



**Effect of gravity on inertial particle clustering and the
Lagrangian attractors in Kinematic Simulation with
different energy spectra**

Muhammad Farhan

A thesis submitted to The University of Sheffield in partial fulfilment of the
requirements for the degree of Doctor of Philosophy

Department of Mechanical Engineering

September 2015

بِسْمِ اللَّهِ الرَّحْمَنِ الرَّحِيمِ

" قالوا سبحانك لا علم لنا إلا ما علمتنا إنك أنت العليم الحكيم "

In the name of Allah, the Beneficent, the Merciful

"They said: Be glorified! We have no knowledge saving that which Thou hast taught us. Lo! Thou, only Thou, art the Knower, the Wise."

Verse 32, Chapter Al-Baqara, The Holy Quran.

DEDICATION

To my respected parents,

To my beloved wife Fariha, my lovely kids Bareen and Ahsan.

Abstract

We study the clustering of inertial particles using a periodic kinematic simulation. A pre-defined Fourier based Eulerian flow field is established. The systematic Lagrangian tracking of particles makes it possible to identify the particles' clustering patterns for different values of particle inertia and drift velocity. The different cases are characterised by different pairs of Stokes number (St) and Froude number (Fr).

The quantification of these clustering patterns is performed for a selection of ranges of non-dimensional parameters and for the present study $0 \leq St \leq 1$ and $0.4 \leq Fr \leq 1.4$. The main focus is to identify and then quantify the clustering attractor - when it exists - that is the set of points in the physical space where the particles settle when time goes to infinity. Depending on gravity effect and inertia values, the Lagrangian attractors have different dimensions varying from the initial three-dimensional space to two-dimensional layers or one-dimensional attractors that can be shifted from a horizontal to a vertical position.

In the absence of gravity, particle clustering is not as significant as when gravity is introduced. It has been noticed that the particle clustering is not obvious for all the values of St and Fr . The particles with low St are more affected by the gravity as compared with high St . In rare cases, the one-dimensional attractors are found and the curtain-like two-dimensional attractors are observed above a certain value of St . The importance of gravity in particle clustering is proved by using the KS model with much more precise data as compared with a complex simulation such as DNS.

KS can be used to model turbulent flow in steps and by construction the KS field has an inertial range equivalent to that of a turbulent flow. The first part of this study is investigated by using the Kolmogorov energy spectrum in the steady flow conditions. Then we proceed our work to further analyse the particle clustering with the modified energy spectral conditions by introducing different energy spectra, unsteadiness frequencies and Reynolds numbers. The variations in the flow change the clustering patterns and it is observed that these changes are more significant for lower values of St and Fr . In addition to this, we also examine the temporal variations of the Lagrangian attractors in the unsteady KS model.

Acknowledgements

Thanks is due to Allah before and after who encourages us to seek for the knowledge for his sake as he says “Lord, Grant me an increase in knowledge” (verse 14, Chapter Taha, The Holy Quran) and who facilitates for us to achieve this work.

I would like to thank my supervisor, Dr. F. C. G. A. Nicolleau, for his thoughtful supervision and guidance throughout this work, whenever I need him he was happy to see me to give me his advice. His understanding and cooperation with me to overcome any problem that I have encountered during my research, are highly acknowledged. Furthermore, his revision and assistance helped me to understand many topics related to my field of study. Also my gratitude is going to Dr. A.F. Nowakowski for his unlimited support and his valuable discussions toward this research.

It goes without saying that the trust and encouragement of my teachers in Pakistan Prof. Dr. Riaz Mirza and Prof. Dr. Nasir Hayat has been a motivation for me to complete this work. I also want to thank Dr. Fahad Noor and Mr. Farrukh Arsalan Siddique, my colleagues in UET Lahore and BZU Multan/Pakistan, for their valuable suggestions during different stages of my project. In addition, my deep thanks are going to all my friends in the Sheffield Fluid Mechanics Group for their great support, discussion and the nice time spent together.

My sincere appreciation and extended thanks go to my beloved family here, for unconstrained support and encouragement throughout this work even in hard times, and also for my family members in Multan/Pakistan although they have been in distress from being away from us, they always give us their moral support and advice.

Contents

Abstract	i
Acknowledgements	iii
Contents	iv
List of tables	vii
List of figures	viii
Nomenclature	xi
1 Introduction	1
1.1 Outline of thesis	4
2 Literature review	5
2.1 Origin of heavy particle in the flow	5
2.2 Approaches to study the particle clustering	6
2.3 Experimental methods	7
2.3.1 Wind-tunnel set-ups	7
2.3.2 Closed turbulent flow	8
2.4 Numerical methods	8
2.4.1 Direct Numerical Simulation (DNS):	9
2.4.2 Large Eddy Simulation (LES):	10
2.4.3 Synthetic flows	11
2.5 Factors affecting particle clustering	12
2.5.1 Flow conditions	12
2.5.2 Seeding of particles	13

2.5.3	Particle characterisation	14
2.5.4	Other factors	16
2.6	Motivation of present study	16
3	Synthetic Kinematic Simulation Model for particle clustering	18
3.1	Periodic KS method for isotropic turbulence	19
3.1.1	The wavenumber distribution:	20
3.1.2	Energy spectrum:	20
3.1.3	Unsteadiness frequency	21
3.1.4	Characteristic time scales and computing time step	21
3.2	Heavy particle equation of motion	22
3.2.1	Forces acting on heavy particle	23
3.2.2	Advancements in equation of motion	24
3.2.3	Assumptions and modified equation	26
3.3	Computing trajectory of particle using KS	28
3.4	Non-dimensional parameters	28
4	Visualisations of particle clustering in Kinematic Simulation	31
4.1	Introduction	31
4.1.1	Time dependency of evolution	32
4.1.2	Visualisation of particle clustering	34
4.2	Visualisations of particle clustering for $St \leq 1$	37
4.2.1	Variation in clustering in relation to St	38
4.2.2	Variation in clustering in relation to Fr	44
4.2.3	Variation in clustering in relation to γ	50
4.3	Visualisations of particle clustering for $St > 1$	52
4.4	Conclusion	55
5	Quantitative analysis of inertial particle clustering	58
5.1	Introduction	58
5.2	Methods of quantification	59
5.2.1	Box-counting method	61
5.2.2	Lacunarity analysis	63
5.2.3	Nearest-neighbour analysis	64
5.3	Application of quantification methods	66
5.3.1	Results using box-counting method	66
5.3.2	Results using Lacunarity analysis	70

5.3.3	Results using Nearest-neighbour analysis	70
5.4	Quantitative analysis of the Lagrangian attractors	74
5.5	Anisotropy of Lagrangian attractor	77
5.6	Conclusion	79
6	Conclusions and considerations for future studies	82
6.1	Conclusion	82
6.2	Considerations for future works	84
	References	86
	Appendix	94
A	Quadrat variance method	95
A.0.1	Results using Quad variance analysis	97
B	Matlab Script to create Q-criterion and vorticity using velocity field	98
	Publications	99

List of tables

3.1	Periodic KS parameters (except modified conditions used in <i>Chapter 8</i>)	22
4.1	Different cases for studying the attractor topology for different ranges of St .	39
4.2	Different cases for studying the attractor topology for different ranges of Fr .	45
4.3	Summary of Observed patterns with varying values of St and Fr	57
5.1	Cases with observed patterns used for method selection	66
5.2	Systematic data set used to quantify the Lagrangian attractors	76

List of figures

1.1	Evolution of particles with increasing values of drift parameter γ	3
3.1	Particles' (a) initial distribution and (b) re-injection	28
3.2	(left) Flow chart of the Modified FORTRAN code for kinematic simulation model of the particle laden clustering (right) Part of code showing re-injection of the particles	29
4.1	Initial distribution of particles in the period box	32
4.2	Time evolution of inertial particles with $St = 0.167$ and $\gamma = 0.689$. . .	33
4.3	Time evolution of inertial particles with $St = 0.413$ and $\gamma = 0.575$. . .	33
4.4	Spatial distribution of inertial particles for eight different values of St_η in a thin layer (width 5η) (a) 0.05, (b) 0.1, (c) 0.2, (d) 0.5, (e) 1, (f) 2, (g) 5 and (h) 10.	35
4.5	(a) The modulus of the pressure gradient, giving the main contribution to fluid acceleration, on a slice $512 \times 512 \times 4$. B/W code low and high intensity, respectively. Particle positions in the same slice are shown for (b) $S_\eta = 0.16$, (c) 0.80 and (d) 3.30. Note the presence of voids with sizes much larger than the dissipative scale.	35
4.6	(a) – (c) Two-dimensional and (d) three-dimensional snapshots of a droplet concentration field that is driven by both gravity and turbulence. The slice thickness in (a) – (c) is one grid box. The snapshots show the curtain-like manifolds of sediment droplets waving in the turbulent field.	36
4.7	Evolution of tracers in the flow field at $t=100s$ (a). without gravity and (b). with gravity	37
4.8	Attractors for $St = 0.167$ with increasing γ run at different times.	38

4.9	Clustering variations at $St = 0.041$ for decreasing value of Fr (increasing gravity) and $t = 300s$	40
4.10	Clustering variations at $St = 0.124$ for decreasing value of Fr and $t = 300s$	40
4.11	Clustering variations at $St = 0.249$ for decreasing value of Fr and $t = 300s$	41
4.12	Clustering variations at $St = 0.331$ for decreasing value of Fr and $t = 300s$	42
4.13	Clustering variations at $St = 0.373$ for decreasing value of Fr and $t = 300s$	42
4.14	Clustering variations at $St = 0.413$ for decreasing value of Fr and $t = 300s$	43
4.15	Clustering variations at $St = 0.456$ for decreasing value of Fr and $t = 300s$	43
4.16	Clustering variations at $St = 0.663$ for decreasing value of Fr and $t = 300s$	44
4.17	Clustering variations at $St = 1.00$ for decreasing value of Fr and $t = 300s$	44
4.18	Clustering variations at $Fr = \infty$ for increasing value of St and $t = 300s$.	45
4.19	Clustering variations at $Fr = 1.89$ for increasing value of St and $t = 300s$	46
4.20	Clustering variations at $Fr = 1.34$ for increasing value of St and $t = 300s$	46
4.21	Clustering variations at $Fr = 1.09$ for increasing value of St and $t = 300s$	47
4.22	Clustering variations at $Fr = 0.849$ for increasing value of St and $t = 300s$	48
4.23	Clustering variations at $Fr = 0.717$ for increasing value of St and $t = 300s$	48
4.24	Clustering variations at $Fr = 0.548$ for increasing value of St and $t = 300s$	49
4.25	Clustering variations at $Fr = 0.490$ for increasing value of St and $t = 300s$	49
4.26	Attractor variation with increasing values St for $\gamma=0.138$ and $t = 300s$.	50
4.27	Attractor variation with increasing values St for $\gamma=0.276$ and $t = 300s$.	51
4.28	Attractor variation with increasing values St for $\gamma=0.345$ and $t = 300s$.	51
4.29	Attractor variation with increasing values St for $\gamma=0.689$ and $t = 300s$.	52
4.30	Attractor variation with increasing values St for $\gamma=2.0$ and $t = 300s$. .	53
4.31	Attractor variation with increasing values St for $\gamma=3.0$ and $t = 300s$. .	53
4.32	Clustering variations at $St = 1.24$ for decreasing value of Fr and $t = 300s$	54
4.33	Clustering variations at $St = 1.63$ for decreasing value of Fr and $t = 300s$	54
4.34	Clustering variations at $St = 1.86$ for decreasing value of Fr and $t = 300s$	55
4.35	Different types of attractors	56
5.1	A relationship between box-counting dimension D_B and Lacunarity Λ .	64
5.2	Example of a nearest-neighbour network. Points are only connected to their nearest neighbours.	65
5.3	Bench mark for box-counting method	67
5.4	(a)-(f) log-log plots showing box-counting dimension for different values of St with varying Fr at $t=300s$, slopes are taken between inertial range of 3.96-15.85	68
5.5	Time evolution of inertial particles with $St = 0.207$ and $Fr = 0.55$. . .	69

5.6	Box-counting slope for very similar cases for different values of Fr at $St = 0.207$	69
5.7	Bench mark of Lacunarity for different clear Lagrangian attractors . . .	71
5.8	Lacunarity curves (a)-(f) for different values of St with varying Fr at $t=300s$	72
5.9	Clustering of inertial particles with $Fr = 1.34$ (a). $St=0.124$ and (b). $St=0.249$	73
5.10	Variation in Δ for decreasing values of Fr for different values of St . . .	73
5.11	Variation in Δ for increasing values of St for different values of Fr . . .	74
5.12	Iso-contours of the attractors fractal dimension D as a function of (St, Fr) . . .	75
5.13	Iso-contours of Δ as a function of (St, Fr)	76
5.14	Iso-contours of Δ as a function of (St, γ)	77
5.15	2D-planar views columns (a)-(d) showing different asymptotic 1-D attractor for $St = 0.207$ with different γ	78
5.16	(a) Iso-contours of Δ as a function of (St, Fr) , (b) Δ_V/Δ when $\Delta \leq 0.006$, (c) Δ_H/Δ when $\Delta \leq 0.006$	78
5.17	(a) Iso-contours of Δ as a function of (St, γ) , (b) Δ_V/Δ when $\Delta \leq 0.006$, (c) Δ_H/Δ when $\Delta \leq 0.006$	79
5.18	Flow chart describing the different attractors in relation to the two critical values of St	81
A.1	Representation of eight-term local quadrats	96
A.2	Representation of twenty seven-term local quadrats	96
A.3	Results using 27-LTQV method for different values of St with varying Fr at $t=300$	97

Nomenclature

Latin

a	particle radius
\mathbf{a}_{ijl} and \mathbf{b}_{ijl}	Fourier coefficient vectors
C_D	drag coefficient
d	particle diameter
D	fractal Dimension
du/dt	time derivative of the moving particle
Du/Dt	total time derivative of the fluid velocity
dt	time increment
$E(k)$	energy spectrum
Fr	Froude number
g	gravity acceleration
k_{ijl}	the wave vector
k_{min}	the smallest wave number
k_{max}	the largest wave number
L	the largest length scale
m_p	particle mass
m_f	equivalent mass of the displaced fluid due to particle existence
N	number of Fourier modes
N_p	number of particles
N_ε	number of boxes needed to cover an object
Δp	pressure drop
$Re(L)$	Reynolds number based on integral length scale
Re	Reynolds number
Re_p	Reynolds number based on particle diameter
St	Stokes number based on eddy turnover time
St_η	Stokes number based on Kolmogorov time
t	time
t_η	Kolmogorov time
t_d	eddy turnover time based on the largest length scale
u_{rms}	r.m.s. of the turbulent velocity fluctuations
$u(x(t), t)$	Eulerian velocity field
$u(x_p(t), t)$	velocity of the fluid at the particle position
V	particle velocity
V_d	terminal fall velocity in still fluid

Greek

Δ	average distance to nearest-neighbour
Δ_H	average horizontal distance to nearest-neighbour
Δ_V	average vertical distance to nearest-neighbour
ε	energy dissipation rate
ε	box size used in fractal dimension calculation
γ	particle drift velocity
ρ_p	particle density
ρ_f	fluid density
Λ	Lacunarity
λ_n	unsteadiness parameter
η	Kolmogorov length scale
μ	fluid viscosity
ω	angular velocity
Ω	vorticity
ω_n	unsteadiness frequency associated with wave mode
\mathcal{L}	integral length scale
\mathcal{T}	eddy turnover time based on integral scale

Subscripts

f	for fluid
p	for particle
i	the i^{th} Cartesian component
j	the j^{th} Cartesian component
k	the k^{th} Cartesian component
E	associated with Eulerian property
n	n^{th} wave mode
η	associated with Kolmogorov scale

Chapter 1

Introduction

The history of turbulent flows is as old as the Universe and owing to non-linear behaviour of turbulent flows, their dynamics are complicated to resolve. Turbulent flow originates from the instabilities present in laminar flow which is affected by perturbations due to imperfections or vibrations of the system or inlet passages. If the fluid viscosity is significant, these perturbations are damped and the flow energy is converted into heat. In a case when the flow rate is very high, the perturbations sustain and amplify in the flow instead of decaying with time such a flow becomes turbulent.

Naturally, turbulent flows can be thought as random in time and space and this randomness in the flow is due to its sensitivity to initial and boundary conditions. This unique feature of turbulence makes it very difficult to rely on deterministic approaches. Rather statistical analyses are considered as more reliable options for turbulence modelling. In addition, turbulent flow has a wide range of scales varying from large scale (size of conduit) to small scales (scales where flow energy dissipated into heat). All these aspects of turbulence make it a complex problem to solve and it is a challenge for researchers and scientists to model the flow close to a real turbulent flow.

In order to simplify the problem, assumptions are normally made during analysis and the most commonly, incompressible homogeneous isotropic turbulence (HIT) is used. That is, the flow has the same structure in all parts and directions. In this work, we are also interested in incompressible homogeneous isotropic turbulence for studying particle clustering.

Clustering could be defined as the propensity of an initially uniformly distributed cloud of particles to accumulate in some regions of the physical space. The clustering phenomenon is frequently referred to as preferential concentration in the flow. This is an important task to understand in order to explore, identify and possibly monitor some natural or hand-made mixing processes such as those causing rain formation (Falkovich *et al.*, 2002), sediment transportation (Pan *et al.*, 2011), fuel mixing and combustion, the development of planetesimals during process of planet formation (Cuzzi *et al.*, 2001).

There are different ways to analyse particle clustering in turbulent flows and Direct Numerical Simulation (DNS) is the most widely used method (e.g., Cencini *et al.* (2006); Saw *et al.* (2012); Falkovich & Pumir (2004)). Particle clustering depends on both the flow conditions and the particle characteristics. Different flow conditions can lead to different clusters. The clustering mechanism would be different in the inertial or dissipation range of turbulent flow (Bec *et al.*, 2007). In this work, we only study the effect of the scales in the inertial range and this is possible by using a synthetic model where forcing and dissipation are not needed to develop the inertial range. While considering particle characteristics, most of the studies on particle clustering have been conducted in the absence of external forces on particles but the effect of gravity(external force) was discussed in relation to cloud physics and rain formation in Falkovich & Pumir (2004); Woittiez & Portela (2008).

More recently, the effect of gravity on clustering mechanism has been further emphasized in Dejoan & Monchaux (2013); Park & Lee (2014); Gustavsson *et al.* (2014); Bec *et al.* (2014). In the present study, to observe the clustering pattern in the presence of gravity, the particles are initially uniformly distributed in the Kinematic Simulation (KS) flow. Though there is no particular difficulty in considering particles with different inertia in Kinematic Simulation, this study is limited to mono-dispersed seeding i.e. particles having the same inertia. Furthermore, the particles are considered small enough so that they neither affect the flow nor interact with each other (one-way coupling). The positions of particles are monitored as a function of time and a Lagrangian attractor is observed for some cases. That is, the initially uniformly distributed cloud of particles will end in a set of loci as shown in Fig. 1.1 that does not evolve any further. The particles move within that set of loci which defines the structure of the Lagrangian attractor and its dependence on St and Fr numbers is studied here.

We only consider attractors with integer dimensions (one-dimensional and two-dimensional structures) which are easy to identify. Different types of methods can be found in the

literature to identify and then quantify particle clustering patterns, e.g.: correlation dimension used in Bec *et al.* (2007), radial distribution function (RDF) Saw *et al.* (2012), average-distance-to-nearest-neighbour method Park & Lee (2014). The selection of a method is mainly based on the objective of the study. For example, the RDF has the advantage of being directly related to the droplet collision rate. For the present work, the Box counting method (BCM) and the nearest-neighbour distance analysis are implemented to identify the integer dimensions of Lagrangian attractor in the presence of gravity.

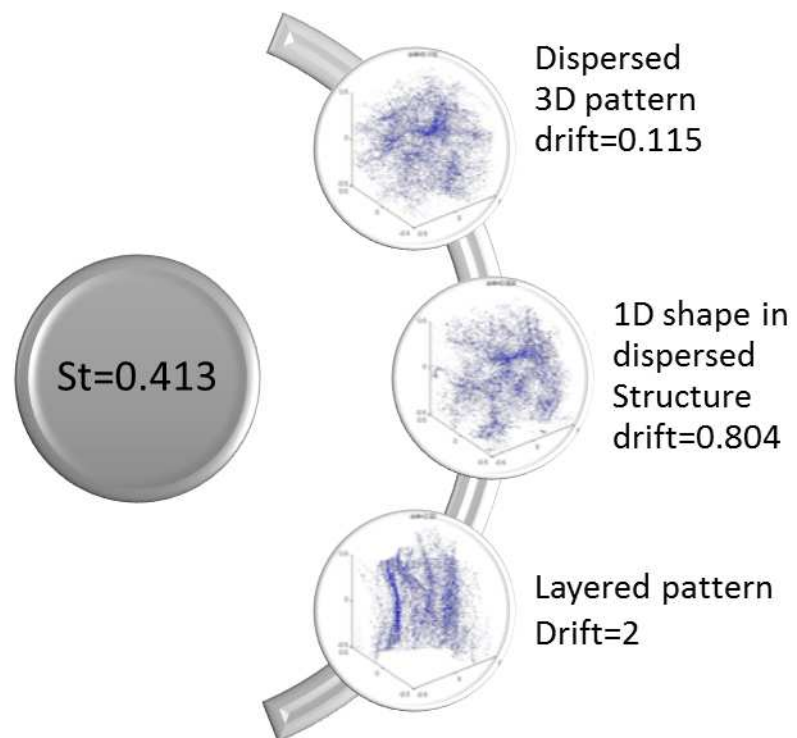


Figure 1.1. Evolution of particles with increasing values of drift parameter γ .

Following the successful findings of clustering patterns in the steady KS with Kolmogorov energy spectrum, we modify the energy and scale distributions in the flow. Using the synthetic KS model, it is quite feasible to modify the flow conditions and investigate the effects of these modifications on the particle clustering. Throughout this thesis, we focus on the effect of gravity in the context of particle clustering.

1.1 Outline of thesis

After a brief literature review and description of methodology in *Chapter 2 and 3* respectively, we present a qualitative analysis to identify the clustering patterns with respect to different pairs of (St, Fr) in *Chapter 4*. In order to quantify the clustering attractors, different types of quantification methods are discussed and applied to the qualitative results in *Chapter 5*. The clustering with modified spectral laws will be part of discussion in *Chapter 6* while in *Chapter 7* the results obtained in *Chapter 5 and 6* are related to the flow vortex structures. In *Chapter 8*, we include the effects of unsteadiness, seeding and Reynolds number on particle clustering. Finally, we conclude our achievements and recommend some future considerations in *Chapter 9*. It should be noticed that each result chapter i.e. *Chapter 4-8* has its own introduction, historical background and conclusion.

Chapter 2

Literature review

In this chapter, we review the particle clustering phenomenon and different ways to analyse it. In particular, we focus on the numerical simulations which have been used to study particle clustering. In addition, we will also discuss different factors affecting particle clustering by relating them with previous studies. As each of the result chapters has a self-contained literature, here we present a brief historical background to set the goals of our study.

2.1 Origin of heavy particle in the flow

A particle whose density is significantly higher than the density of the fluid is termed as a heavy particle. It is important to know how the heavy particles behave in turbulent flow to understand natural and artificial phenomena. Historically, a hydrostatic force on an immersed body was first investigated by Archimedes. He described the hydrostatic forces on the immersed object for all shapes and densities as well as concept of integration of these forces. His idea was implemented to develop instrument like pycnometer. Further advancement in the field of floating bodies was made by Galileo who elaborated the correct use of principle of Archimedes and its application for immersed and partially immersed objects.

A few years later, Newton further explained the mechanics of immersed object. His publication “monumental Principia” is considered as a mainstay of recent developed mechanics. In addition to this, the first attention to hydrostatic forces on the spherical objects in a inviscid flow was given by Poisson by calculating the force exerted by the inviscid fluid on sphere. They achieved this by solving the equation of the potential flow

around the sphere. In continuation, Green extended the results obtained by Poisson and he studied the flow around an ellipsoid in an inviscid fluid. Furthermore, Poiseuille studied experimentally the motion of spheres in a solid conduit in order to understand the flow of blood corpuscles. These early researches help us to develop basic understanding of particle motion in a fluid.

Stokes was the first who analysed the motion of solid sphere in a viscous fluid. Using the Navier-Stokes equation, he found the solution of a steady state flow around the sphere and defined a force which is now known as the ‘Stokes drag force’. Further detailed discussion on the forces acting on the spherical particles will be presented in *Chapter 3*. Now we discuss the literature relevant to inertial particle clustering, methods of analyses and factors affecting the clustering mechanism.

First qualitative measures of particle dispersion was tracked back by Crowe *et al.* (1988). He reported the first experimental evidence related to preferential concentration of the heavy particles by Brown & Roshko (1974) who discovered the interaction of the heavy particles with large-scale turbulent structure. In most of the early researches (Squires & Eaton, 1990, 1991; Tang *et al.*, 1992; Fessler *et al.*, 1994) etc.), a common phenomenon of preferential concentration was analysed i.e. settling of particles in the saddle regions of the flow ejected from the vortical regions was revealed.

Since these early developments on clustering, the number of contributions (experimental, theoretical and numerical) have significantly increased. Mainly based on numerical simulations, different particle mechanisms such as dispersion, diffusion and clustering have been investigated. Also by taking into account the interaction of particles within themselves and with the surrounding fluid, a few number of studies have also figured out the effect of particles on turbulence structure. In order to achieve the desired objective of a study, the specific flow conditions are designed according to given particle characteristics. In the following sections we describe the different approaches have been adopted for studying particle clustering.

2.2 Approaches to study the particle clustering

The particle laden turbulent flows can be studied either experimentally or numerically. Most of early researches (before 90’s) on this topic are based on experimental results and it is found that experimental set-up could generate a limited amount of results because of complex constraints of the multi-particle flows. Another common way to see the particle

clustering is by using numerical method which provide more flexibility in the methodology, designs and degree of precision. Therefore, numerical simulations are presently preferred over experimental methods. Depending on the type of problem, precisions of results and available computing facilities, different types of numerical techniques have been employed. Before discussing the numerical simulation in detail, we would like to describe some experimental works.

2.3 Experimental methods

Particle clustering has been mostly studied using the numerical simulations as state of the art computing facilities are available. Instead of the structured flows, homogeneous isotropic turbulence (HIT) is under consideration and a number of anisotropic flows have been used to study the preferential concentration or clustering of inertial particles including boundary layers flows, free shear flows, jet flows, etc. Main experimental researches can be classified into two types and these are briefly discussed here.

2.3.1 WIND-TUNNEL SET-UPS

Wind-tunnel experiments are widely used to analyse the single-phase or multiphase turbulence problems. In such experiments, a flow is developed by using the fans/propellers and particles are injected randomly or uniformly later in the flow. In case of particle clustering, it is utmost difficult to build a new wind-tunnel set-up which can track a few hundreds of particles to generate sophisticated results. Normally, turbulent flows are created using a grid of uniform section that is positioned downstream in the convergent section of tunnel and a large variety of grids have been deployed to investigate statistical properties of turbulence. An optimum design of mesh grid actually controls the integral length scales and Taylor micro-scales in turbulent flow. Eventually, these parameters are used to define the Reynolds number which is a key factor in defining the turbulence. In single-phase flow, depending on the size of wind-tunnel, one can achieve Reynolds number starting from hundreds to a few thousands. Recently, an active-grid technology has been introduced to increase the Reynolds number in small laboratory experiments (Saw *et al.*, 2008), but it creates the problems in measuring the turbulence statistics because of the continuous motion of the grid.

Even after successful generation of turbulence in a controlled environment, other issues those can restrict the use of wind-tunnel experiments to study particle clustering are:

- It is difficult to inject and track inertial particles under unsteady flow conditions,

specially at high Reynolds numbers. Therefore, a few hundreds of particles can be tracked using the high speed cameras (Ayyalasomayajula *et al.*, 2006).

- The selection of size and types (solid, liquid, synthetic, etc.) of particles is another critical issue which may restrict the use of wind-tunnel experiments. Normally, it is difficult to inject the large number of solid particles as they can wear and destroy the mechanical parts of the wind tunnel. On the other hand, it is equally tricky to inject the liquid particles of same size in a controlled flow conditions.

2.3.2 CLOSED TURBULENT FLOW

During the past few years, turbulent flows enclosed by a box or vessel had been extensively investigated in relation to particle clustering. In a close flow, particles remain in a confined space and not in contact with the fan or propeller as happen in wind-tunnel. Therefore, seeding is not an issue with this type of flow and particles with different densities can be injected with ease. The most common closed flow is Von Kármán experiment which used the counter rotating propellers to generate an inhomogeneous anisotropic flow of $Re_\lambda=400$. Later, other researchers (Salazar *et al.*, 2008; Zimmermann *et al.*, 2010; Gibert *et al.*, 2012) extended Von Kármán experiment to achieve the homogeneous and isotropic turbulent flow.

Another kind of closed flows to produce an isotropic turbulence, using eight synthetic jets, is proposed by Hwang & Eaton (2004) and their approach is followed by Goepfert *et al.* (2010) to study the evaporation of droplets in turbulence.

It has been noted that different experiments have the different kind of limitations. Though the findings of an experimental work can be more realistic and closer to nature, difficulty of building a new set-up and tracking of particles restrict the application of this approach, specially in the present era of state-of-the-art computing.

2.4 Numerical methods

At the present moment, it is considered as the most promising way to study turbulence problems as the sources available today for this method are much sophisticated than what we had twenty years ago. Of course, the cost of computing is one of the limitations of this method, but this can be overcome by using simpler flow conditions. In general, numerical simulations are used for two purposes as follows:

- (1). The first is to understand and control the physical mechanisms governed by fluid

dynamics and usually highly accurate results are generated by using all space-time scales of turbulence. These types of simulation become complicated with increasing range of scales and hard to simulate.

- (2). Numerical simulations are also used to predict some design parameters instead of flow characteristics. Normally, flow conditions are kept constant and some engineering analysis is performed which depends on the flow, such as the forces acting on the inertial particles in the flow. The purpose is to get a less expensive and quick development of the prototype.

In the context of particle clustering, numerical simulations are the most widely used method. Most of the numerical methods are based on the Maxey & Riley (1983) equation of motion of particle with some assumptions. On the basis of flow tracking mechanism, we can classify numerical methods into two different classes i.e., Eulerian approach and Lagrangian approach. Here we are interested in discussing major types of numerical simulation in relation to particle clustering.

2.4.1 DIRECT NUMERICAL SIMULATION (DNS):

Direct numerical simulation is the first and most developed method to deal with turbulence by solving the unsteady three-dimensional Navier-Stokes equation. DNS has been established as an extremely reliable tool for investigating inertial particle dynamics. Due to the heavy computational demands of resolving all the scales (temporal and spatial), modest values of Taylor Reynolds number ($Re_\lambda \simeq 500$) have been achieved. When dealing with particle clustering, a 3D flow is normally generated as a box of turbulence and then particle phase is resolved in the flow.

One way is to simulate particle phase through a fully resolved particle-fluid DNS, but this approach has limited application because of time and cost expenses. On the other hand, Lagrangian tracking is another way to deal with DNS. With Lagrangian tracking much detailed statistics of particles in the flow can be achieved (Holzner *et al.*, 2008; Tagawa *et al.*, 2012). As a fully resolved turbulence, DNS can be used to study particle clustering in dissipative and inertial ranges (Bec *et al.*, 2007). They found that clustering mechanism is different in inertial and dissipative length scales.

In addition to this, we also refer to some DNS studies dealing with particle dynamics by applying the well-defined inertial ranges (Bec *et al.*, 2010; Pan *et al.*, 2011; Ray & Collins, 2011; Rosa *et al.*, 2013). All of these studies considered different values of Reynolds number $Re \leq 500$ and further work is required to fully understand the natural

phenomena such as rain formation, planet formation, etc. In the presence of gravity, previous DNS studies emphasized on how turbulence changes settling velocity of particle (Good *et al.*, 2014; Bec *et al.*, 2014; Park & Lee, 2014) or collision rate (Woittiez & Portela, 2008; Rosa *et al.*, 2013).

Apart from physical space, DNS can also be run as a pseudo-spectral method in which linear terms are solved in spectral space while physical space is adopted for non-linear terms. For producing a link between two spaces normally fast Fourier transform is used. Using a pseudo-spectral 2D DNS, Coleman & Vassilicos (2009) proposed a new mechanism (sweep-stick mechanism) to investigate the clustering of inertial particles. They found that heavy particles at zero-acceleration points move with the local fluid velocity. Jin & He (2013); Bec *et al.* (2014) considered pseudo-spectral models to investigate the clustering of particles in the presence of gravity.

2.4.2 LARGE EDDY SIMULATION (LES):

Another way to efficiently simulate the particle laden flow, with lower computation cost as compared to DNS, is Large eddy simulation (LES). Using this method, the large scales are computationally resolved while the smaller scales are represented through a sub-grid model. The main advantage of LES over DNS is easy achievement of high Reynolds numbers and its ability to simulate the complex shapes and geometries. In terms of particle clustering, LES is only capable with particles sized larger than grid size. As most of the flows consists of the particles much smaller than the smallest-resolved scale, the accuracy of LES depends on the sub-grid model.

Early researches (Wang & Squires, 1996; Yang & Lei, 1998) used LES to study the particle dynamics in a isotropic homogeneous turbulence. Recently, Ray & Collins (2011, 2013) applied sub-grid models in LES to investigate the particle-pair dynamics at small separations and to reproduce the particle clustering. They showed that their results in terms of critical St are in agreement with DNS Salazar & Collins (2012). Moreover, Jin *et al.* (2010) studied the collision of heavy particles in isotropic turbulence by using filtered direct numerical simulation (FDNS) and large eddy simulation (LES). They found the critical value of $St_k > 3$ above which collision rate can be predicted using both numerical methods. While for low and intermediate St , selection of sub-grid scale for LES is crucial. Besides a few attractive features of LES, selection of sub-grid model for the small scales is considered as a drawback of LES and further work is required to resolve this.

2.4.3 SYNTHETIC FLOWS

Synthetic flows are used to test various ideas by isolating particular physical mechanisms in turbulent flows. In general, these flows consist of analytical vortices whose positions and intensities can be deterministically or randomly defined. Specifically, these less physical models have been used to test basic centrifuging phenomenology, such as those experimentally reported by Eaton & J.R.Fessler (1994). Kinematic simulation (KS) is one of the established synthetic flows and it has been successfully applied to study particle dispersion and diffusion.

The first KS Eulerian flow was generated by Fung *et al.* (1992) for an isotropic homogeneous turbulence. They produced some new results for the statistics of the velocity and pressure fields in a high Reynolds number turbulent flow, whereas the particle statistics were obtained by tracking the trajectories of many particles and then taking the ensemble average.

After the evolutionary findings by Fung *et al.* (1992), many studies have been presented either for validating the KS model or for analysing the different aspects of particle dynamics. For example, two-particle diffusion in the turbulent flow was investigated by Fung & Vassilicos (1998) while first comparison between DNS and KS was made by Malik & Vassilicos (1999). Further to this, Nicolleau & Vassilicos (2003) studied the particle-pair diffusion and their results were compared to previous experiments. They investigated the effect of second order structure function of one particle Lagrangian velocity, $\langle v^2(t) \rangle$, as a function of energy spectrum power law and the unsteadiness parameter.

Nicolleau & Yu (2004) Examined one-particle and two-particle diffusion in a 3D homogeneous isotropic KS. They found the effect of changing the power law exponent on two-particle diffusion and also revisited the locality assumption. Furthermore, Thomson & Devenish (2005) used a variable time-step in KS (varied with the particle pair separation) with particular attention paid on the problem caused by the lack of sweeping of the small scales by the large scales. After Thomson & Devenish (2005) findings, Osborne *et al.* (2006) also chose to investigate the separation of particle pairs in kinematic simulation. They simulated the inertial sub-range in the range of $k_N/k_1 = 10^4$ and concluded that KS reproduces Richardson's power law over a wide range of scales in the inertial range.

KS has also been complemented with other simulations in order to understand the clustering. Such as, clustering of stagnation points and inertial particles in turbulent flow

is investigated by Chen *et al.* (2006). They found the simultaneous sweeping of zero-acceleration points and inertial particles by the large scales thus implying the kind of persistence in time which might well cause droplet spectral broadening to occur as a result of clustering. This phenomenon of sticking and sweeping is further explained by Coleman & Vassilicos (2009) using the three-dimensional KS model.

The results in all above studies motivate us to study the clustering of laden particles using KS. The detailed discussion on selected KS model and recent literature will be provided in *Chapter 3*. We close this section by listing the reasons for choosing the KS model. The less physical KS flow has eddying, straining and streaming regions similar to real turbulent flows. Though the sweeping from large to small scales is missing, centrifugal effect created by the rotational eddies is enough to study the clustering. The major advantages of KS over DNS are as follows:

- It is computationally cheap in comparison to DNS.
- High Reynold numbers can be achieved with fully developed turbulence.
- The energy spectrum can be chosen arbitrarily according to the nature of the problem.
- Efficient for parallel computing
- No forcing (no decay)

2.5 Factors affecting particle clustering

Once a method (experimental or numerical) to analyse particle clustering is decided, next step is to control the flow conditions and particle characteristics. Depending on the experimental or numerical technique, particles' characteristics are chosen accordingly. Usually, numerical simulations can be devised to investigate the clustering with a much more precise data and flexible flow conditions. In the following sections, we discuss different factors which have been related to particle clustering in the previous numerical studies.

2.5.1 FLOW CONDITIONS

As mentioned earlier, most of the studies have adopted for incompressible homogeneous isotropic turbulence (HIT) to study particle clustering. In such a complex flow, the most important flow controlling parameter is Reynolds number and until now a few hundred

values of Reynolds number have been achieved using DNS. It has been found that after a certain particle size, Reynolds number does not affect the particle clustering (Collins & Keswani, 2004; Bec *et al.*, 2014). Collins & Keswani (2004) studied the clustering of aerosols with the different values of Reynolds number and found that clustering of particles is independent of Reynolds number. Similarly, Bec *et al.* (2014) observed same trend of clustering variation with the different values of Reynolds number in DNS.

Furthermore, laden particles are mostly studied in an unsteady flow as it is difficult to produce the steady flow conditions in an experimental method or DNS. In contrast, it is quite viable to develop the steady flow using an analytical method. For example, Sapsis & Haller (2010) defined a clustering criterion for the inertial particles in a three-dimensional steady flow. They found that particles' clusters are attracting towards the inertial Lagrangian coherent structures. In similar way, Kinematic simulation has also the capacity to produce a steady flow and then unsteadiness can be increasingly introduced.

2.5.2 SEEDING OF PARTICLES

Depending on particles' inertia and sizes, they can be seeded as mono-dispersed, bi-dispersed or poly-dispersed. For the sake of convenience and better understanding, mono-disperse particle seeding is frequently used method in the previous numerical studies. On the contrary to this, a few of studies (Woittiez & Portela, 2008; Saw *et al.*, 2012) considered bi-disperse and poly-disperse particle seeding as inestimable to study the particle clustering. Woittiez & Portela (2008) compared the collision rate of mono-disperse or bi-disperse inertial particles. It was found that for mono-disperse distributions, gravity decreases the collision probability. On the other hand, the collision kernel is increased by the gravity for bi-disperse distributions as a result of the fact that droplets of unequal size possess different terminal falling velocities. In addition to this, Saw *et al.* (2012) found that the effect of poly-disperse seeding is to diminish the particle clustering by calculating the RDF for an arbitrary particle size distribution.

In terms of coupling of particles with flow structures, both one-way and two-way coupling techniques have been employed to examine particle clustering. Clustering by considering particles as the passive tracers is a common approach used in the numerical simulations. In such simulations, particle motion is affected by the fluid phase and there is no influence of the particle phase on the fluid. While in case of two-way coupling, the fluid phase affects the particle dynamics via aerodynamic drag and turbulence transfer and also particle motion reduces the mean momentum and turbulent kinetic energy of

the fluid phase.

Squires & Eaton (1990) were among the first who considered the two-way coupling in DNS. An increase in turbulent kinetic energy was found at higher wavenumbers. Recently, effect of St and mass loading on turbulence characteristics was further analysed by Ferrante & Elghobashi (2003); Lucci *et al.* (2010, 2011). Ferrante & Elghobashi (2003) related the particle dispersion with energy spectrum modification with and without gravity using different aerodynamic response time. They found that spectrum of turbulence with particles becomes anisotropic as compared to the particle-free turbulence.

Furthermore, the modification in mean settling velocity is another parameter which has been examined using two-way coupling. In this regard, Maxey (1987); Wang & Maxey (1993) revealed an increase in mean settling velocity compared to the terminal velocity of a single particle in a still fluid. Referring to their works, Bosse *et al.* (2006) strengthened the argument of an increase in settling velocity using the two-way coupling.

Regardless of coupling and types of particles, numerical simulations are normally initiated with a uniform distribution of the particles. Then the particles are tracked by solving the equation of motion. Corresponding to flow conditions and seeding mechanisms, particle characterisation is one more considerable feature needing to be discussed.

2.5.3 PARTICLE CHARACTERISATION

In order to relate with the pre-defined flow field, particle phase are usually characterised using different non-dimensional parameters. Among these non-dimensional parameters, Stokes number (St) is the mainly considered parameter which is defined as the ratio between aerodynamic response time of particle and Kolmogorov or integral time-scale of turbulence. A wide range of Stokes numbers ($0 \leq St \leq 100$) has been used in the literature. Although St is considered as a representative of inertial effect of particles (based on size and density of particles), a few of studies such as Qureshi *et al.* (2008) considered size and density separately to measure the acceleration statics of inertial particles in the turbulent flow. Using two-way coupling Lucci *et al.* (2010, 2011) also showed that particles with different diameters but same response time have different impact on the flow. Further to this, it has also been observed (Bec *et al.*, 2007a, 2008) that scale-by-scale clustering can be better understood by considering the local Stokes number (related to local eddy-turn over time). Hence, the Stokes number for a particular study must be defined on the basis of time-scale of local turbulence.

Gravity-driven particles:

In the turbulence dominating regime, particles form clusters due to the centrifugal force acting on particles and as a result particles accumulate in the strain region. This phenomenon strongly linked with particles' St . Other than the inertia, external forces (gravity, electrical charge, etc.) can also affect particle clustering. In most of the previous studies, the effect of gravity has been ignored either to avoid complexity in simulation or insignificance of the effect was found on the clustering mechanism.

Under the effect of gravity, particles have an average relative velocity to the surrounding flows that may decrease the interaction time scale between the turbulent structures and particles, thus it could change the particle clustering. Therefore, it is important to consider the gravity for better understanding some of the natural process such as rain-formations (Falkovich *et al.*, 2002; Falkovich & Pumir, 2004). The Combined effects of turbulence and gravity on droplet collisions in clouds (Woittiez & Portela, 2008) also revealed the significance of gravity on particle clustering.

Most recently, gravity has been taken into account (Rosa *et al.*, 2013; Dejoan & Monchaux, 2013; Jin & He, 2013; Bec *et al.*, 2014; Gustavsson *et al.*, 2014; Angilella *et al.*, 2014; Park & Lee, 2014) in order to analyse the inertial particle motion in turbulence. In terms of particle characterisation, different research teams used various Fr ranges to include the role of gravity with different flow conditions.

Rosa *et al.* (2013) specifically addressed the role of gravity on collisions of cloud droplets for a range of flow with Taylor micro-scale Reynolds numbers up to 500, using a highly scalable hybrid direct numerical simulation approach. They found a critical value of droplet size below which gravity is not affected. For larger particles they observed that the collision rate alters with the effect of gravity and also noted that the effect of gravity is not same for different sized particles.

Jin & He (2013) elaborated the effect of gravity in relation to some chemical engineering applications. A pseudo-spectral method along with the particle tracking was implemented to compute the point particle clustering in a forced isotropic turbulent flow, while the finite-size particles were tracked by applying the lattice Boltzmann method in a decaying isotropic turbulent flow. They found that the mean drift velocity could reduce the point particles' clustering. However, for the particle sized larger than characteristic viscous scales, clustering is very weak.

Bec *et al.* (2014) analysed the particle clustering to understand the intriguing interplay between turbulence, gravity, and particle sizes. They used three different values of Taylor scale Reynolds number $Re_\lambda = 130, 290$ and 460 to investigate the particle clustering with various values of St and Fr . On the basis of their quantified results, the effect of gravity is confirmed depending on the particles' St .

Further to this, Gustavsson *et al.* (2014) also reported the possible reduction or enhancement of small particles clustering (depending on the Stokes number of the particles) using incompressible velocity field and also found strong anisotropic clustering as the result of gravity. Most recently, Park & Lee (2014) discovered the vertical stripe patterns under the effect of gravity by quantifying the clustering using different St and Fr . In all of the above studies of particle clustering shows that the Stokes number is not enough to characterise the clustering of inertial particles and the effect of gravity must be included.

2.5.4 OTHER FACTORS

So far we have discussed different factors affecting the clustering mechanism. On top of this, post processing and quantification methods are other important considerable aspects to reveal the clustering patterns. Such as, in dissipative range, particles may cluster as an invariant fractal structure and this kind of differentiation is made by Bec *et al.* (2007) who quantified the clustering in both inertial and dissipation ranges. It has been found that different types of quantification methods are employed to quantify the clustering patterns in different turbulence scales. Further details on quantification methods will be provided *Chapter 5*.

2.6 Motivation of present study

On the basis of previous studies on inertial clustering, we infer that there is a huge demand of research to fully understand the clustering mechanism, particularly in the presence of gravity. The effect of gravity on particle clustering has already been studied, but there are some open questions to answer and these are main source of motivation for the present work. In the light of our discussion, we set our goals as follows:

- In order to identify the clustering of inertial particles in turbulent flow, we aim to use different ranges of St (based on particles inertia) and Fr (based on gravity). Owing to simplicity of the KS model, more precise data can be generated as compared to DNS.

- After identification of clustering patterns, it is schemed to apply different quantification methods to our visualised results. In this way, we can classify different clustering attractors.
- The interpretation of clustering mechanism is very important to understand the physical mechanisms such as, rain formation, mixing process, etc. So, we aim to define inertial particle attractors with respect to critical values of St and Fr . Using these critical values, we can define the importance of gravity effect for different industrial and natural processes.
- By using KS, it is feasible to start the simulations with the simplest case of steady homogeneous turbulence and then on later stages, we can impose the unsteady conditions to flow field to study the particle clustering.
- Similarly, Kolmogorov spectrum is set as an input for the KS model which is then modified to different power laws of energy spectrum in order to see the difference in the attractors.
- Following the centrifugal phenomenology, it is very interested to see the particles' positions among flow vortices under the effect of gravity. In order to do so, we first consider different approaches to develop the vorticity structures and then locate the inertial particles' attractors in those flow vortices.
- The main objective of this work is to link the effect of gravity to the inertial particles clustering in different spectral conditions. Whether it is steady or unsteady flow condition with Kolmogorov or non-Kolmogorov energy spectrum, our goal is to emphasize the effect of gravity on inertial particle clustering using specific ranges of St and Fr .

Chapter 3

Synthetic Kinematic Simulation Model for particle clustering

Kinematic Simulation (KS) is a particular case of synthetic turbulence where the focus is on particle's trajectory at the expense of solving the Navier-Stokes equation. An analytical formula 'synthetic flow' is used for the Eulerian flow field. The simplicity of the KS model excludes some features of real turbulent flow but capture the part of the physics which is required to perform Lagrangian particle tracking. Such is the idea with synthetic turbulence which retains less information than the whole flow, but tries to keep what is paramount for the Lagrangian story.

KS modelling has been successfully employed and validated (Fung *et al.*, 1992; Elliott & Majda, 1996; Malik & Vassilicos, 1999). This kind of simulation is much less computing-time consuming than DNS which is important for the present study where we need to run many cases (about 2000 cases for different perspective up to different eddy turnover time). Each case corresponds to a given flow conditions and particle characteristics (St , Fr) and involves 15625 particles.

With synthetic simulations, one can develop models where turbulence ingredients and complexity can be added step by step helping to understand their respective importance. These synthetic models can be a useful complement to Direct Numerical Simulation. In particular, KS was instrumental in discriminating between the role of Lagrangian and Eulerian correlations for vertical diffusion in stratified and rotating flows (Nicolleau & Yu, 2007). With KS it is also possible to play with the spectral law (Nicolleau & Nowakowski, 2011) and its consequences in terms of particle's dispersion. We also refer to the work of (Malik, 2014*a,b*) for a discussion on how the work on KS can help

to understand the sweeping effect on two-particle dispersion.

KS was first introduced as a way to understand particle dispersion rather than particles clustering and in the last decades most of the attention has turned around its ability to predict Richardson's t^3 . That is

$$\Delta^2(t) \sim t^3 \quad (3.1)$$

where Δ is the average distance between two particles initially separated by Δ_0 . We propose here a work getting back to the main strength of KS. That is to provide a coherent Lagrangian framework where some parameters (e.g. spectra Nicolleau & Nowakowski (2011), waves Nicolleau & Yu (2007); Nicolleau *et al.* (2013)) can be studied in detail posing the basis for a comparison with experiments. Previous work (Ijzermans *et al.*, 2010; Meneguz & Reeks, 2011) particularly supports the use of KS for studying the evolution of the particle cloud in the absence of gravity effect which made the study more about segregation than clustering.

As we are not interested in two-particle dispersion, we limit our study to small Reynolds numbers, more precisely to scale ratio $k_{imax}/k_{imin} = 9^1$.

3.1 Periodic KS method for isotropic turbulence

In Kinematic Simulation the underlying Eulerian velocity field is generated as a sum of random incompressible Fourier modes with a prescribed energy spectrum $E(k)$. For most part of study, spectrum is limited to a Kolmogorov type spectral law $E(k) \sim k^{-5/3}$ which does not have delta-correlation in time at any level. The velocity field is a continuous function of space and time and incorporates turbulent-like flow structure, such as eddying, straining and streaming regions similar to those expected and observed in turbulent flow.

In the KS Eulerian velocity field (\mathbf{u}_E) takes the form of a truncated Fourier series, sum of $N_k = N^3$ Fourier modes:

$$\mathbf{u}(\mathbf{x}, \mathbf{t}) = \sum_{i=1}^N \sum_{j=1}^N \sum_{l=1}^N \mathbf{a}_{ijl} \cos(\mathbf{k}_{ijl} \cdot \mathbf{x} + \omega_{ijl} \cdot \mathbf{t}) + \mathbf{b}_{ijl} \sin(\mathbf{k}_{ijl} \cdot \mathbf{x} + \omega_{ijl} \cdot \mathbf{t}) \quad (3.2)$$

where \mathbf{a}_{ijl} and \mathbf{b}_{ijl} are the decomposition coefficients corresponding to the wavevector \mathbf{k}_{ijl} while ω_{ijl} represents the unsteadiness frequency.

¹ $i = 1, 2$ or 3

3.1.1 THE WAVENUMBER DISTRIBUTION:

Unlike the classic KS decomposition (Fung & Vassilicos, 1998; Nicolleau & ElMaihy, 2006), in our study the wavevectors $\mathbf{k}_{ijl} = (k_i, k_j, k_l)$ are implemented arithmetically to enforce a periodic condition for the flow field:

$$k_i = \frac{2\pi}{L_x}(n_i - 1) \quad (3.3)$$

$$k_j = \frac{2\pi}{L_y}(n_j - 1) \quad (3.4)$$

$$k_l = \frac{2\pi}{L_z}(n_l - 1) \quad (3.5)$$

where (n_i, n_j, n_k) are integers satisfying $1 \leq n_i \leq N$. In practice, we choose $(L_x = L_y = L_z)$ for creating an isotropic turbulence and to ensure the flow incompressibility the Fourier coefficient vectors \mathbf{a}_{ijl} and \mathbf{b}_{ijl} are set orthogonal to the wavevector:

$$\mathbf{a}_{ijl} \cdot \mathbf{k}_{ijl} = \mathbf{b}_{ijl} \cdot \mathbf{k}_{ijl} = 0 \quad (3.6)$$

Their magnitude is fixed by the energy spectrum, $E(k)$

$$|\mathbf{a}_{ijl}|^2 = |\mathbf{b}_{ijl}|^2 = 2E(k)\Delta k_{ijl}/m_k \quad (3.7)$$

where m_k is the number of wavevectors of wavenumber $k = \|\mathbf{k}_{ijl}\|$.

3.1.2 ENERGY SPECTRUM:

The fully developed turbulence consists of a large number of different scales. Each scale is associated with a certain kinetic energy; the smallest scale is associated with the maximum wave number and the largest scale is associated with the smallest wave number. The large scale eddies, which receive energy from the mean flow, are unstable and able to break up easily transferring their energy to the smaller eddy. These smaller eddies undergo the same process and transfer their energy to the smallest eddies.

This process is called energy cascade in which the energy is transferred successively to smaller and smaller eddies until it reaches a stable scale. The molecular viscosity takes place in order to be effective in dissipating the kinetic energy. At these small scales the kinetic energy of turbulence is converted into heat. The range between the largest scale, L , and the smallest scale, η , is called the inertial sub-range. The dissipation process of energy can be neglected and this range is characterised by a power law with an exponent of $-5/3$. We use an energy spectrum which does not change with time (non-decaying turbulence).

Nicolleau & Vassilicos (2003) and Khan *et al.* (2003) showed that kinematic simulation

is in a good agreement with experiments for statistics of multi-particle when the Kolmogorov energy spectrum is used as an input. In this study, an energy spectrum has the following form:

$$E(k) = Ak^{-5/3} \text{ for } k_{min} \leq k \leq k_{max} \quad (3.8)$$

where A is a constant. From the spectral law, the rms velocity and the integral length scale can be defined as follows:

$$u_{rms} = \sqrt{\frac{2}{3} \int_{k_{min}}^{k_{max}} E(k) dk} \quad (3.9)$$

$$\mathcal{L} = \frac{3\pi}{4} \frac{\int_{k_{min}}^{k_{max}} k^{-1} E(k) dk}{\int_{k_{min}}^{k_{max}} E(k) dk} \quad (3.10)$$

The Kolmogorov length scale is defined as $\eta = 2\pi/k_{max}$, whereas the largest physical scale is $L = 2\pi/k_{min}$ which determines the inertial range $[\eta, L]$ over which (3.8) is observed. It is worth noting that $\mathcal{L} \simeq L$ for sufficiently large inertial ranges. However, here in contrast to other KS studies the inertial range is small and $L \simeq 5\mathcal{L}$. In this work, non-dimensional numbers (St and Fr) are based on the integral length scale \mathcal{L} and for the sake of comparisons both are reported in Table 3.1. The ratio between the largest length scale and the Kolmogorov length scale is k_{max}/k_{min} and the associated Reynolds number is: $Re_L = (k_{max}/k_{min})^{4/3}$. This is the standard way to define a Reynolds number in KS and a DNS or an experiment yielding the same ratio k_{max}/k_{min} would have a much larger Reynolds number.

3.1.3 UNSTEADINESS FREQUENCY

In its general form the KS field can also be a function of time by introducing the frequency ω_{ijl} that determines the unsteadiness associated with the n^{th} wave mode. The effect of introducing a time-dependence in the Fourier modes will be the objective of the study in chapter 8 and discussed in detail.

3.1.4 CHARACTERISTIC TIME SCALES AND COMPUTING TIME STEP

It is equally important to define the time scales of turbulence. The eddy turn over time scale is related to integral length scale. It is defined as the time taken by an eddy to turn itself around. Mathematically:

$$t_d = L/u_{rms}. \quad (3.11)$$

$$\mathcal{T} = \mathcal{L}/u_{rms}. \quad (3.12)$$

As we use the integral length scale \mathcal{L} for defining the non-dimensional parameters, the eddy turnover time \mathcal{T} is considered throughout the study. Before the eddy turnover time, the particle remembers its initial position, while after this time, the particles are free to move randomly. The Kolmogorov time scale is another important time scale which is defined as the time taken by a fluid particle to move a distance η (Kolmogorov length scale) when its velocity is equal to Kolmogorov velocity u_η and is mathematically expressed as follows:

$$t_\eta = \eta/u_\eta. \quad (3.13)$$

Both characteristic times can be related as follows:

$$t_\eta = \mathcal{T}(\eta/\mathcal{L})^{2/3}. \quad (3.14)$$

The time step, Δt , must be smaller than both the eddy turnover time and the Kolmogorov time scale. According to Fung (1990), a time step equal to 1/10 of the Kolmogorov time scale is enough to ensure that the results are independent of the time step within the statistical errors. All the periodic KS parameters are gathered in table 3.1.

$L_x = L_y = L_z$	1
N	10
N_p	15625
u_{rms}	0.8703
\mathcal{L}	0.2106
L	1
η	0.0642
\mathcal{T}	0.2420
t_d	1.1491
k_i/k_{imin}	9
k_{max}/k_{min}	15.5885
Re_L	38.94

TABLE 3.1. Periodic KS parameters (except modified conditions used in *Chapter 8*)

3.2 Heavy particle equation of motion

In continuation of the brief introduction of forces on immersed objects in *Chapter 2*, we discuss the major types of forces acting on the spherical particles moving in a fluid.

The selection of the equation of motion for inertial particles is still the subject of much interest in current research. It could consist of all the forces acting on the particle and these forces are of following types:

- The non-uniform distribution of the flow field around the particle causes lift force,
- The relative motion between the particle and the surrounding fluid elements produces the drag force,
- Force of gravity,
- Buoyant force,
- force due to the unsteadiness in flow.

3.2.1 FORCES ACTING ON HEAVY PARTICLE

Let us consider a heavy particle with mass m_p centrally positioned \mathbf{x} at time t , it moves with a velocity $\mathbf{V}(t)$ in a flow of velocity $\mathbf{u}(\mathbf{x}, t)$. The equation of motion can be introduced in a fixed frame of reference originated from the centre of the particle as derived by Maxey & Riley (1983) and it is expressed as follows:

$$m_p \frac{d\mathbf{V}}{dt} = \sum \mathbf{F}_{acting}. \quad (3.15)$$

The drag force:

The drag force can be defined as the resistance to the movement of the heavy particle in turbulent flow. As a result it is opposite to the flow direction and can be calculated from the relative velocity of the particle and the surrounding fluid as follows:

$$F_D = -\frac{1}{2}\pi a^2 C_D \rho_f \mathbf{V}_{rel}^2, \quad (3.16)$$

$$F_D = -\frac{1}{2}\pi a^2 C_D \rho_f (\mathbf{V} - \mathbf{u})^2, \quad (3.17)$$

where C_D is the drag coefficient and depends on the particle Reynolds number, Re_p , based on the particle diameter. The Stoke drag coefficient for a spherical particle, in which the drag is assumed to be linear given that the particle Reynolds number is to be less than unity $Re_p \ll 1$, is:

$$C_D = \frac{24}{Re_p} = \frac{24\mu}{\rho_f |\mathbf{V}_{rel}| A} = \frac{24\mu}{2\rho_f |\mathbf{V} - \mathbf{u}| a}, \quad (3.18)$$

where μ is fluid dynamic viscosity and A is the diameter of the spherical particle. Then by substituting the equation 3.18 in the equation 3.17:

$$F_D = -6\pi a\mu(\mathbf{V} - \mathbf{u}). \quad (3.19)$$

The Stokes drag can be revised to include both non-linear drag and the Faxén effect. The later effect is due to the curvature in the velocity profile (second- order gradients of the velocity field) by replacing in the relative velocity component $(\mathbf{V} - \mathbf{u})$ in equation 3.19 with the following to include such that effect:

$$\mathbf{V} - \mathbf{u} - \left(\frac{a^2}{6}\right)\nabla^2\mathbf{u}. \quad (3.20)$$

So the drag force can be revised to be as follows:

$$F_D = -6\pi a\mu\left(\mathbf{V} - \mathbf{u} - \left(\frac{a^2}{6}\right)\nabla^2\mathbf{u}\right). \quad (3.21)$$

Basset history force:

The friction effect in a viscous fluid flow in the transient state is known as the Basset history force. This effect results from the diffusion of vorticity from the particle as the particle is moving unsteadily. The past acceleration is included in this effect weighted with $(t - \tau)^{1/2}$, where $(t - \tau)$ is the time lag from the past acceleration. It can be written in the form (Maxey & Riley, 1983):

$$F_s = -6\pi a^2\mu \int_0^t \left(\frac{d\mathbf{H}}{d\tau}[\pi\nu(t - \tau)]^{-1/2}\right)d\tau, \quad (3.22)$$

where ν is the fluid kinematic viscosity and the term $H(t)$ is represented as follows:

$$\mathbf{H}(t) = \mathbf{V}(t) - \mathbf{u}(\mathbf{x}_p(t), t) - \frac{a^2}{6}\nabla^2\mathbf{u}. \quad (3.23)$$

3.2.2 ADVANCEMENTS IN EQUATION OF MOTION

Basset (1888); Boussinesq (1903); Oseen (1927) are among those early researchers who examined the motion of a sphere settling in a fluid under the effect of gravity that was otherwise at rest. The disturbance in the flow as a result of sphere motion was assumed to be at sufficiently low Reynolds number. The forces acted by the fluid on the sphere could be calculated as the results of unsteady Stokes flow. In actual, the flow near the particle was split into two parts: the original fluid flow without the particle and the particle affected flow. After calculating the forces separately for both parts, they were summed up.

Since Tchen (1947), who first proposed an equation for the motion of a rigid sphere in a non-uniform flow, several studies have been established either to correct or modify the terms in his equation. His assumption (the Eulerian velocity at the particle location is the same as the fluid velocity along a fluid element trajectory) provided the first approximate solution. This assumption required that both drift velocity and inertia of the particle set

to be small.

Tchen (1947) extended his work first to a sphere settling under gravity in an unsteady uniform flow. Later, it is further extended to an unsteady and non-uniform flow with a view to apply it in different situations. He stated that it becomes necessary to introduce an extra pressure term representing an extra force due to the fluid acceleration.

Corrsin & Lumley (1956) addressed some of the inconsistencies in Tchen's equation. They highlighted the role of the pressure gradient of the basic flow contributing also to the net fluid force on the particle. They proposed a new equation, appears to be non-linear with respect to velocities, for a small rigid sphere of radius 'a' and mass m_p instantaneously centred at $x(t)$ and moving with velocity $V_p(t)$ as follows:

$$\sum \mathbf{F}_{acting} = (m_p - m_f)\mathbf{g} + \frac{3}{2}m_f \frac{D\mathbf{u}}{Dt} - 6\pi a^2 \mu \int_0^t \left(\frac{d\mathbf{H}}{d\tau} [\pi v(t - \tau)]^{-1/2}\right) d\tau. \quad (3.24)$$

The terms on the right-hand-side of equation 3.24 are corresponding to the effects of the pressure gradient of the undisturbed flow, added mass, viscous Stokes drag, Basset history term and the buoyancy force. The fluid acceleration as observed at the instantaneous center of the sphere is:

$$\frac{D\mathbf{u}_i}{Dt} \Big|_{\mathbf{x}_p(t)} = \left[\frac{\partial \mathbf{u}_i}{\partial t} + \mathbf{u}_j \frac{\partial \mathbf{u}_i}{\partial x_j} \right]_{\mathbf{x}=\mathbf{x}_p(t)}. \quad (3.25)$$

The pressure gradient term was written in the following form on the assumption that the flow is incompressible:

$$\frac{D\mathbf{u}_i}{Dt} = \frac{-1}{\rho} \frac{\partial p}{\partial x_i} + \mathbf{g}_i + \nu \nabla^2 \mathbf{u}_i. \quad (3.26)$$

The equation 3.26 is not consistent. In fact, the effect of pressure gradient on the undisturbed flow has not been considered which may affect the particle motion as the result of a viscous shear stress.

Buevich (1966) derived a new equation of motion by changing the frame of referencing of the Basset-Boussinesq-Oseen to a coordinate system moving with the particle. He concluded that the second term in the equation 3.24 should be replaced by a term

$$m_f \frac{d\mathbf{u}_i}{dt}. \quad (3.27)$$

Riley (1971) used a similar analysis and concluded that the term describing the effect of the pressure gradient in the flow field should be

$$m_f \frac{D\mathbf{u}_i}{Dt} \Big|_{\mathbf{x}_p(t)}. \quad (3.28)$$

This result is more physically realistic for small sphere because the effect of the undisturbed fluid stress (both from the pressure and viscosity) is to produce the same net force as would act on the fluid sphere of the same size. This force must equal to the product of the fluid mass and the local acceleration of the fluid which opposes the equation described by Buevich (1966).

Maxey & Riley (1983) studied the problem of disturbed flow around a rigid Stokes sphere in non-uniform undisturbed flow. They derived an equation of motion for the sphere following the approach of Riley (1971). This equation differs from the previous versions as the velocity gradient is introduced, known as Faxén correction (second-order gradients of the velocity). This leads to modifications of the added mass terms, the Stokes drag and the Basset history term due to the curvature in the velocity profile. While in low Reynolds number limit there is no force due to shear or particle spin besides the difference in the form of the fluid acceleration term.

The equation proposed by Maxey & Riley (1983) is the most recent full derivation of the equation of motion for a sphere particle in a non-uniform unsteady flow with the particle starting at rest relative to the fluid. Wang & Maxey (1993) used equation of motion without the limitation of the initial velocity of the heavy particle to be equal to that of the fluid. The equation of motion for a sphere heavy particle can be written as the following:

$$m_p \frac{d\mathbf{V}_p}{dt} = m_f \frac{D\mathbf{u}}{Dt} \Big|_{\mathbf{x}_p(t)} - \frac{1}{2} m_f \frac{d}{dt} \{ \mathbf{V}_p(t) - \mathbf{u}(\mathbf{X}_p(t), t) - \frac{1}{10} a^2 \nabla^2 \mathbf{u} \Big|_{\mathbf{x}_p(t)} \} - 6\pi a \mu \mathbf{H}(t) + (m_p - m_f) \mathbf{g} - 6\pi a^2 \mu \int_0^t \left\{ \frac{d\mathbf{H}(\tau)}{d\tau} [\pi \nu (t - \tau)]^{-1/2} \right\} d\tau. \quad (3.29)$$

where the first term represents the force exerted by the undisturbed fluid on the particle. The second term is accounted for the added-mass effect which is defined as the mass added to the particle when it moves relative to the fluid. The third term describes Stokes drag due the fluid's viscosity while the fourth represents the drag created by the force of buoyancy. The last right-hand-side term of the equation 3.29 is the Basset Boussinesq history term (discussed in previous section). It should be also noticed that the Faxén correction is also included in the terms except the first term.

3.2.3 ASSUMPTIONS AND MODIFIED EQUATION

In our case, the motion of heavy spherical particles is studied in a uniform homogeneous isotropic turbulence. The flow has a constant mean velocity taken to be zero. To consider the Lagrangian tracking, the following assumptions are applied to simplify the equation

of motion of the heavy particle in turbulent flow studied:

- (1). The radius of the particle sphere is small enough such that $Re_p \ll 1$ to consider linear drag force on the inertial particle. It means that we can apply equation 3.29 as it is valid for small particles at low Reynolds number and Faxén correction can be neglected.
- (2). The inertial particles are much heavier than the fluid particles i.e $\rho_p \gg \rho_f$. Using this assumption, the added mass and the Basset history terms can be ignored.
- (3). It is also assumed that there is no initial relative velocity of the particle with respect to fluid velocity. With this assumption, we can exclude the last term of the equation 3.29.
- (4). The radius of the particle (a) is assumed to be smaller than the Kolmogorov length scale of turbulence (η). So, the particle can respond to all the scales without affecting the turbulence.
- (5). The radius of particle is considered to be large enough as compared to fluid molecules free path. The particle aerodynamic response time is much longer than the mean molecular collision time. So, the effect of Brownian motion can be ignored.
- (6). The particle concentration in a flow must be dilute enough to ensure that the interaction between the particles could be ignored and also to avoid the modification in flow structure.
- (7). The relative fluid approaching the particle is assumed to be uniform such that no lift force is present.

Simplified equation of motion:

After applying the assumptions 1-3, the equation of motion of heavy particle derived by Maxey & Riley (1983); Gatignol (1983) can be simplified to achieve our goal and it reduces the computing time with less cost. It is considered to be done in a fixed frame of reference as follows:

$$m_p \frac{d\mathbf{V}_p}{dt} = m_p \mathbf{g} - 6\pi a \mu (\mathbf{V}_p(t) - \mathbf{u}(\mathbf{x}_p(t), t)), \quad (3.30)$$

where m_p is the mass of the particle, \mathbf{g} the gravity, a the spherical particle's radius and μ the dynamic viscosity of the fluid. Another form of the equation 3.30 is:

$$\frac{d\mathbf{V}_p}{dt} = \frac{\mathbf{u}(\mathbf{x}_p(t), t) - \mathbf{V}_p(t) + \mathbf{V}_d}{\tau_a}, \quad (3.31)$$

where $\tau_a = m_p/6\pi a\mu$ is the particle's aerodynamic response time and $\mathbf{V}_d = \tau_a \mathbf{g}$ the particle's terminal fall velocity or drift velocity.

3.3 Computing trajectory of particle using KS

The particles are initially homogeneously distributed as shown in Fig. 3.1a and whenever a particle leaves the turbulence box domain (e.g. $\mathbf{x}_1 > L_x$), then it is re-injected from the opposite side as shown in Fig. 3.1b to keep the periodic condition.

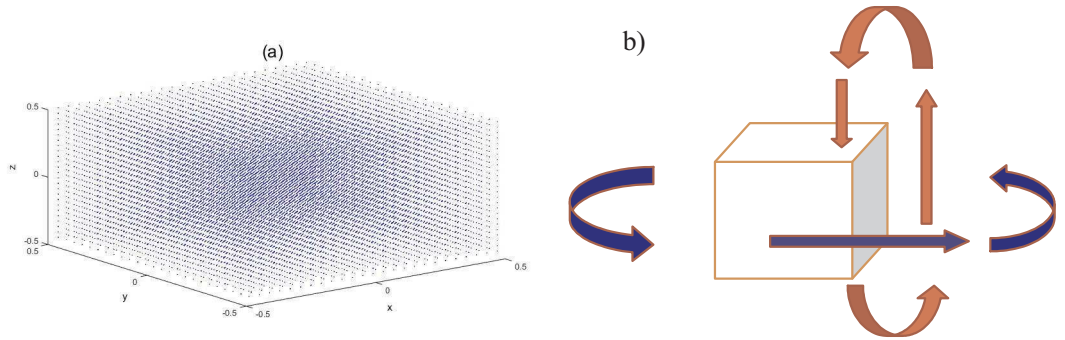


Figure 3.1. Particles' (a) initial distribution and (b) re-injection

Using KS, the computational task reduces to calculate the trajectory of each particle placed in the turbulent field initially at \mathbf{X}_0 . Each trajectory is, for a given initial condition, solution of the differential equation set:

$$\frac{d\mathbf{X}}{dt} = \mathbf{V}(t), \quad (3.32)$$

$$\frac{d\mathbf{V}}{dt} = \mathfrak{F}(\mathbf{u}_E(\mathbf{X}, t), \mathbf{V}, t), \quad (3.33)$$

where $\mathbf{X}(t)$ is the particle's position, $\mathbf{V}(t)$ its Lagrangian velocity and \mathbf{u}_E the analytical Eulerian velocity used in KS. \mathfrak{F} is a function relating the Lagrangian acceleration to the Eulerian and Lagrangian velocities. The flow charts of the KS model used for studying the particle clustering are illustrated in Fig. 4.2.

3.4 Non-dimensional parameters

Three non-dimensional parameters are introduced to make qualitative and quantitative analyses of the particle clustering.

- (a). The Stokes number expresses the ratio between the particle's response time (inertia effect) and the turbulence characteristic time

$$St = \tau_a u_{rms} / \mathcal{L}. \quad (3.34)$$

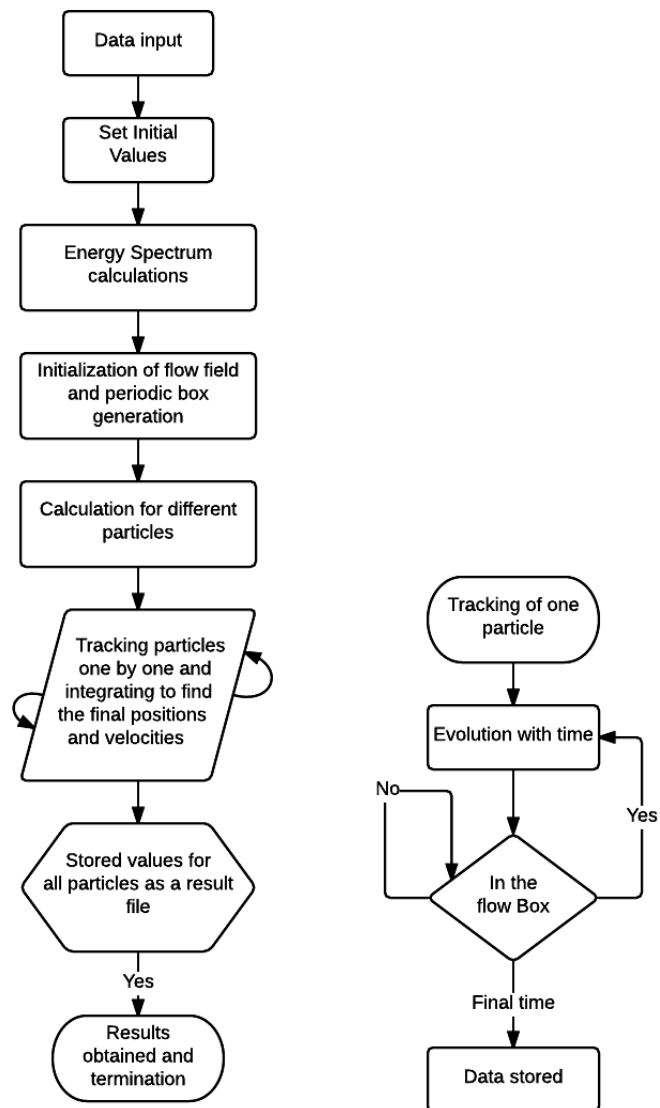


Figure 3.2. (left) Flow chart of the Modified FORTRAN code for kinematic simulation model of the particle laden clustering (right) Part of code showing re-injection of the particles

It is relative of the particle inertia. In the limiting case $St \rightarrow 0$; the particles recover the motion of the fluid tracers; whereas for $St \rightarrow \infty$, the particles are less affected by the fluid.

- (b). The Froude number is the ratio between inertial forces and gravitational forces.

$$Fr = u_{rms}/\sqrt{g\mathcal{L}}. \quad (3.35)$$

In our study the rms velocity u_{rms} and inertial length scale are constant and g is varied.

- (c). The Drift parameter is the ratio between the particle's drift velocity and the turbulence rms velocity:

$$\gamma = V_d/u_{rms}. \quad (3.36)$$

The Drift parameter can still be defined without gravity. Then γ can be considered as measuring the effect of a mean velocity V_d .

If V_d is caused by gravity, then

$$\gamma = \tau_a g/u_{rms}. \quad (3.37)$$

In this case the drift parameter is affected by both the gravity and the particle's inertia. γ can be expressed as a function of Stokes and Froude numbers so for a given turbulence the case corresponding to a constant gravity, that is varying τ_a only, is given by

$$Fr = \text{constant} \quad (3.38)$$

$$\gamma \sim St \quad (3.39)$$

In this work, all the three non-dimensional parameters (defined by 3.34-3.36) are used for initial quantification in *Chapter 4 and 5*, but we only emphasize on St and Fr for the most part of the thesis.

Chapter 4

Visualisations of particle clustering in Kinematic Simulation

4.1 Introduction

We analyse the clustering of inertial particles using a periodic kinematic simulation. Practically, the shape of clustering pattern depends on flow conditions and particle characteristics. In the KS model, the flow conditions are kept constant and the particle characteristics can be changed by varying the inertial and gravity effects to observe the variation in clustering. We use Stokes number St as the main non-dimensional number to control the inertial effect of the particles, while Froude number Fr and drift parameter γ are used to define the role of gravity on clustering. In order to identify and characterise the particle clustering in turbulent flow on the basis of non-dimensional numbers, many qualitative and quantitative methods have been employed. In this Chapter, we only discuss the qualitative visualisations of clustering patterns evolved as the results of particles' motion in flow. The corresponding quantitative analysis will be presented in the next chapter.

To observe the clustering variations, particles are initially uniformly distributed in the Kinematic simulation flow. Though there is no particular difficulty in considering particles with different inertia in Kinematic Simulation, this study is limited to mono-dispersed seeding, i.e. particles having the same inertia for each case. Furthermore, the particles are considered small enough so that they neither affect the flow nor interact with each other (one-way coupling). The particle ($N_p = 25^3$) grid distribution is shown in Fig. 4.1 and the values of St and Fr are randomly selected to see the evolution of

the particles. It is clearly observed that the particles gather and produce some low and high concentration regions as St and Fr are varied. For some pairs of (St, Fr) , a strong attractor hereinafter referred to as a Lagrangian attractor appears in the KS.

The topological dimension of the Lagrangian attractor is varied from one-dimensional to two-dimensional or three-dimensional with varying values of St and Fr . The range of Stokes number St and Froude number Fr can be selected depending on the objective of the study. In the literature, the value of St is chosen from 0 to 10 while Fr is selected ranging $[0, \infty]$. In our study, we particularly focus on Stokes number ranging $0 \leq St \leq 1$ and the Froude number Fr is ranged as $0.3 < Fr < 1.4$.

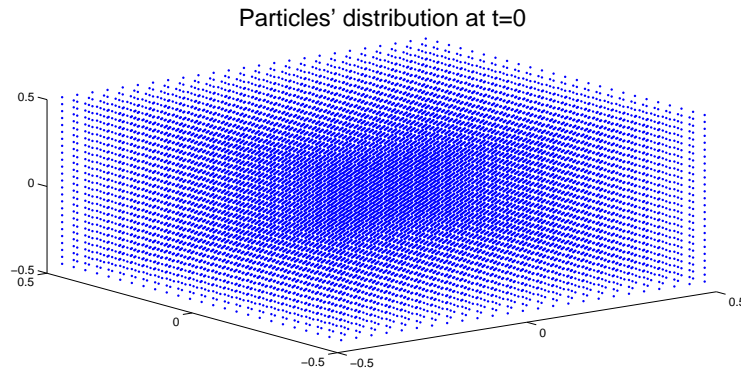


Figure 4.1. Initial distribution of particles in the period box

4.1.1 TIME DEPENDENCY OF EVOLUTION

Initially uniformly positioned particles are monitored as a function of time in the flow and a Lagrangian attractor is observed in some cases depending on St and Fr . That is, the initially uniformly distributed cloud of particles will end in a set of loci that does not evolve any further. The particles move within that set of loci which defines the structure of the Lagrangian attractor and its dependence on St and Fr numbers is studied here. For short times the attractor shape is time-dependent as shown in Figs 4.2 and Fig. 4.3. The time evolution of the cluster depends on the non-dimensional parameters St and Fr as illustrated in Fig. 4.2 where it takes 4 times longer to reach the one-dimensional Lagrangian attractor than in the case of Fig. 4.3. We do not intend to investigate the temporal evolution of attractor in this chapter and are only interested in attractor's asymptotic form (i.e. for $t \rightarrow \infty$).

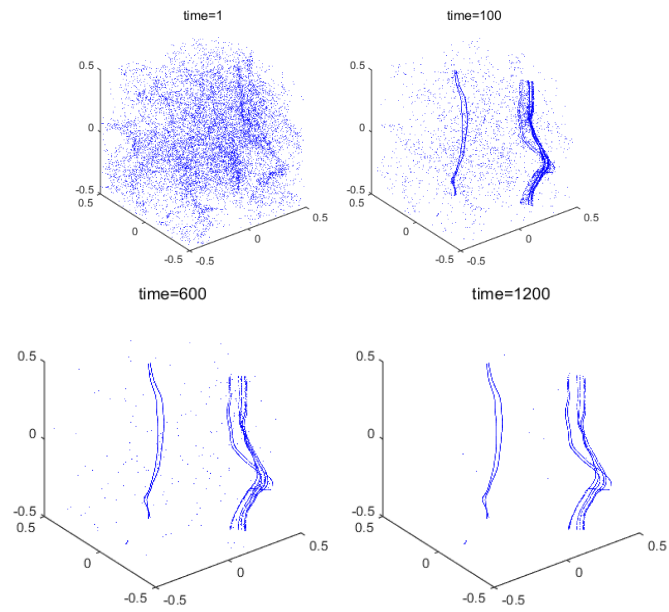


Figure 4.2. Time evolution of inertial particles with $St = 0.167$ and $\gamma = 0.689$

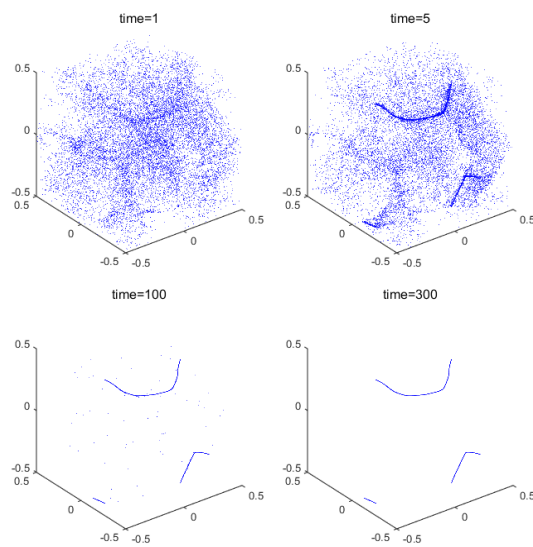


Figure 4.3. Time evolution of inertial particles with $St = 0.413$ and $\gamma = 0.575$

4.1.2 VISUALISATION OF PARTICLE CLUSTERING

Visualisation is one of the methods used to identify the particle clustering for varying flow conditions and particle characteristics. Though these types of measures are very limited to use in experimental set up, they have been successfully implemented to capture the clustering variations in many of the simulations such as DNS, LES, Stochastic models, synthetic models, etc. Whether it is a two-dimensional simulation or three-dimensional, visualisation can provide the initial idea on how particles are moving in the flow. Normally, researchers consider the visualisation to start clustering analysis before applying the detailed quantitative measures. Chen *et al.* (2006) used visualisation to identify the self-similar clustering of inertial particles and zero-acceleration points in fully developed two-dimensional DNS. Similarly, Goto & Vassilicos (2006) showed the particle distributions in two-dimensional DNS turbulence to see the clustering with varying values of St .

In addition to 2D simulations, visualisation has also been used as the qualitative measures in a three-dimensional simulations. Beside the fact that three-dimensional flows are more complex than two-dimensional flows in order to detect the particle clustering, visualisation can still be considered as a successful tool to initiate the clustering analysis. Using three-dimensional DNS, Yoshimoto & Goto (2007) have shown a series of pictures as shown in Fig. 4.4 to see the spatial distribution of inertial particles in the flow. Similar kinds of visuals are also described in 3D DNS by Bec *et al.* (2007) as shown in Fig. 4.5. From Fig. 4.5, it is clear that fluctuation in the particle spatial distribution extends to scales far inside the inertial range. Moreover, the large eddy simulation LES (Jin *et al.*, 2010) and the Stochastic models (Bec, 2005) also used visualisation to observe the particle distribution in flow. Whatever are the methods of simulation, there are following common observations:

- Inertial particles tend to accumulate in the preferential regions of flow by increasing Stokes number St .
- The particle clustering is not noticeable for any value of Stokes number when $St \rightarrow 0$ and $St \rightarrow \infty$.

Furthermore, the clustering patterns have also been visualised by considering additional external forces on inertial particles like gravitational force, Basset history force, added mass term, etc. Usually, the effect of gravity has been ignored by most of the researchers to avoid complexity of simulation and hence; to reduce the computing time, but the effect of gravity can entirely change the particle clustering for a given St . Woittiez &

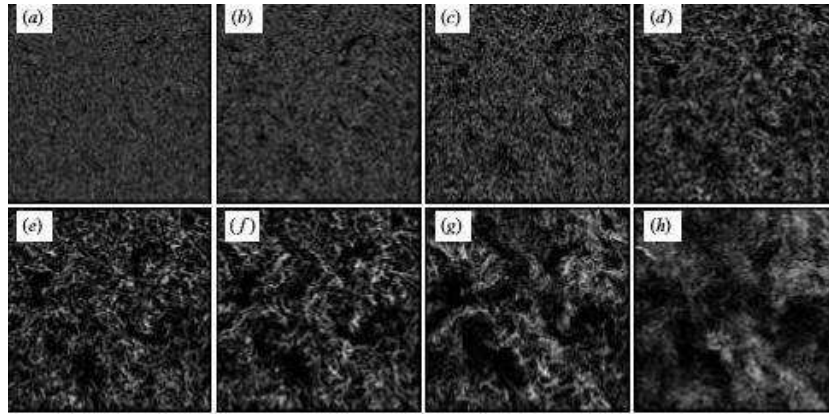


Figure 4.4. Spatial distribution of inertial particles for eight different values of St_η in a thin layer (width 5η) (a) 0.05, (b) 0.1, (c) 0.2, (d) 0.5, (e) 1, (f) 2, (g) 5 and (h) 10.

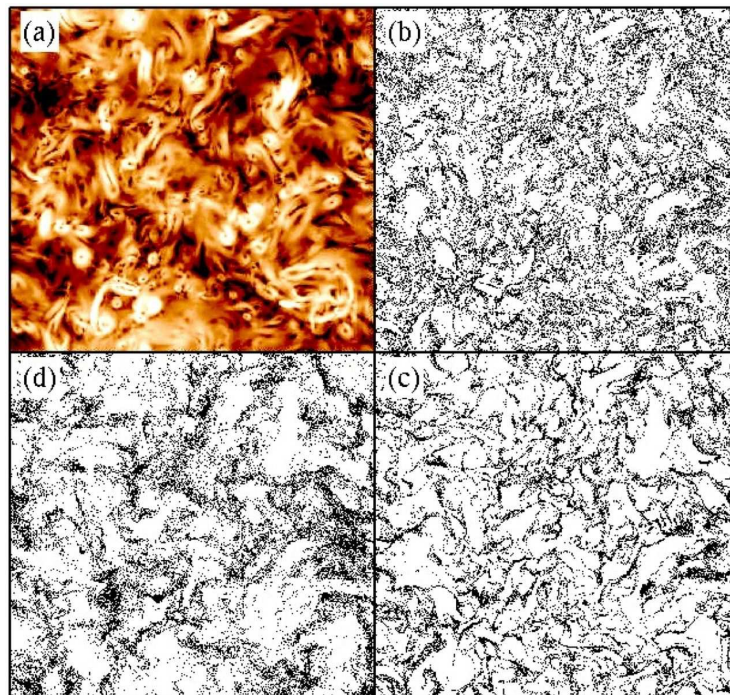


Figure 4.5. (a) The modulus of the pressure gradient, giving the main contribution to fluid acceleration, on a slice $512 \times 512 \times 4$. B/W code low and high intensity, respectively. Particle positions in the same slice are shown for (b) $St_\eta = 0.16$, (c) 0.80 and (d) 3.30. Note the presence of voids with sizes much larger than the dissipative scale.

Portela (2008) investigated the clustering by considering both mono-dispersed and poly-dispersed particles in the presence of gravity. They observed the curtain-like manifolds as shown in Fig. 4.6 which do not appear without gravity. Similar kinds of vertical stripe patterns are also found by Park & Lee (2014) and Bec *et al.* (2014). This new type of two-dimensional cluster shows the significance of gravity on inertial particle clustering. Recently, Olivieri *et al.* (2014) analysed clustering of inertial particles in the presence of Basset history force. They visualised snapshots of the clustering to sight the reduction in clustering using Basset history term. In fact, visualisation is the simplest method to estimate the variations in clustering and set proceedings for quantitative analysis.

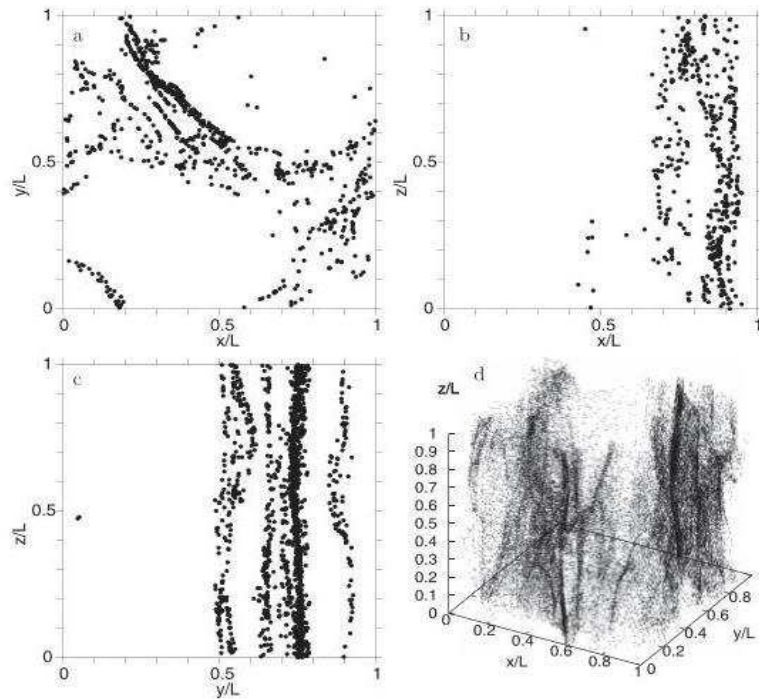


Figure 4.6. (a) – (c) Two-dimensional and (d) three-dimensional snapshots of a droplet concentration field that is driven by both gravity and turbulence. The slice thickness in (a) – (c) is one grid box. The snapshots show the curtain-like manifolds of sediment droplets waving in the turbulent field.

We make a qualitative analysis in the steady KS flow and the study is classified into two parts for different ranges of Stokes number. The main focus is on the Stokes number ranged from $0 \leq St \leq 1$ (discussed in § 4.2) as we found the clearest variations in the Lagrangian attractor within this range. We also run a few cases for particles with $St > 1$ to determine the clustering patterns (discussed in § 4.3). All the cases are run for a sufficient time of evolution to see the definite patterns of clustering. As some new types of clustering structures are found in the KS and it is very important to categorically define them in relation to non-dimensional the parameters St and Fr or γ . Therefore, we describe the Lagrangian structure in detail in the following section.

4.2 Visualisations of particle clustering for $St \leq 1$

Before applying the Stokes number St to the particles, we look into the variations in clustering for the particles with $St = 0$, i.e. the fluid tracers. These fluid tracers behave differently from the inertial particles in turbulent flow and the evolution of the fluid tracers is examined to differentiate the clustering inertial particle motion in the flow. In Fig. 4.7a, it can be clearly noticed that there is no significant variation in fluid tracer accumulation even at a longer time of evolution $t = 100s$. The effect of gravity is also introduced to see whether there is any of inhomogeneity under action of drift but still no clear variation is observed as shown in Fig. 4.7b. So, the particles with $St = 0$ follow the flow structures and do not show any significant clustering.

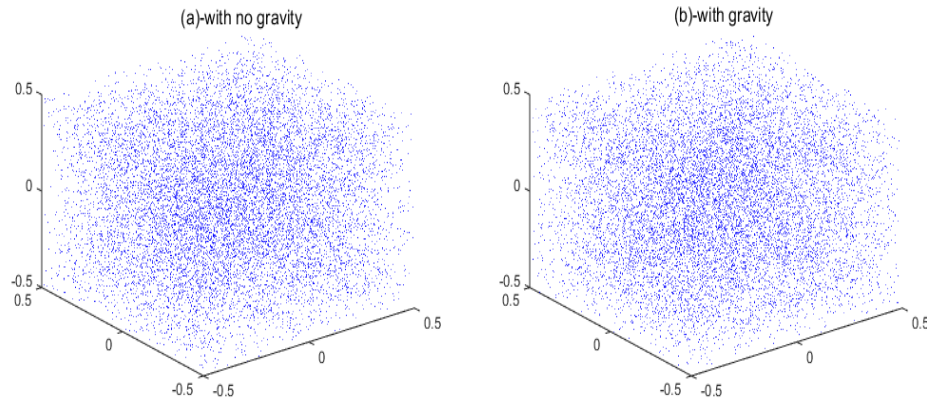


Figure 4.7. Evolution of tracers in the flow field at $t=100s$ (a). without gravity and (b). with gravity

We now study the clustering by applying different values St to the particles in the presence of gravity (Fr). The random selection of St and Fr showed the different shapes of Lagrangian attractor whose dimensions are varied from 1D to 3D. It is rather difficult to establish a relationship between the attractor patterns and non-dimensional parameters. So, the study is organised for different values of St , Fr and/or γ and we choose the different pairs of St and γ to observe the clustering variations. Three different values of Stokes numbers are picked namely 0.167, 0.413, 0.827. Each St case is run with varying values of drift parameter ranging $0 \leq \gamma \leq 1$ till the uniform distribution of particles converts into an asymptotic Lagrangian attractor. We found that the dimensionality of a Lagrangian attractor depends on both St and γ and the stronger clustering is observed for the lower values of St . Such as, different types of one-dimensional Lagrangian attractors are observed for $St=0.167$ as shown in Fig. 4.8.

On the basis of the final shapes of the attractors, the Lagrangian attractors are classified and we use following nomenclature;

- i) 1D-H : horizontal one-dimensional Lagrangian attractor as in Fig. 4.8a.

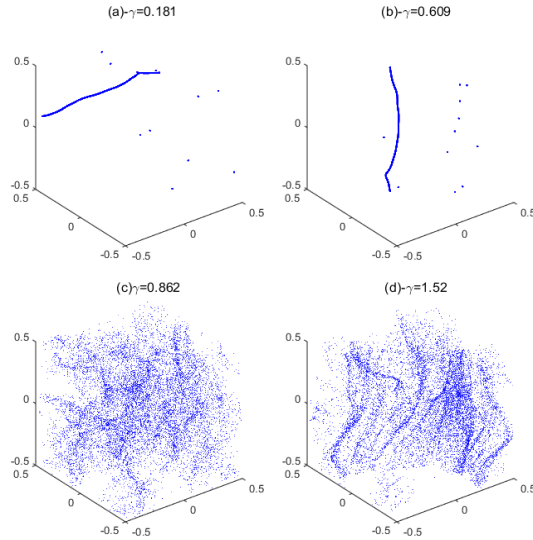


Figure 4.8. Attractors for $St = 0.167$ with increasing γ run at different times.

- ii) 1D-V : vertical one-dimensional Lagrangian attractor as in Fig. 4.8b.
- iii) 1D-HV : Intermediate one-dimensional Lagrangian attractor as in Fig. 4.3.
- iv) 2D-L : two-dimensional vertical curtain-like layer as in Fig. 4.8d,
- v) 3D : any three-dimensional structure without any particular structure in the cloud as in Fig. 4.8c.

The qualitative results are split into three different categories which can take into account the effect of gravity and/or inertia:

- i) keeping St constant §4.2.1.
- ii) keeping Fr constant §4.2.2.
- iii) keeping γ constant §4.2.3.

4.2.1 VARIATION IN CLUSTERING IN RELATION TO St

In this sections, the variation in the clustering is analysed by fixing the St and varying the Fr . The effectiveness of the gravity for a St is evident with different clustering patterns. An adequate classification of St is adopted for a given range of Fr listed in Table 4.1 and we run each case for an arbitrary time of $t = 300s$ to track Lagrangian attractors. As these Lagrangian attractors are never found in the past studies, therefore, it is important to discuss them in detail. We detect the different clustering patterns according to set

nomenclature and marked them in the last column in the Table 4.1 (ticked after detailed visualisations).

Case	St range	Fr range	observed patterns			
			1D-H	1D-V	2D-L	3D
A	0.0-0.2	0.42-1.34	✓			✓
B	0.2-0.4	0.42-1.34	✓	✓		✓
C	0.4-0.5	0.42-1.34		✓	✓	✓
D	0.5-1.0	0.42-1.34			✓	✓

TABLE 4.1. Different cases for studying the attractor topology for different ranges of St .

Clustering patterns for range $0 \leq St \leq 0.2$:

As the flow conditions are constant, the particles are likely to be trapped in the preferential localised regions and as a result, the accumulation of particles can be in a horizontal or vertical direction. For the St values closer to 0, case A, the particle relaxation time is much less than the flow integral time scale and no significant clustering is observed as shown in Fig. 4.9.

When St is slightly increased, the relatively heavier particles depart from the initial grid positions and start clustering with decreasing values of Fr (increasing gravity) as shown in Fig. 4.10. The particles coagulate and one-dimensional attractors are observed for some particular values of Fr . For a higher value of Fr , a 1D-H attractor is visualised as shown in Fig. 4.10a. Further decreases in the Froude number Fr destroys the one-dimensional structure and particles redistribute evenly in the flow as 3D structure as shown in Fig. 4.10d. It means the high gravitational force pulls the particles out of that one-dimensional space of the attractor.

Clustering patterns for range $0.2 < St \leq 0.4$:

In continuation to previous range, the Stokes number is further increased to examine the Lagrangian attractors. The range of $0.2 \leq St \leq 0.4$ is found to be the most difficult to analyse as all types of attractors are observed within this range. We found that the 1D-H attractor still appears with the decreasing values of Fr . Rather than having only 1D-H attractor, a 1D-V attractor is also discovered for this range of St . For low value of Stokes number ($St = 0.249$), case B, a 1D-H is observed at high Fr as shown in Fig. 4.11a which converts into a 1D-V attractor as the Fr is further decreased as shown in Fig. 4.11b. Further increases in the gravity eradicate the one-dimensional attractor

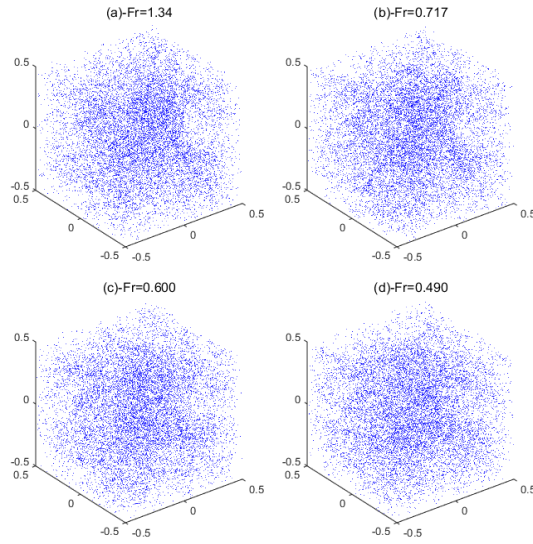


Figure 4.9. Clustering variations at $St = 0.041$ for decreasing value of Fr (increasing gravity) and $t = 300s$

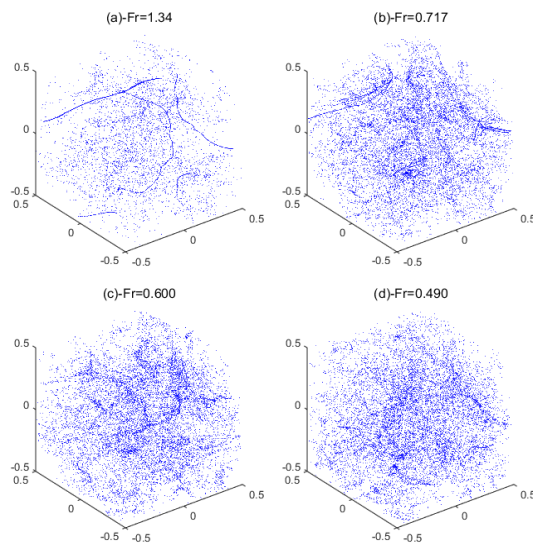


Figure 4.10. Clustering variations at $St = 0.124$ for decreasing value of Fr and $t = 300s$

and the particles rearrange themselves as the 3D attractors as seen in Figs. 4.11c and d.

Progressively, for $St = 0.331$, the 1D-H attractor is no longer observed and a 1D-HV attractor starts appearing as shown Fig. 4.12b. This 1D-HV attractor restructures into a 1D-V attractor with decreasing values of Fr as shown in Fig. 4.12c. Ultimately, these one-dimensional attractors transform into two-dimensional 2D-L patterns for very low values of Froude number such as $Fr = 0.49$ as shown in Fig. 4.12d. The two-dimensional structures confirm that the particles do not move randomly with the flow and are forced to move on the planar structures in the direction of gravity. This shows the dominance of gravity over turbulence structure and we can say that the gravity starts playing a more important role on the particle clustering after a particular St range. The last important

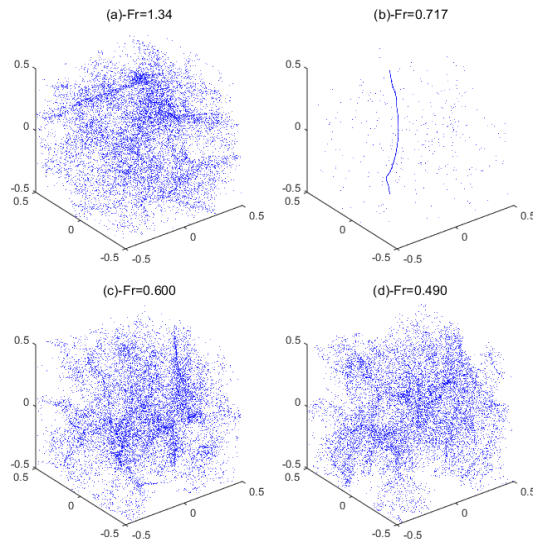


Figure 4.11. Clustering variations at $St = 0.249$ for decreasing value of Fr and $t = 300s$

noticeable feature for this range of St is appearance of a 1D-V attractor for a high value of Fr as illustrated in Fig. 4.13a. This 1D attractor does not stay longer with the further increases in gravity and reproduces as the 2D-L pattern at $Fr = 0.49$ as shown in Fig. 4.13c,d. Overall, we can state that the clustering stretch in the direction of gravity either in the form of 1D-V attractor or 2D-L attractor depending on value of St .

Clustering patterns for range $0.4 < St \leq 0.5$:

The particles with the relaxation time almost half of the integral time scale, case C, do not converge into the 1D-H or 1D-V structures, but still a 1D-HV attractor is observed as shown in Fig. 4.14b for $St = 0.413$. When Froude number Fr is reduced, the 1D-HV attractor reshuffles into a 2D-L structure as shown in Fig. 4.14d. A similar kind of 1D-HV attractor can also be seen in Fig. 4.15a for $St = 0.456$. The difference in both cases

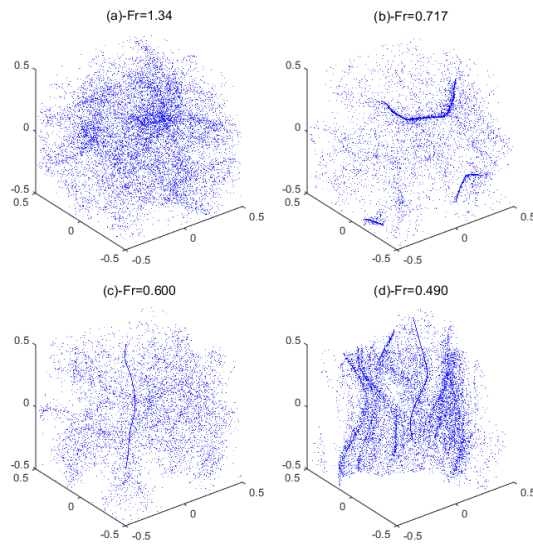


Figure 4.12. Clustering variations at $St = 0.331$ for decreasing value of Fr and $t = 300s$

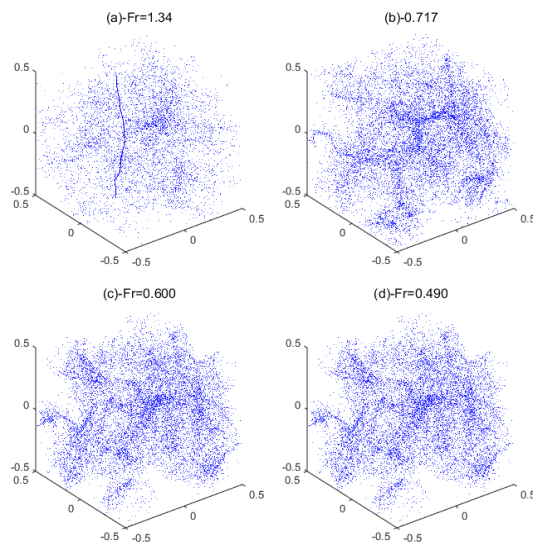


Figure 4.13. Clustering variations at $St = 0.373$ for decreasing value of Fr and $t = 300s$

is the value of Fr at which the attractor appears, i.e. less gravity is required for higher value of Stokes number $St = 0.456$ than that of $St = 0.413$.

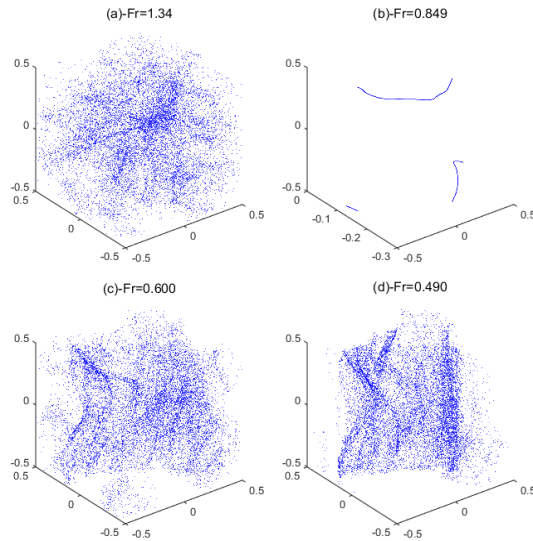


Figure 4.14. Clustering variations at $St = 0.413$ for decreasing value of Fr and $t = 300s$

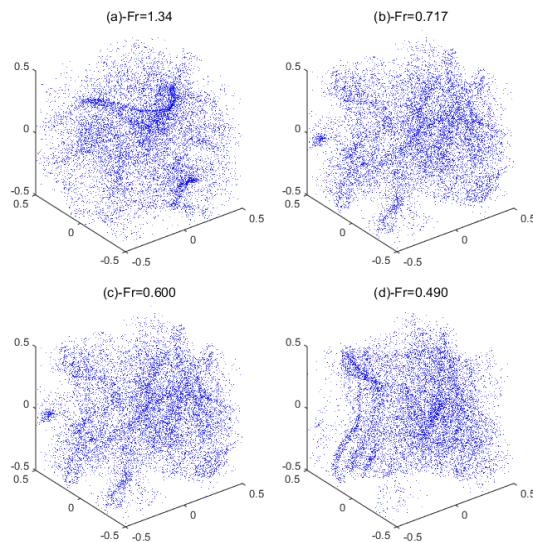


Figure 4.15. Clustering variations at $St = 0.456$ for decreasing value of Fr and $t = 300s$

Clustering patterns for range $0.5 < St \leq 1.0$:

The one-dimensional Lagrangian attractors are the indicators of strong clustering and we do not observe any of them for $St > 0.5$. For this range of St , case D, the particles settle predominantly as the 2D-L attractors at relatively higher values of Fr as shown in Fig. 4.16b and Fig. 4.17b. There is also notable variations in clustering within the

2D-L attractors as the Fr is decreased but the overall shape remains same as shown in Fig. 4.16c,d and Fig. 4.17c,d. This type of 2D layered clustering pattern shows that gravity holds the particles together on the attractor for a specific value of St .

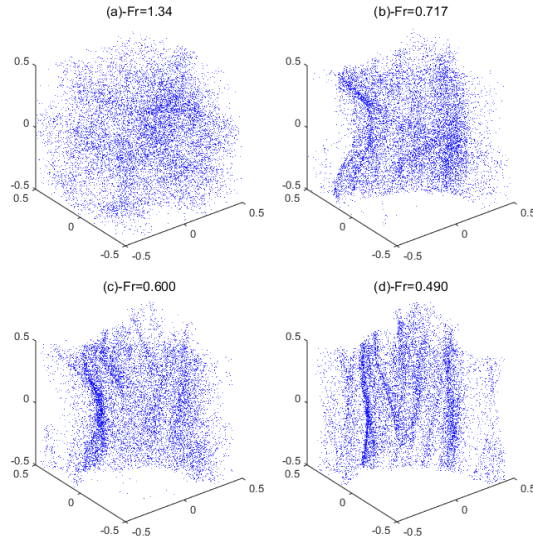


Figure 4.16. Clustering variations at $St = 0.663$ for decreasing value of Fr and $t = 300s$

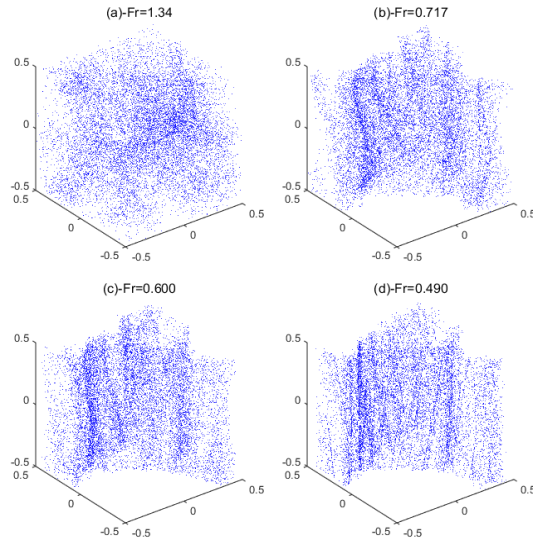


Figure 4.17. Clustering variations at $St = 1.00$ for decreasing value of Fr and $t = 300s$

4.2.2 VARIATION IN CLUSTERING IN RELATION TO Fr

A constant Froude number corresponds to the case of varying the particle's property (τ_a) for a given environment (turbulence and gravity) which exists in most of the experimental situations. The variations in clustering patterns are identified by keeping Fr constant

while varying St . For the purpose of qualitative measures, three different ranges of Fr listed in Table 4.2 are considered with small increments in St ranging [0-1].

Case	Fr	St range	observed patterns			
			1D-H	1D-V	2D-L	3D
E	> 1	0-1	✓	✓		✓
F	0.6-1.0	0-1	✓	✓	✓	
G	< 0.6	0-1		✓	✓	

TABLE 4.2. Different cases for studying the attractor topology for different ranges of Fr .

Evolution of particles without gravity:

First we observe the case with no gravity and the variation in the clustering is studied for $Fr = \infty$. There is no noticeable variation observed in clustering with the increasing values of St as shown in Fig. 4.18. An insignificant difference still exists between clustering patterns for the low and high values of St . The cases in Fig. 4.18a,b illustrate relatively more clustering than the cases presented in Fig. 4.18c,d.

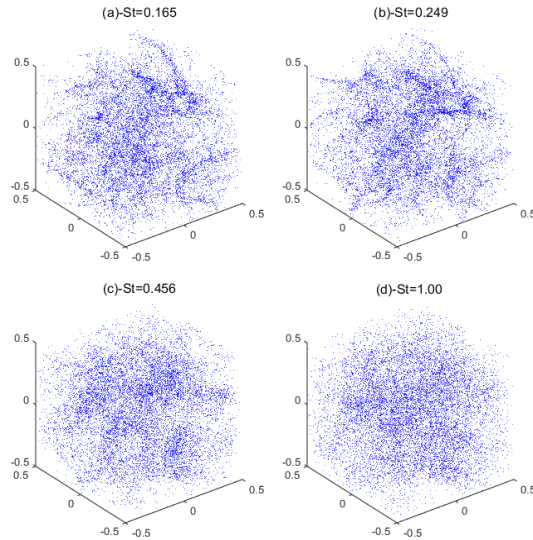


Figure 4.18. Clustering variations at $Fr = \infty$ for increasing value of St and $t = 300s$

For high range $Fr > 1$:

A slight increase in gravity, in case E, can force the particles to come together and start accumulating. A clear 1D-H attractor can be seen for a higher value of $Fr=1.89$ with a low St as shown in Fig. 4.19b. As the St number is increased, the 1D-H attractor

disappears and the particles repositions evenly in the flow as shown in Fig. 4.19d. It illustrates that the relatively heavier particles are less affected by the gravity.

Further increases in gravity, relatively lower Froude number $Fr = 1.34$, shows the same picture and the 1D-H attractor appears at higher values of Stokes number Fig. 4.20a,b as compared to the case with $Fr=1.34$. The 1D-H attractor converts into a 3D attractor with increasing values of St .

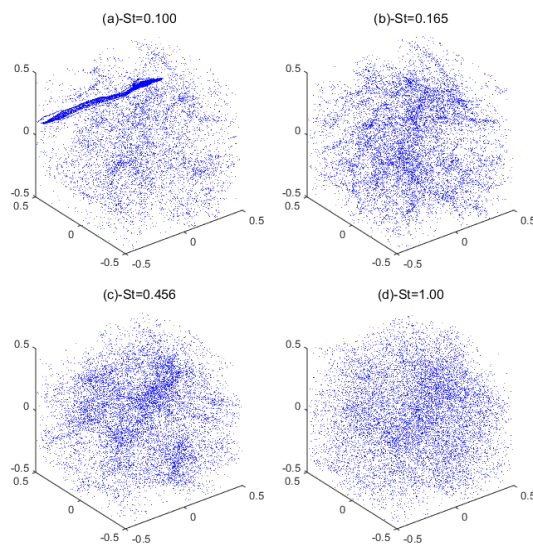


Figure 4.19. Clustering variations at $Fr = 1.89$ for increasing value of St and $t = 300s$

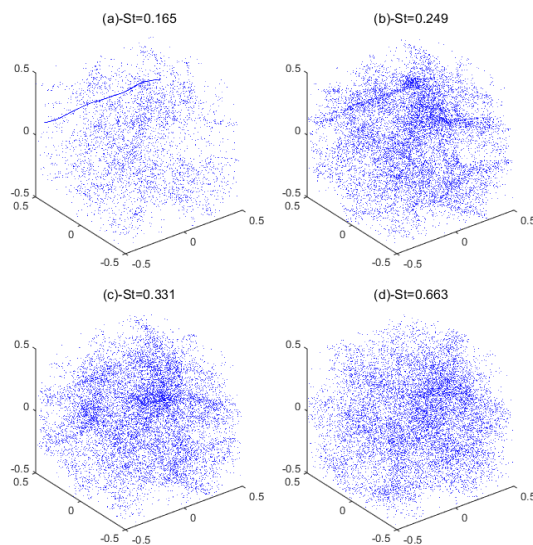


Figure 4.20. Clustering variations at $Fr = 1.34$ for increasing value of St and $t = 300s$

Another prosperous feature of the clustering observed within this range of Fr is existence of both $1D-H$ and $1D-V$ attractors for a given value of Fr for a range of St . This elaborates that different particles can respond differently to a combined gravity-turbulence effect. These variations can be observed in Fig. 4.21 where (a) and (b) represent the horizontal one-dimensional attractor while a vertical one-dimensional attractor can be seen in Fig. 4.21c.

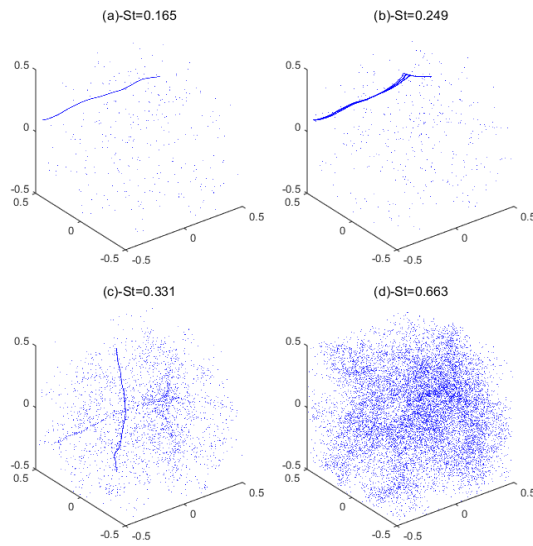


Figure 4.21. Clustering variations at $Fr = 1.09$ for increasing value of St and $t = 300s$

For medium range $0.6 < Fr < 1.0$:

The mid-ranged values of Fr , in case F, show different settlement of particles in the flow. The particles accumulate as different one-dimensional attractors for some pairs of (St, Fr) . First, the particles with low St cluster as a $1D-H$ attractor for high value of Fr (as shown in Fig. 4.22a and Fig. 4.23a). Then these $1D-H$ attractors switch into the $1D-V$ attractors with the increasing values of St as shown in Fig. 4.22b and Fig. 4.23b. The switching of a horizontal attractor into a vertical confirms that the heavier particles respond better to the gravity than the lighter ones.

Further increment in St repositions the $1D-V$ attractor as $1D-HV$ attractor for an intermediate value of St as shown in Fig. 4.22c and Fig. 4.23c. Finally, $St \rightarrow 1$, these $1D$ attractors get the shape of $2D$ -layered structure as shown in 4.22d and Fig. 4.23d. These layered structures are the rare feature which generates as the result of gravity for the relatively higher St particles.

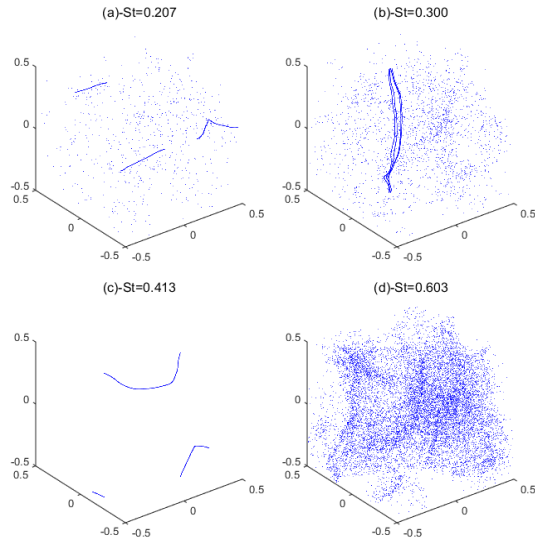


Figure 4.22. Clustering variations at $Fr = 0.849$ for increasing value of St and $t = 300s$

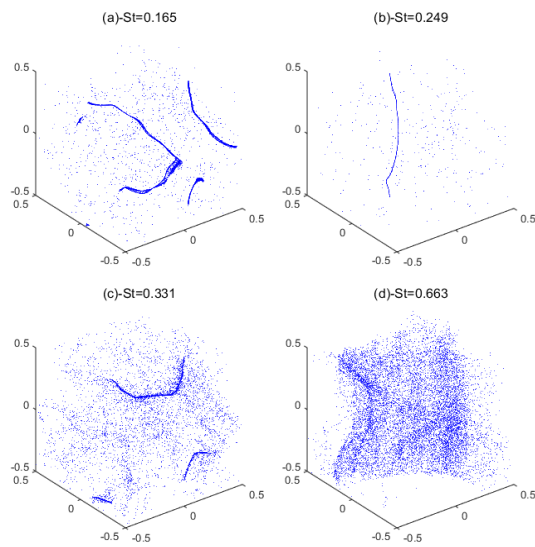


Figure 4.23. Clustering variations at $Fr = 0.717$ for increasing value of St and $t = 300s$

For low range $Fr < 0.6$:

The gravitational force is kept very high to achieve $Fr \rightarrow 0$. For this range of Fr , in case G, the 1D-V attractor is identified for a very low value of St as shown in Fig. 4.24a and Fig. 4.25a and it converts into the 2D-L attractors for high values of St as shown in Fig. 4.24d and Fig. 4.25d. It is clearly evidenced that the higher values St and Fr reduce the chances of appearance of the one-dimensional attractor while the 2D-L attractors predominantly come out.

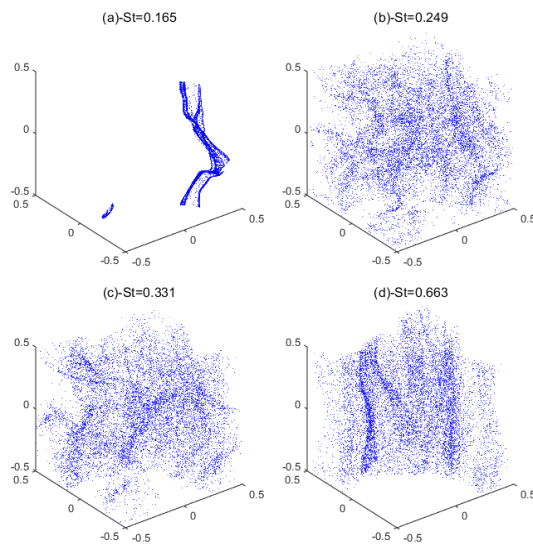


Figure 4.24. Clustering variations at $Fr = 0.548$ for increasing value of St and $t = 300s$

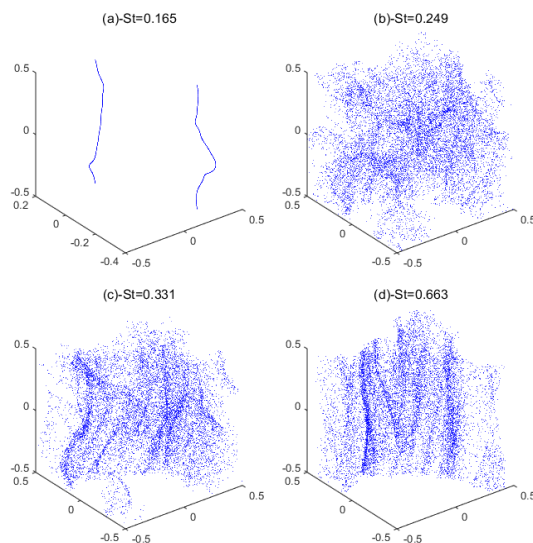


Figure 4.25. Clustering variations at $Fr = 0.490$ for increasing value of St and $t = 300s$

4.2.3 VARIATION IN CLUSTERING IN RELATION TO γ

It results from the previous discussion that the variations in inertial and gravity effects do not have a monotonic effect on the particle clustering. Physically gravity and inertia are combined effects but one can consider a particle subjected to a drift velocity without referring explicitly to gravity. This effect of drift can be assessed by identifying the patterns with the drift parameter γ instead of Fr . So here we want to observe the variation in the particle attractor by keeping the drift parameter γ constant. For the purpose we have chosen three different ranges of γ .

For low drift parameter γ :

For very low range of drift parameter $0 < \gamma \leq 0.2$, the 1D-H attractors appear at low St as shown in Fig. 4.26b and the particles redistribute evenly in the flow field when St approaches to 1 as shown in Fig. 4.26d. The increment in γ forces the particles to move in the direction of gravity and the 1D-H attractor transforms into a 1D-V attractor for an intermediate value of St as shown in Fig. 4.27c. But the particles remain dispersed in the flow for low and high values of St shown in Fig. 4.27a and d respectively. The constant drift parameter γ can produce the same types of attractors for different St , and these attractors are very sensitive to the gravity variations. Therefore, the range of the drift parameter γ would be very limited for which the similar attractors can appear specially for the lighter particles, i.e. for $St < 0.3$.

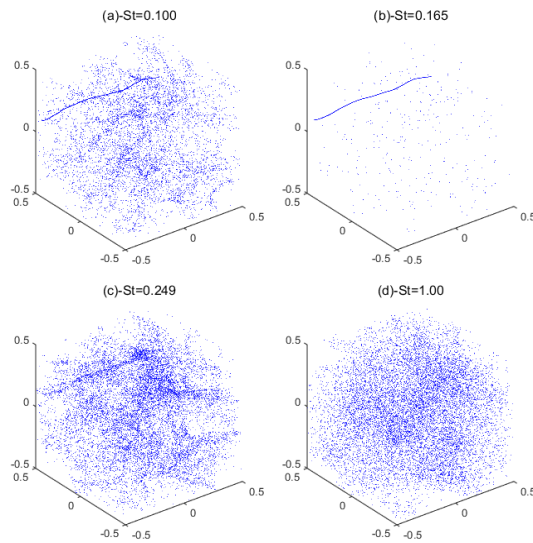


Figure 4.26. Attractor variation with increasing values St for $\gamma=0.138$ and $t = 300s$

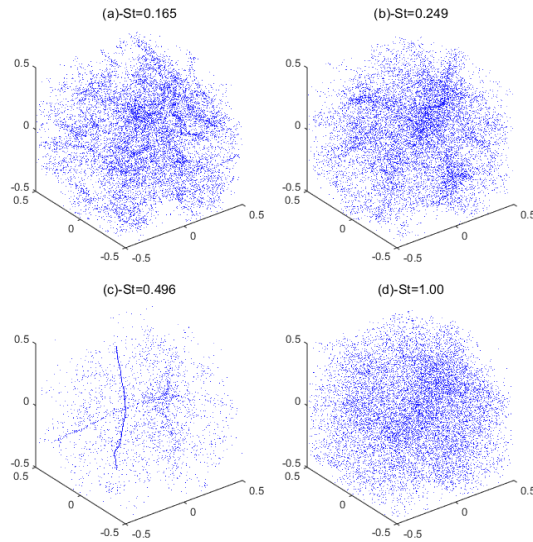


Figure 4.27. Attractor variation with increasing values St for $\gamma=0.276$ and $t = 300s$

For medium drift parameter γ :

When the drift parameter γ is increased to mid-ranged values $0.3 \leq \gamma \leq 0.8$, instead of 1D-H attractors, the 1D-HV attractor appears as illustrated in Fig. 4.28c. Another significant observation can be made at $\gamma = 0.689$ where a 1D-V attractor is observed at low values of Stoke number $St = 0.165$ Fig. 4.29b. This shows that the particles with low inertia can also be accumulated in a vertical direction by keeping the γ very high. Furthermore, the particles do not show any apparent clustering for high values of St as shown in Fig. 4.28d and Fig. 4.29d.

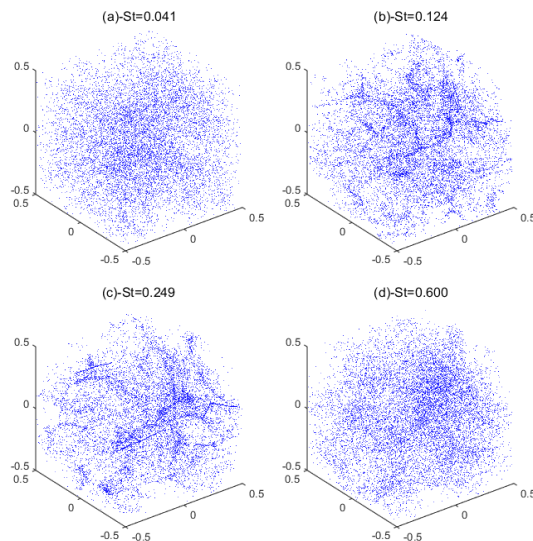


Figure 4.28. Attractor variation with increasing values St for $\gamma=0.345$ and $t = 300s$

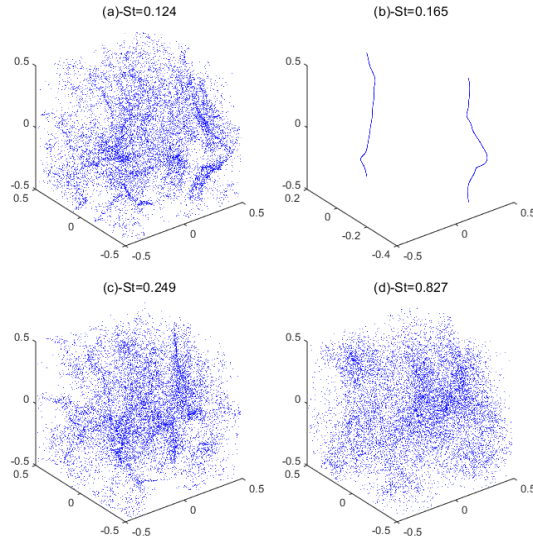


Figure 4.29. Attractor variation with increasing values St for $\gamma=0.689$ and $t = 300s$

For high drift parameter γ :

By increasing the drift parameter $\gamma > 1.0$, we do not provide the enough time to the particles for settling in the flow as compare to the low drift γ . The 2D-L layered patterns are mostly observed for $St > 0.3$ and $0.8 \leq \gamma \leq 3$ as shown in Fig. 4.30 and Fig. 4.31. We also found that for a given γ , only one type of attractor is predominantly evolved. As a result, we can have similar type of attractor for a very high gravity or inertia providing γ constant for a specific flow conditions. This type of information is of extreme importance in the practical situations where mean velocity can change the process altogether.

4.3 Visualisations of particle clustering for $St > 1$

We discussed the visualisations of the Lagrangian attractors in the KS flow for $St \leq 1$, and now intend to confirm the continuation of clustering patterns for $St > 1$. We run a few cases with $1 < St \leq 2$ and found that with low gravity effect particles like to stick with their initial positions and somewhat distributed structures are observed in Fig. 4.32a, Fig. 4.33a and Fig. 4.34a. As Fr is decreased, the two-dimensional layered attractors appear as shown in Fig. 4.32b, Fig. 4.33b and Fig. 4.34b whose dimensions decrease with the decreasing values of Fr . It shows that the gravity is still effective for Stokes number $1 < St \leq 2$ for a given inertial range scales of turbulence.

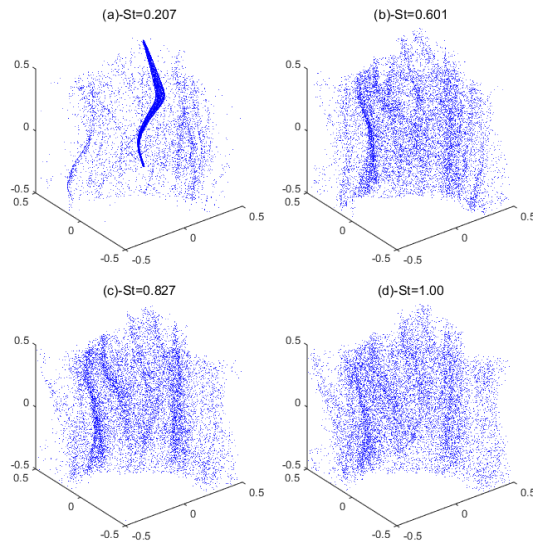


Figure 4.30. Attractor variation with increasing values St for $\gamma=2.0$ and $t=300s$

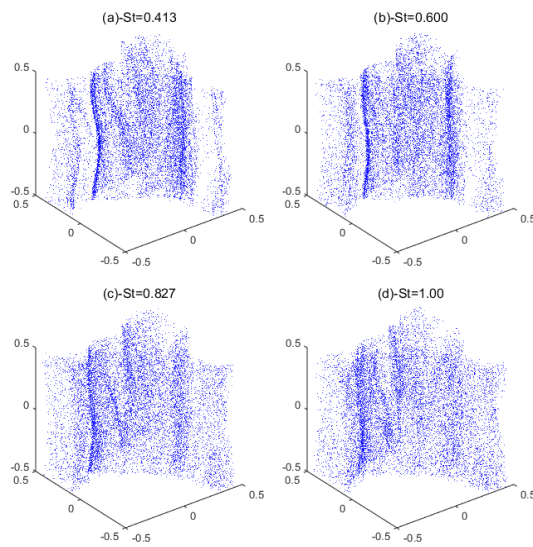


Figure 4.31. Attractor variation with increasing values St for $\gamma=3.0$ and $t=300s$

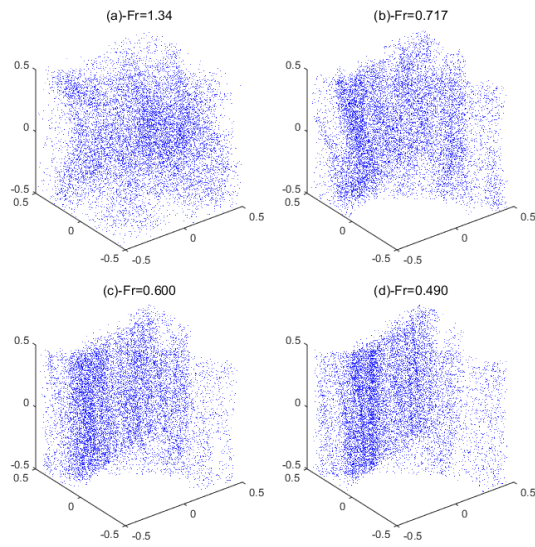


Figure 4.32. Clustering variations at $St = 1.24$ for decreasing value of Fr and $t = 300s$

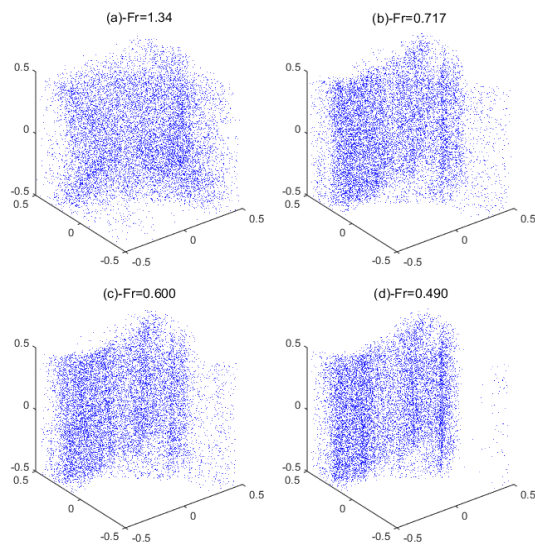


Figure 4.33. Clustering variations at $St = 1.63$ for decreasing value of Fr and $t = 300s$

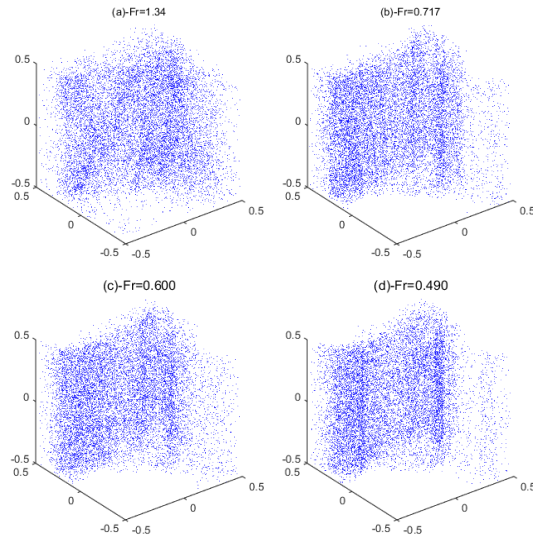


Figure 4.34. Clustering variations at $St = 1.86$ for decreasing value of Fr and $t = 300s$

4.4 Conclusion

In this chapter, the effect of gravity on inertial particle clustering and variations in Lagrangian attractor is visualised. The evolution of particles in the homogeneous isotropic flow provide a thorough information about the clustering depending on non-dimensional parameters St and Fr . The topological dimension of the clustering pattern varies from 1D to 3D as described by different of attractors in Fig. 4.35. Because of the KS model (a less time-computing), we able to run a number of cases to identify the shapes of the Lagrangian attractor. The outcomes of this chapter are summarised in table 4.3 and these will be used to quantify the clustering patterns. We conclude this part of study as follows:

- Particle inertia in the absence of gravity does not affect much the clustering patterns which can be visualised for the given inertial range of flow.
- The variations in clustering pattern become more observable as the gravity is increased for a given Stokes number. These variations are clearly different for the various ranges of St .
- It is found that particles with very low Stokes number (St) remain dispersed in the flow even at the high gravity. This shows that particles' inertia should be enough to sense the effect of gravity.
- As St is slightly increased, the particles start accumulating as a one-dimensional attractor for some particular values of Fr . The orientation of this one-dimensional

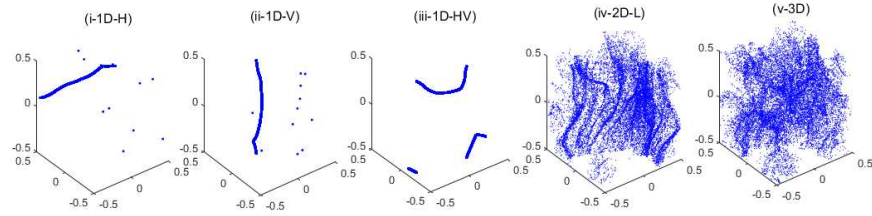


Figure 4.35. Different types of attractors

attractor (1D-H, 1D-V or 1D-HV) depends on Fr . It means that the effect of gravity does not only change the attractors shape but can also vary its orientation for a given value of St .

- Normally a 1D-V attractor appears at a low Fr (high gravity), but we also identified some cases with low St and Fr which produced a 1D-V attractor. This shows that the one-dimensional attractors appear as the combined effect of gravity and inertia.
- For some specific values of St , one type of Lagrangian attractor (1D-H) can switch into another (1D-V or 1D-HV) with varying values of Fr .
- The one-dimensional attractors are not observed after a particular St and rather two-dimensional curtain-like layered patterns predominantly appear with low Fr .
- The 2D layered patterns are considered as a sign of dominance of the particle inertial over the gravity. It is also observed that for the heavier particles, an increase in gravity enhances the clustering within 2D-L structures.
- Finally, we found that particles clustering persists with $St > 1$ with the decreasing values of Fr and the 2D-L attractors are mostly observed.

Froude Number (Fr)	Structure	Range of St		
		Low range	Medium range	High range
∞ (gravity=0)	1D-H	No	No	No
	1D-V	No	No	No
	2D-L	No	No	No
	3D	Yes	Yes	Yes
High Fr (Low gravity)	1D-H	Yes	Yes	No
	1D-V	No	Yes	Yes
	2D-L	No	No	No
	3D	Yes	Yes	Yes
Low Fr (High gravity)	1D-H	No	Yes	No
	1D-V	Yes	Yes	Yes
	2D-L	No	Yes	Yes
	3D	Yes	No	No

TABLE 4.3. Summary of Observed patterns with varying values of St and Fr

Chapter 5

Quantitative analysis of inertial particle clustering

5.1 Introduction

The qualitative visualisation revealed the clustering of inertial particles in the KS flow and the different types of Lagrangian attractor were identified in the previous chapter. In particular, we noticed the topological variations in the Lagrangian attractors according to the observed shapes of the attractor. Beyond the simple visualisation it is important to analyse the Lagrangian attractors using an appropriate quantification and visualisations of the particle cloud for small discrete increments of the non-dimensional parameters St and Fr can be tedious. In this chapter, dependence of clustering pattern on St , Fr and γ is quantified to establish a relationship, that is we aim to determine the critical values of the non-dimensional parameters to identify the different types of attractors.

In the previous studies, the clustering has strongly been linked to the flow conditions and these conditions are considered as the decisive factor for the selection of quantification method. Bec (2005) developed a statistical description of heavy particle clustering and showed that, differently from smooth flows, particles do not form fractal clusters in the rough flows (variable velocity). They rather distribute inhomogeneously with a statistics that only depends on a local Stokes number. In addition to this, Bec *et al.* (2007) conclusively found that the particles with same St can evolve differently by varying the length scales in turbulence. They investigated the clustering in the dissipative and inertial ranges of scales and it is concluded that particles form fractal clusters with properties independent of the Reynolds number in the dissipative range. On the other

hand, the clustering is characterised by voids generation in the inertial range scales. On the basis of flow conditions and respective clustering mechanism, the fractal analysis methods are normally chosen when finding fractal dimension in dissipative scales while integer dimensions are considered for the clustering variation in the inertial range.

In the present study, we use a confined inertial range of scales specified by a set of wave-numbers. Therefore, we aim to measure the integer dimension of the Lagrangian attractors. In order to achieve this, we first discuss the methods generally used in the literature to quantify the clustering patterns in turbulent flow. Then we apply some of these methods to quantify the qualitative shapes of the Lagrangian attractors. The selection of the quantification method also depends on outcomes of a particular study and for our work, the methods find:

- The critical values of Stokes number St and Froude number Fr at which the Lagrangian attractors can be differentiated as 1D-H, 1DV, 1D-HV, 2D-L, etc.
- The anisotropic behaviour of the Lagrangian attractors i.e. the value of St at which the switching of one attractor from a horizontal to vertical direction occurs.

5.2 Methods of quantification

A number of methods have successfully been used to quantify the clustering patterns in turbulent flow such as Box counting method (BCM), Correlation dimension (D_2) analysis, Voronoï diagram analysis, Minkowski functional analysis, Radial distribution function (RDF) or Particle-pair correlation, nearest neighbour (NN) analysis, etc. We briefly introduce some of these methods along with their applications. Eventually, the quantification methods will be proposed for the final quantitative analysis by comparing the different aspects of methods.

Starting discussion from box-counting method (BCM), this simpler method has been successfully used to characterise the voids by identifying the number of boxes required to cover the particle positions. Though the prime application of Box counting method is to find the fractal dimension, it can also be used to determine integer dimension. The method has been applied by Aliseda *et al.* (2002) to figure out that clustering effect is maximum at scales of order $10\eta_K$. The same kind of analysis repeated by Monchaux *et al.* (2010) on a experimentally collected data. They found that the clustering effect is maximum when St is about 1.

Another widely used method, to find the fractal dimension of clustering patterns, is the

correlation dimension (D_2). This method was first introduced by Tang *et al.* (1992) for quantifying the relative organization of the dispersion patterns as a function of the particle time scale ratio. Since then, many researchers (Fessler *et al.*, 1994; Hogan & Cuzzi, 2001; Bec *et al.*, 2007) have successfully applied this method to quantify the particle clustering in turbulent flow. The correlation dimension (D_2) is defined as the exponent of the power-law behaviour at small scales of the probability $P_2(r)$ to find two particles at a distance less or equal to r . In practice, D_2 reveals the space dimension when particles are uniformly distributed and in case of clusters (as a fractal patterns), D_2 decreases. Fessler *et al.* (1994); Bec *et al.* (2007) found that the correlation dimension is minimum for Stokes numbers around unity.

When interesting in scale by scale quantification of clusters along with particle collision rate Radial distribution function (RDF) is preferred. It is calculated as the ratio of the probability of finding a particle pair separated by a distance r normalized by the same probability for a randomly distributed mixture. This clustering indicator has widely been used in the literature, also referred to as particle-pair correlation. Many studies (Chun *et al.*, 2005; Salazar *et al.*, 2008; Saw *et al.*, 2012) have applied RDF to look into the clustering of particles with varying Stokes number and at the same time they also investigated the collision rate of particles.

Another reliable method is proposed by Monchaux *et al.* (2010) who used Voronoï diagrams to quantify the particle clustering. Each particle in a Voronoï diagram for a nD space is associated with an independent cell. One cell is characterised as the collection of close points for a particle than any other. As the volume (V) of a Voronoï cell is related to local concentration in particles, the measure of Voronoï volumes illustrates local concentration field. Moreover, Voronoï volumes also allow the Lagrangian particle tracking to investigate the particle concentration along the trajectories. Monchaux *et al.* (2010) directly linked the PDF of Voronoï volumes to particle clustering. As no prior scaling is required, one can measure local concentration for any given intrinsic resolution.

After Monchaux *et al.* (2010) this method of quantification is also applied by others. More recently, using Lagrangian autocorrelation of the Voronoï volume, Tagawa *et al.* (2012) found that inertial particles (light or heavy) cluster significantly in the flow structures because of the inertial bias between particles and fluid tracers. Furthermore, Dejoan & Monchaux (2013) extended the application of this method of quantification while considering the gravity effect on inertial particle clustering.

Minkowski functional has been implemented by Calzavarini *et al.* (2008) to geometrically characterise the clustering patterns in turbulence. The method is widely used in cosmology and normally, a collection of balls of radius r is centrally positioned with initial particle cloud. Then morphological variations are calculated indicating as the surface, the volume, etc. and these variations in structure provide an indirect measure particle clustering. Calzavarini *et al.* (2008) evidently found the filamentary and tube-like structures of bubble and heavy particle clusters respectively. As these results only provides the global topological indications on clustering, individual cluster identification is not possible with this method.

Furthermore, Jin & He (2013) applied wavenumber spectra of particle concentration fluctuations to analyse the multi-scale nature of particle clusters. These methods have restrictive applications as a long computational time is required to resolve the flow contained a number of particles. In order to quantify the clustering phenomenon, another promising spatial analysis technique (successfully adopted by Park & Lee (2014)) is the nearest-neighbour analysis. Using the average distance to nearest neighbour, they found the clustering variations with respect to St and Fr in the horizontal and vertical directions which revealed the anisotropic behaviour in the particle clustering.

Because the different methods catch different features in a data set, it is good practice to use more than one method to analyse the data and then the results can be compared for a greater insight into the clustering characteristics. In this regard, we have selected four different methods to analyse the spatial distribution of the Lagrangian attractors in the KS flow. Two of these methods (box-counting method and nearest-neighbour analysis) have already been used for the quantification of inertial particle clustering in turbulent flow while Lacunarity analysis and Quadrat variance are applied here as a new tool for spatial analysis of the Lagrangian attractors. In the following section, we discuss these methods in detail. It has been found that the results obtained using Quadrat variance methods are very similar to Box-counting method, this method has been reported in the Appendix A to avoid any kind of confusion.

5.2.1 BOX-COUNTING METHOD

In ordinary geometry, where topological dimension is always a non-negative integer, the Euclidean dimension represents the number of coordinates necessary to define an object. For instance, the Point is of Euclidean size 0; the plane curves, segment and contour, are of dimension 1; the surfaces, disc and planes, are of Euclidean size 2 and the volumes, a ball and sphere, are of size 3.

In real life, dimension enclosed by a space and time frame can be considered as fractal dimension which is different from topological dimension. The word fractal is sourced from Latin word of “fractus” meaning discontinuous feature. Fractal geometry can be defined as the geometry of irregular shapes where an identical pattern repeats itself on an ever-diminishing scale. The fractal geometry is a branch of the classical geometry but does not replace it. Rather, it is used to figure out some hidden features of object which cannot be identified by using simple geometrical shapes. The repeated or self similar structure are found in nature configurations like clouds, rock formation, soft tissue of human body etc. Despite of simple outlook of these features, detailed insight observations can emphasize the fractal features.

The fact of fractal has been addressed from long time ago and described on mathematical foundation in the year 1975, when a mathematician Mandelbrot assigned the word “fractal” to describe such that non-smooth edged shapes of self-similar characteristics or irregular shapes. Since that time, fractals have been received more attention due to their graphic art potential in describing some complicated shapes, for example: mountains, clouds and landscapes, in fact most computers graphic techniques actually employ a stochastic approximation of true fractal functions.

The use of the fractal analysis spread to many directions because of its relatively many applications to various fields. One of the methods for estimating D is the box-counting method. The box-counting method (BCM) is the most popular way of estimating the fractal dimension because of its simplicity. The problem with this method is that it finally produced results with high percentage of error as its structure is based on the choice of a unit square box and then select a fraction of its side length to generate the sequence.

The box-counting dimension (BCM) is applied to any structure in the plane and can be adapted for structures in three-dimensional space. This dimension is sometimes called grid dimension because for mathematical convenience the boxes are usually part of a grid. In general, the “rougher” the line, the steeper the slope, the larger the fractal dimension.

The fractal dimension, D , represents the relation between the box counted needed to cover that object, N , and the box side, r , as the following relation:

$$N \sim r^D. \quad (5.1)$$

By taking the natural log of both sides, one could get the following relation:

$$\ln N = D \ln r. \quad (5.2)$$

Then, the fractal dimension can be found as follows:

$$D = \frac{\Delta \ln N}{\Delta \ln r} \quad (5.3)$$

This is known as the Hausdorff dimension. Examined this way, fractal dimension, D , needs not to be an integer as it was in Euclidean geometry, it could be a fraction, as it is in fractal geometry. So, a general definition of D , representing the fractal dimension, is given by the following equation.

$$D = \frac{\Delta \ln N_{boxes}}{\Delta \ln (1/box\ size)}. \quad (5.4)$$

The determination of the value of the fractal dimension is depending on the algorithm used, the range selected and the resolution of the used image. Furthermore, this D is not an absolute measure, thus the parameters associated with the given D value should be specified to reproduce the results for comparison case and D can only be calculated for a deterministic fractal.

5.2.2 LACUNARITY ANALYSIS

The word ‘‘Lacunarity’’ extracted from the word for ‘‘lake’’ means a gap or pool, but in dimensional analysis it is defined as measure of gappiness, inhomogeneity, visual texture, etc. It is usually denoted as ‘ Λ ’. Lacunarity shows both gaps and heterogeneity in the pattern distribution and measures the clustering by identifying the voids. It has been widely used in ecology, medical sciences, environmental sciences and palaeontology for spatial pattern analysis.

Lacunarity and fractal dimension can work together to identify and characterise patterns i.e. it is possible to distinguish between two identical fractal dimensions by using Lacunarity and vice versa as demonstrated in Fig. 5.1. In order to calculate the Lacunarity in a three-dimensional space, the gliding box method is normally used. Lacunarity depends on the size of box(scale) and for a given scale (b), it is expressed as the ratio of the first and second moments of counts within all possible boxes of that size. The first moment is the average sum of values in all possible blocks of size b , while the second moment is the average squared sum of values in all possible blocks of size b . Mathematically, Lacunarity can be mathematically be defined as;

$$\Lambda(b) = \frac{\mu_2(b)}{[\mu_1(b)]^2} \quad (5.5)$$

where

$$\mu_1(b) = \frac{\sum_{x=1}^{n_x+1-b} \sum_{y=1}^{n_y+1-b} \sum_{z=1}^{n_z+1-b} (\sum_{i=x}^{x+b-1} \sum_{j=y}^{y+b-1} \sum_{k=z}^{z+b-1} d_{ijk})}{(n_x + 1 - b)(n_y + 1 - b)(n_z + 1 - b)} \quad (5.6)$$

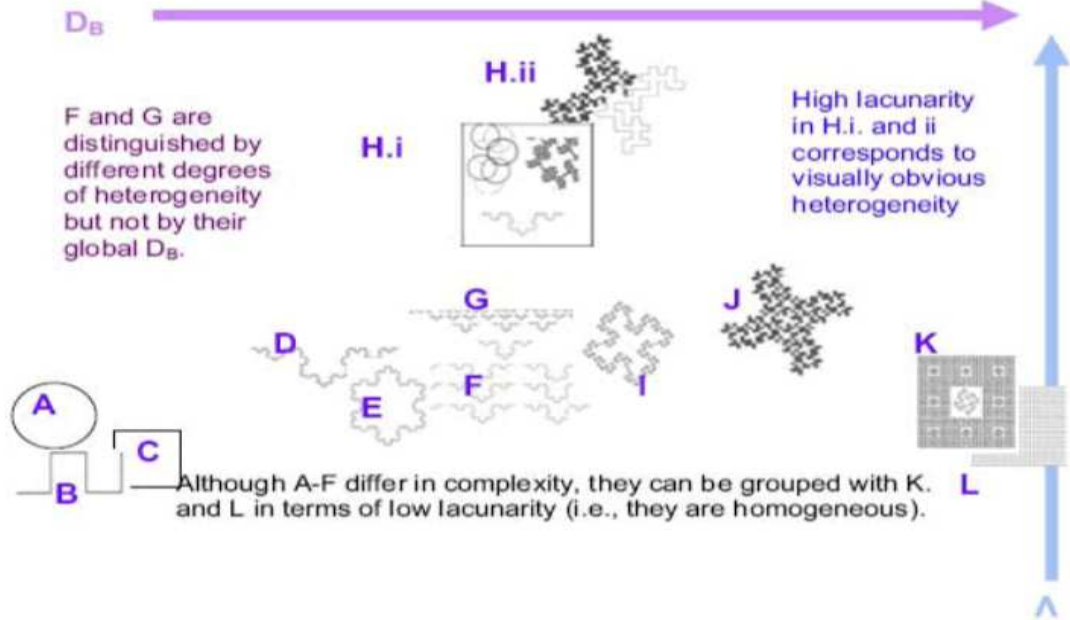


Figure 5.1. A relationship between box-counting dimension D_B and Lacunarity Λ

$$\mu_2(b) = \frac{\sum_{x=1}^{n_x+1-b} \sum_{y=1}^{n_y+1-b} \sum_{z=1}^{n_z+1-b} \left(\sum_{i=x}^{x+b-1} \sum_{j=y}^{y+b-1} \sum_{k=z}^{z+b-1} d_{ijk} \right)^2}{(n_x + 1 - b)(n_y + 1 - b)(n_z + 1 - b)} \quad (5.7)$$

where n_x is the size of the volume along the x-axis, n_y is the size of the volume along the y-axis and n_z is the size of the volume along the z-axis, while d_{ijk} is the value of count at grid point (i, j, k) . Moreover, Lacunarity results are usually presented as a log-log plot of Lacunarity Λ and scale b . In practice, random data produces a curve which is concave upwards, clumped data possess more gaps and results in a curve which is concave downwards. The regularly spaced data produces less Lacunarity and creates a curve initialising with a straight line. Dale (2000) and Plotnick *et al.* (1996) discussed the interpretation of the Lacunarity curves with examples. Lacunarity analysis can provide different results for the identical looking patterns, which is considered as an advantage of Lacunarity over BCM. However, the method is not precise in determining the scale or the patch size in pattern with known properties.

5.2.3 NEAREST-NEIGHBOUR ANALYSIS

This is the procedure of finding a nearest neighbour to every point. The nearest neighbour for a given point is simply the point that is closest to it. A nearest-neighbour connections matrix does not have to be symmetric as shown in Figure 5.2, because the

nearest neighbour of one point is not necessarily the neighbour of the other point. Furthermore, a nearest-neighbour network does not have to completely span the points; usually it will not. One also has the option of specifying the number of neighbours to connect; the standard default is one, which is the traditional nearest-neighbour network, but one can choose to connect the closest two neighbours, or closest three, etc.

The nearest neighbour method is widely used for the purpose of clustering identification in Planetology and Ecology. The nearest neighbour method is chosen for analysing particle clustering as it can provide a direct numerical outcome rather than graphs. In our case, this method of quantification can easily capture the clustering pattern varies from initial 3D-distribution to strong clusters.

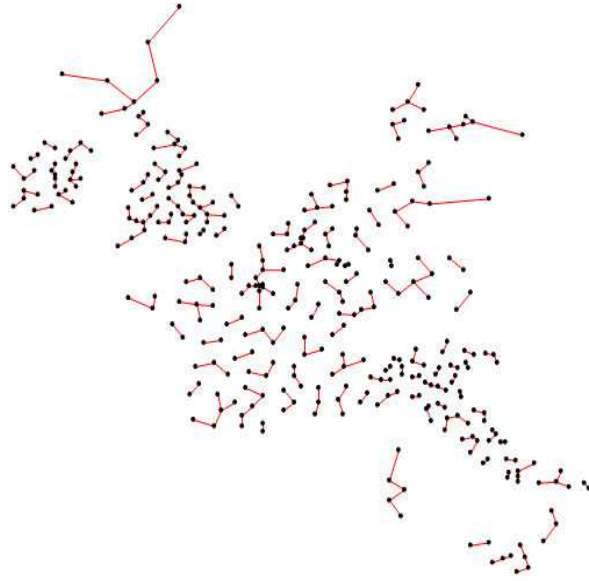


Figure 5.2. Example of a nearest-neighbour network. Points are only connected to their nearest neighbours.

In recent literature (Park & Lee, 2014), the average distance to the nearest neighbour (Δ) is introduced to clearly and systematically quantify the cluster patterns. At a given time for each particle \mathbf{X}_m its nearest neighbour \mathbf{X}_n is such that;

$$\Delta_{mi}^2 = (x_m - x_i)^2 + (y_m - y_i)^2 + (z_m - z_i)^2 \quad (5.8)$$

is minimum for $i = n$. Then we define the average distance to the closest neighbour as

$$\Delta = \frac{1}{N_p} \sqrt{\sum_{n=1}^{N_p} \Delta_{mn}^2} \quad (5.9)$$

Where $\mathbf{X}_n = (x_n, y_n, z_n)$ is the nearest particle's neighbour.

5.3 Application of quantification methods

Now we apply the three methods (discussed in the previous section) to already attained qualitative results. Initially, a small set of data mentioned in Table 5.1 is chosen to see the differences in the results created by applying the different quantitative methods. The advantages and limitations of each method are identified. On the basis of these results, a quantitative relationship is established between particle clustering and non-dimensional parameters (St, Fr).

Stokes number	Froude Number	Observed Patterns
0.124	(1.34,0.717,0.600,0.490)	(1D-H,3D,3D, 3D)
0.249	(1.34,0.717,0.600,0.490)	(1D-H,1D-V,3D, 3D)
0.331	(1.34,0.717,0.600,0.490)	(3D,1D-HV,1D-V,2D-L)
0.373	(1.34,0.717,0.600,0.490)	(1D-V,3D,2D-L, 2D-L)
0.663	(1.34,0.717,0.600,0.490)	(3D,2D-L,2D-L,2D-L)
1	(1.34,0.717,0.600,0.490)	(3D,3D,2D-L,2D-L)

TABLE 5.1. Cases with observed patterns used for method selection

5.3.1 RESULTS USING BOX-COUNTING METHOD

The box-counting method (BCM) is a commonly used method to determine the fractal dimension of an object. Though in our simulation the range of scales is too short to observe the fractal patterns described in Nicolleau & ElMaihy (2004), BCM remains a useful tool to discriminate between one-dimension, two-dimension and three-dimension clustering patterns.

First, box-counting method is validated for three clear identified shapes, namely the one-dimensional Lagrangian attractor, the two-dimensional curtain-like layered pattern and a three dimensional distribution. As shown in Fig. 5.3, the difference between these three patterns is clearly captured by box-counting method. The method is then applied to the set of data mentioned in Table 5.1 and the results are plotted as a log-log plot for each case between number of boxes (N) and box size ($1/r$) as shown in Fig. 5.4. It is clearly evident from Fig. 5.4(b), BCM can only identify the structure with a definite 1D-V attractor with $Fr = 0.717$ while it misses out the 1D-H attractor (surrounded by a cloud of particles) created with $Fr = 1.34$.

In order to investigate this discrepancy of BCM, we run a case with different time of

evolution as shown in Fig. 5.5 and then, apply BCM. We found that the BCM is sensitive to the achievement of the attractor, that is if few particles have not settled on the attractor they can alter the box-counting results. So, with this method it is necessary to make sure that the cloud shape is the asymptotic final one which requires a very long time. As illustrated in Fig. 5.5: though at a very short time $t = 10s$ the position and shape of the 1D-V is obvious, it is necessary to wait up to $t = 1200s$ to get the final cluster position that will allow a correct measure for the BCM.

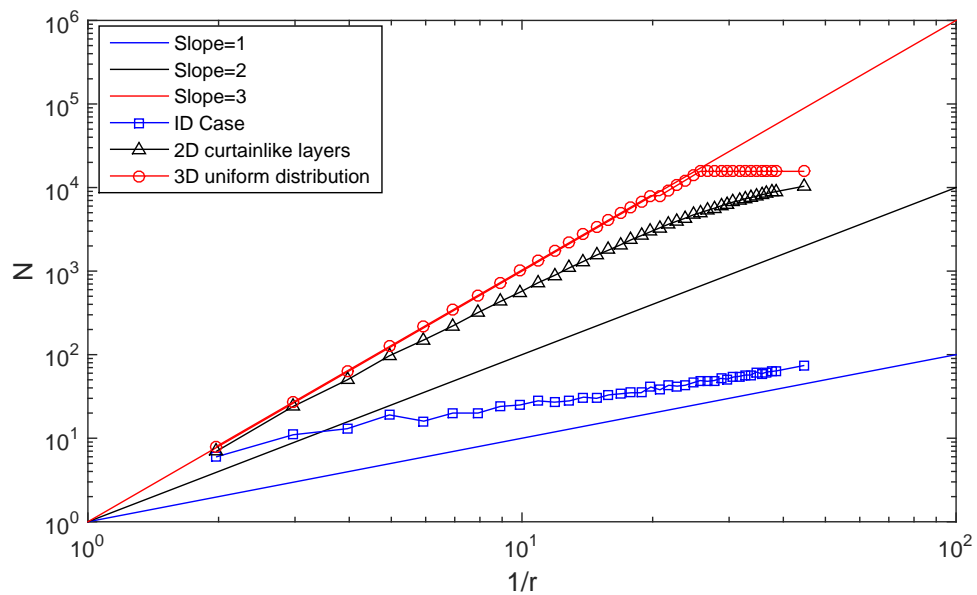


Figure 5.3. Bench mark for box-counting method

Limitation of box-counting method

A major problem with the box-counting method is to identify the integer dimension D of a pattern when particles do not reach asymptotic state. Therefore, we cannot find the significant difference in the box-counting results of two different attractors as shown in Fig. 5.6. As mentioned earlier, in order to be accurate, the BCM must be applied to the Lagrangian attractor. If the particle cloud has not settled on the attractor as at time $t = 10s$ in Fig. 5.5, the BCM will not educe the 1D patterns. So, in practice, it means running the cases for long times until the particles have all settled on the Lagrangian attractor. In addition to this, BCM is also incapable of finding directional variations in the attractors.

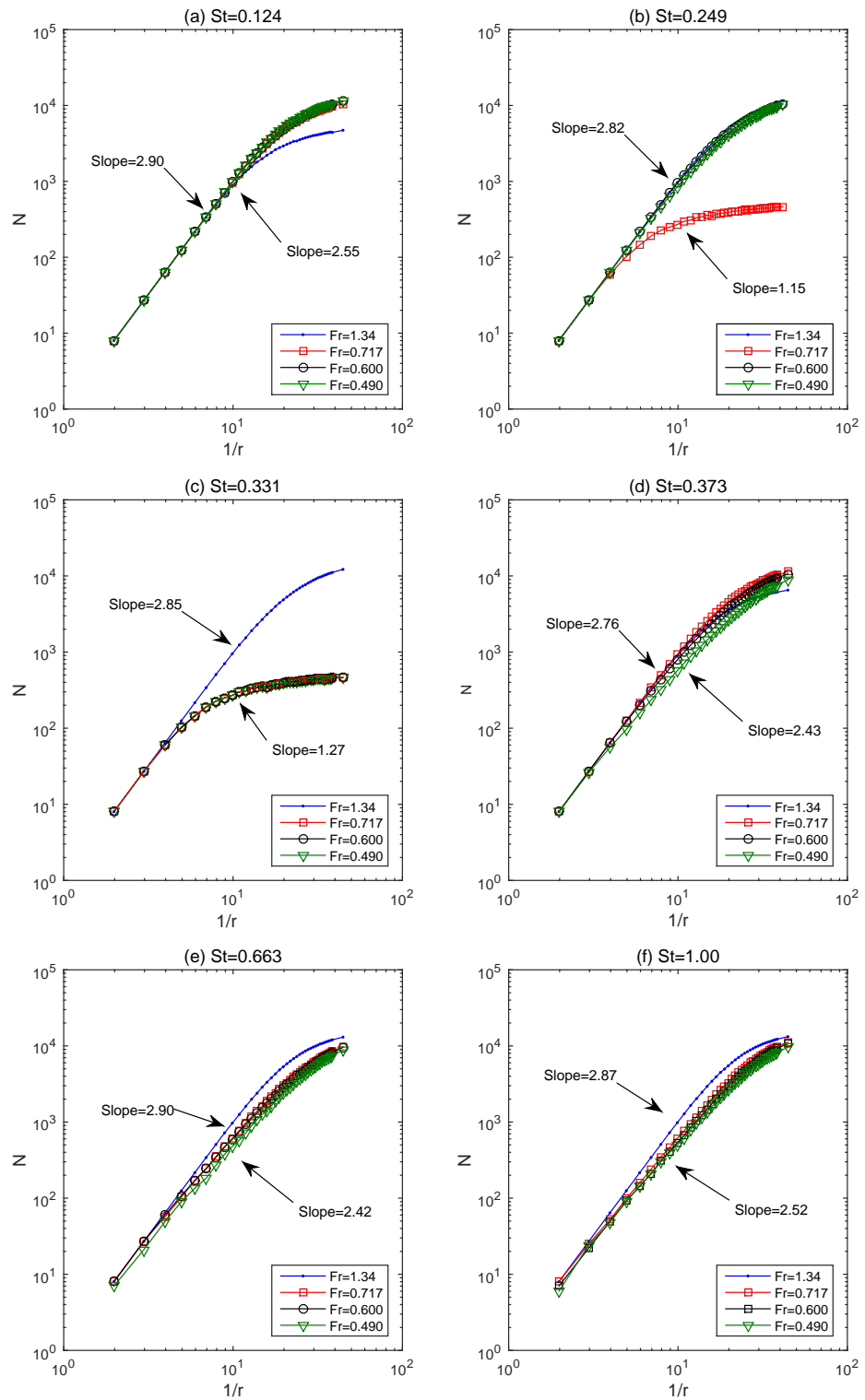


Figure 5.4. (a)-(f) log-log plots showing box-counting dimension for different values of St with varying Fr at $t=300s$, slopes are taken between inertial range of 3.96-15.85

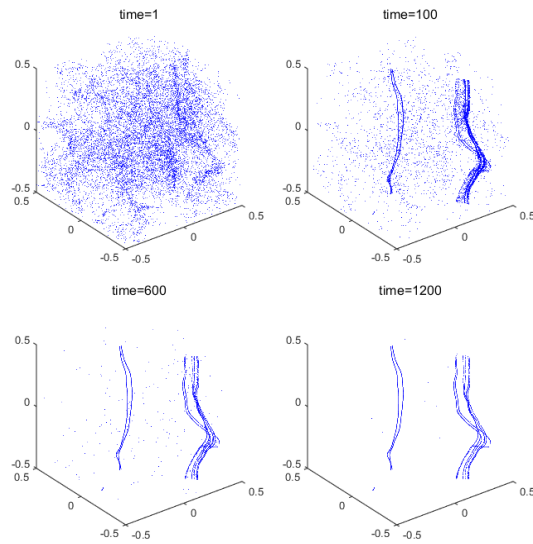


Figure 5.5. Time evolution of inertial particles with $St = 0.207$ and $Fr = 0.55$

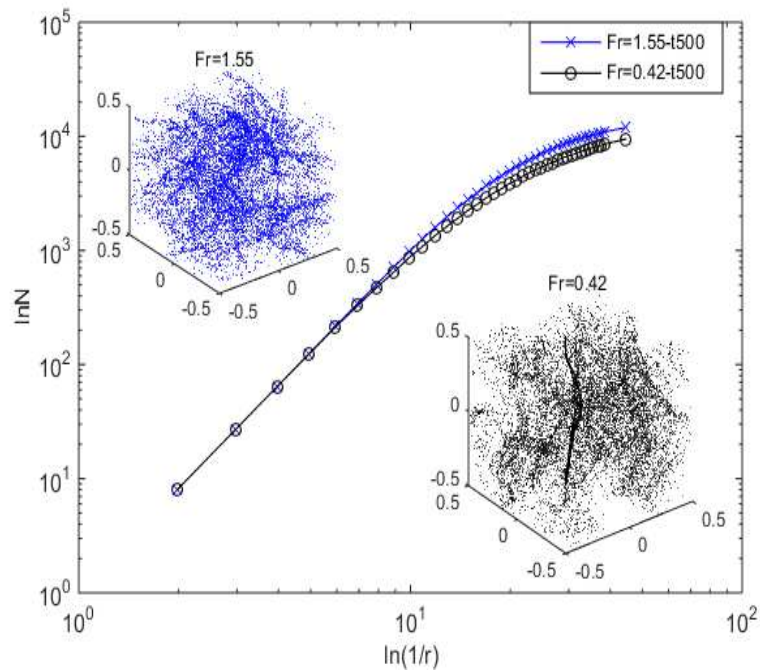


Figure 5.6. Box-counting slope for very similar cases for different values of Fr at $St = 0.207$

5.3.2 RESULTS USING LACUNARITY ANALYSIS

Using Lacunarity analysis, clustering patterns in the flow can also be quantified. For this purpose, the gliding box method is used to the distribution of particles at a given time to see the variations in the patterns. Lacunarity analysis is found to be a useful tool to recognise clearly varied patterns, but the obtained results depend on the scale. After running a number of cases with the different range of scales, we set a benchmark for comparing different types of attractors as shown in Fig. 5.7. In practice, a one-dimensional attractor is represented by a straight line and a three attractor creates a curve initialising with a straight line. In between these two extremes, intermediate attractors can be identified by concave downward curves. Moreover, the strength of one-dimensional clustering is determined by the slope of the line. It means that the larger slope represents the stronger clustering and vice versa.

Now we apply the Lacunarity analysis to each case presented in Table 5.1 and a better outcome is achieved as shown in Fig. 5.8. Regardless of the scale of gliding box b , the curves variation matches the patterns' dimensions as reported in the column 3 of Table 5.1. In this way, the incapability of BCM can be overcome without achieving the final asymptotic patterns as illustrated in Fig. 5.8(b). Contrary to the BCM, Lacunarity for $Fr=1.34$ and $Fr=0.717$ represented by straight lines shows the strong one-dimensional clustering and the difference in slopes confirms that how close the particles are on the attractors. Similarly, we can also compare the blue lines in Figs. 5.8(a) and (b). It can be observed that there is stronger clustering in case of $St = 0.124$ and $Fr = 1.34$ than in the case of $St = 0.249$ and $Fr = 1.34$ as illustrated in Fig. 5.9.

Limitation of Lacunarity analysis

Similar to BCM, Lacunarity is also sensitive to the scale and is normally considered as a complementary tool in the fractal analysis. The output as curves with no defined scale is a most prominent drawback of this method. Furthermore, Lacunarity analysis cannot identify the directionality of the Lagrangian attractors as well. Hence, we can only use this method as an additional tool along with another established method in order to identify the clustering patterns.

5.3.3 RESULTS USING NEAREST-NEIGHBOUR ANALYSIS

Unlike above two methods, the results of nearest-neighbour analysis does not depend on measuring scales and can provide the singularity to the result. We get three obvious benchmark values for the average distance to nearest neighbour.

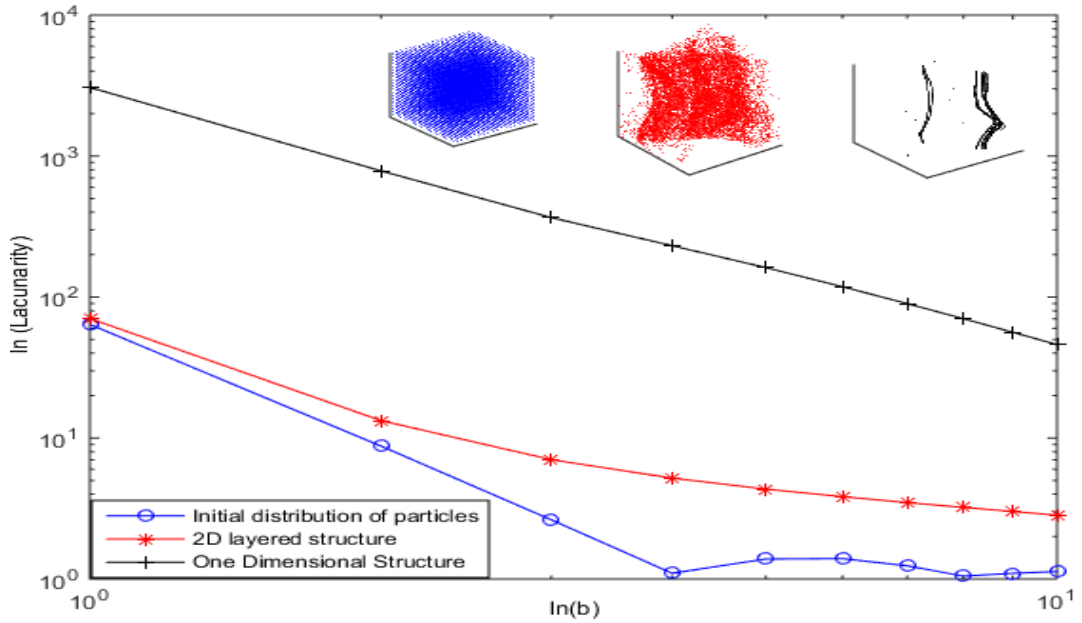


Figure 5.7. Bench mark of Lacunarity for different clear Lagrangian attractors

- i) If the particles are homogeneously distributed as at time $t = 0$, then $\Delta \simeq L_x/N = 1/25 = 0.04$.
- ii) If the particles are distributed on a surface-like attractor 2D-L then $\Delta \simeq L_x/N^{3/2} = 1/25^{3/2} = 0.008$.
- iii) If the particles are distributed on a line-like attractor then $\Delta \simeq L_x/N^3 = 1/25^3 = 6.4 \cdot 10^{-5}$.

In practice, the method will detect a one-dimensional structure (1D-H or 1-DV) for $\Delta \leq 0.008$ while 2D layered structures are observed for $0.01 \leq \Delta \leq 0.014$. In Fig. 5.10, the plots between Fr and Δ for different St clearly shows the pattern variations by using the nearest-neighbour method. Basically, there can be one or more than minimum points for each St representing the strongest clustering. For very low Stokes number ($St = 0.041$), no significant variation is observed with the decreasing values of Fr and same observation is noted in case when $St \rightarrow 1$. Moreover, we notice that the average distance to the nearest neighbour is saturated for low Fr values irrespective of Stokes numbers (encircled portion in Fig. 5.10).

Using the nearest-neighbour analysis, we can easily differentiate the variations in the clustering patterns for constant Froude number Fr as shown in Fig. 5.11. In the absence of gravity, the minimum points (at $St = 0.13$) indicates the insignificant clustering while the gravity consideration decreases the average distance to nearest neighbour (Δ).

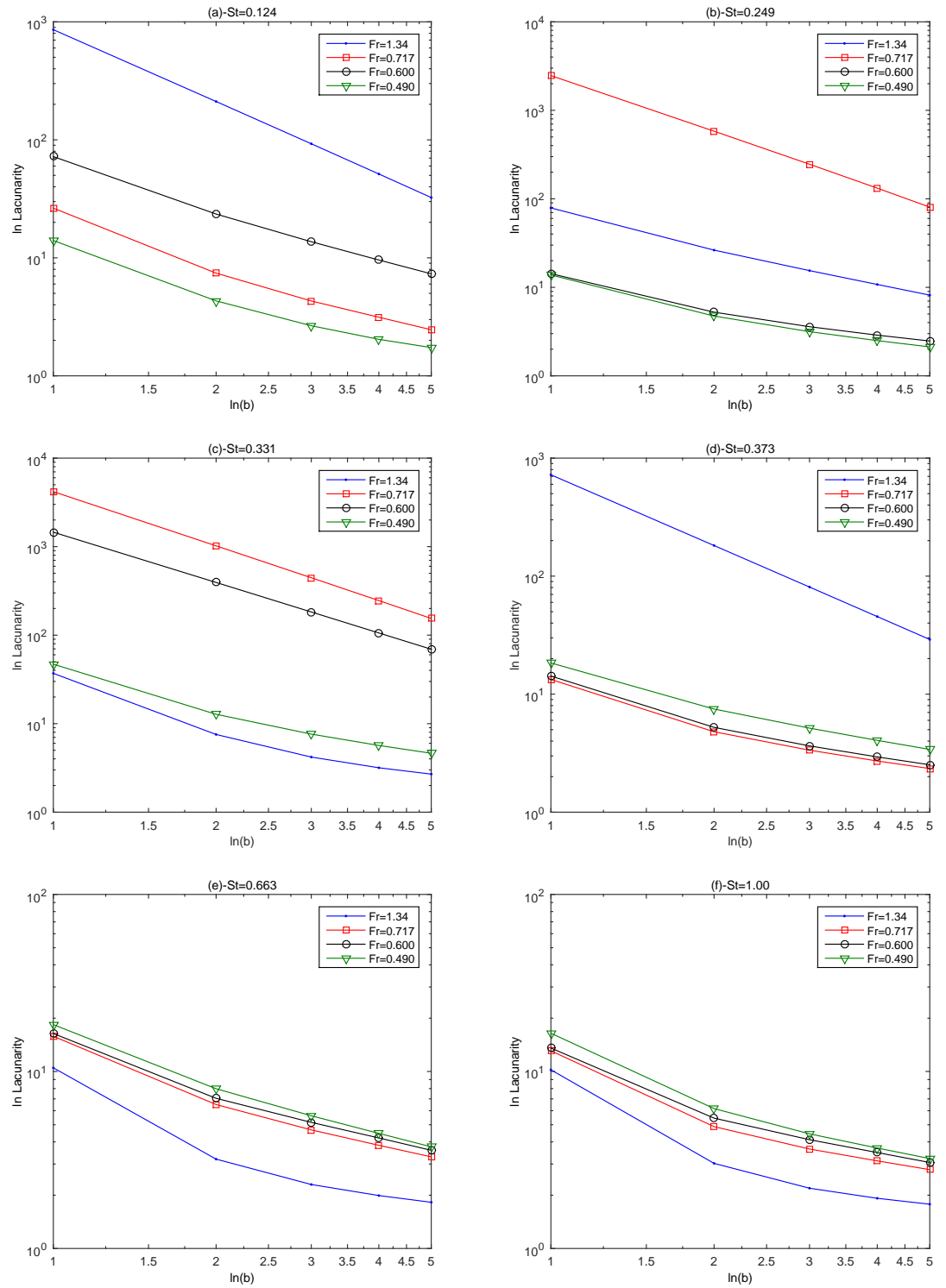


Figure 5.8. Lacunarity curves (a)-(f) for different values of St with varying Fr at $t=300s$

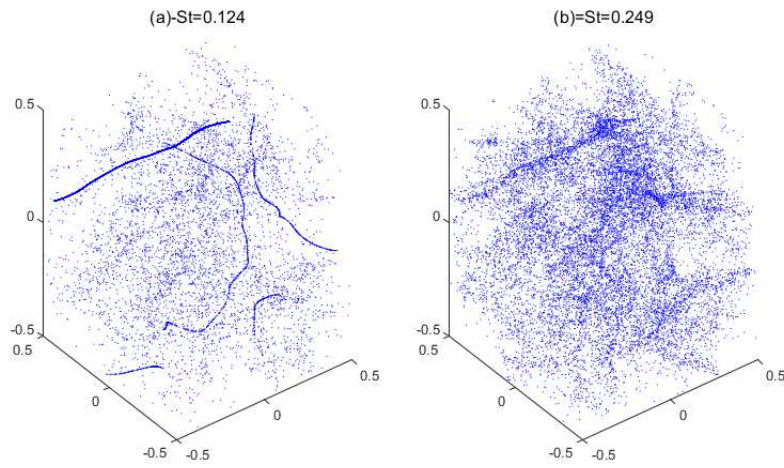


Figure 5.9. Clustering of inertial particles with $Fr = 1.34$ (a). $St=0.124$ and (b). $St=0.249$

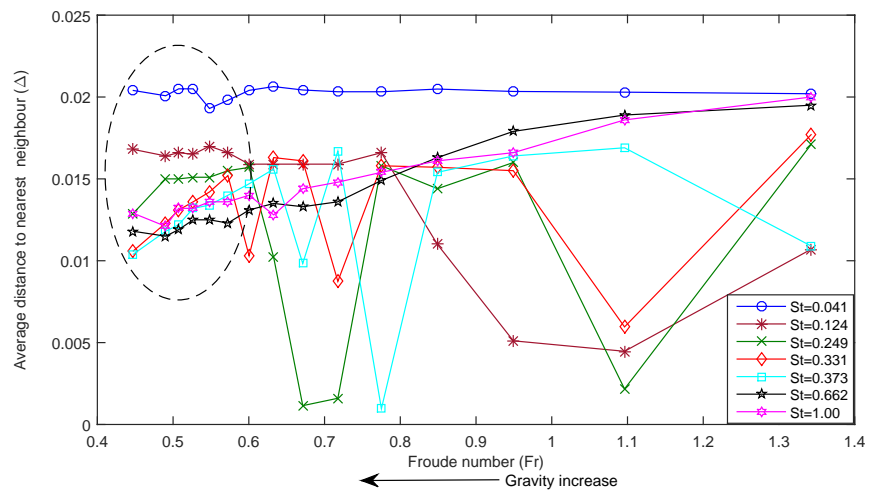


Figure 5.10. Variation in Δ for decreasing values of Fr for different values of St

Hence for a gravitational conditions (constant Fr), we can have strong clustering (as represented by the very sharp dips in 5.11) by changing the particle's inertia (St).

By comparing the results obtained from the three quantification methods, we choose the nearest neighbour (NN) analysis as the best method to quantify the Lagrangian attractors because of a well-defined outcome. In the following section, we apply NN analysis along with BCM to figure out the critical values of St and Fr in the following section.

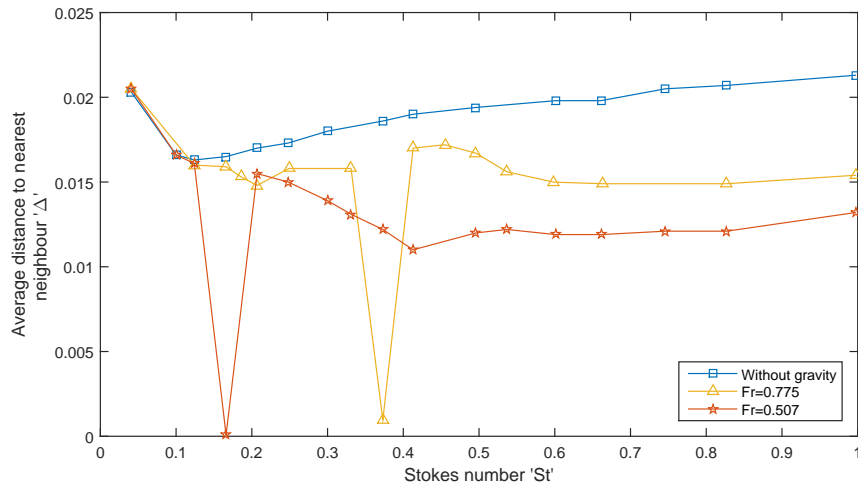


Figure 5.11. Variation in Δ for increasing values of St for different values of Fr

5.4 Quantitative analysis of the Lagrangian attractors

In this discussion, we aim to determine the critical values of St and Fr and preliminary apply the box-counting method for a few cases with different times till the asymptotic patterns achieved. In Fig. 5.12, iso-contours of box-counting dimension (D) as a function of (St, Fr) are plotted for the clusters which reached their final shapes (attractors) and it is observed that strong one-dimensional clustering disappears for $St > 0.45$. Moreover, the different coloured regions identifies the variable clustering patterns in the presence of gravity.

For further detailed analysis, the nearest neighbour analysis is complemented with BCM in order to reduce the computing time for each case. The method is employed to a more systematic data (listed in Table 5.2) and each case is run for an arbitrary time of $t=300s$. Iso-contours of Δ are plotted as a function of (St, Fr) in Fig. 5.13 to see the effect of the variations in gravity and inertia on the Lagrangian attractors. Colour-wise blue corresponds to the 1D Lagrangian attractor, yellow-green to the 2D-L and dark red to 3D

structures. Fig. 5.13 confirms that the clustering of inertial particles is not a monotonic function of either St or Fr number. However, it is possible to identify regions in the plane (St, Fr) .

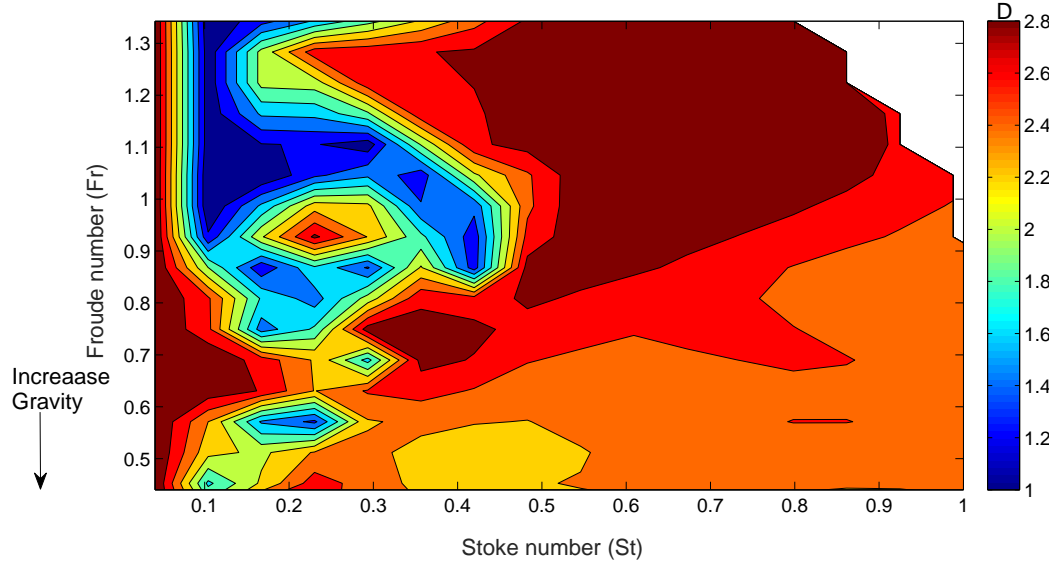


Figure 5.12. Iso-contours of the attractors fractal dimension D as a function of (St, Fr) .

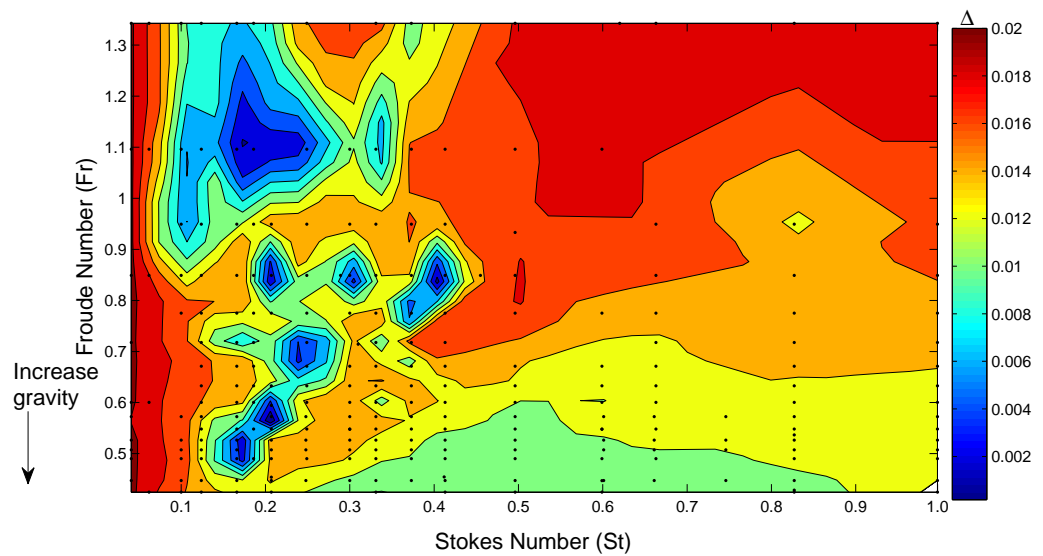
- i) There is no one-dimensional structure for $St \geq 0.5$ in agreement to Fig. 5.12 .
- ii) The 2D-L attractors predominantly appear at low values of Fr and with the sufficient high values of St .
- iii) The lower half of the iso-contours plot (for $Fr < 0.9$ and $St < 0.4$) shows that strong one-dimensional clustering depends on St i.e. for increasing values of St less gravity is required to achieve the one-dimensional attractor and vice versa.

Furthermore, to examine the combined effect of gravity and inertia on the clustering, we further extend the analysis in terms of γ . A few cases with high drift parameter (very low values of Froude number $Fr \rightarrow 0$) are included to find the existence of attractor at lower St . Iso-contours of Δ are plotted as a function of (St, γ) in the Fig. 5.14 which shows the clear blue area for low St and high drift parameter γ . So, further remarks can be added in relation to γ as follows:

- i) For low values of the Stokes number ($St < 0.3$), relatively high drift parameter $\gamma > 1.5$ is required to achieve the vertical one-dimensional attractors.

Cases	Stoke Number	Froude Range
A1	0.04	0.42-1.34
B1	0.1	0.42-1.34
C1	0.12	0.42-1.34
D1	0.17	0.42-1.34
E1	0.21	0.42-1.34
F1	0.25	0.42-1.34
G1	0.3	0.42-1.34
H1	0.33	0.42-1.34
I1	0.37	0.42-1.34
J1	0.41	0.42-1.34
K1	0.5	0.42-1.34
L1	0.6	0.42-1.34
M1	0.66	0.42-1.34
N1	0.83	0.42-1.34
O1	1	0.42-1.34

TABLE 5.2. Systematic data set used to quantify the Lagrangian attractors

Figure 5.13. Iso-contours of Δ as a function of (St, Fr)

- ii) For higher values of the Stokes number ($St > 0.3$) and gravity effects ($\gamma > 0.8$) the 2D-L structures are predominant. This is also in agreement with Gustavsson *et al.* (2014); Park & Lee (2014) whose calculations show that for large values of St particles may cluster strongly.
- iii) In short, we can say that an increase in γ for a given St can create a 1D-V or 2D-L while an increase in St destroys the one-dimensional attractor leading to a 2D-L or 3D attractor. As a result, we often found 2D-L attractors for high γ and St .

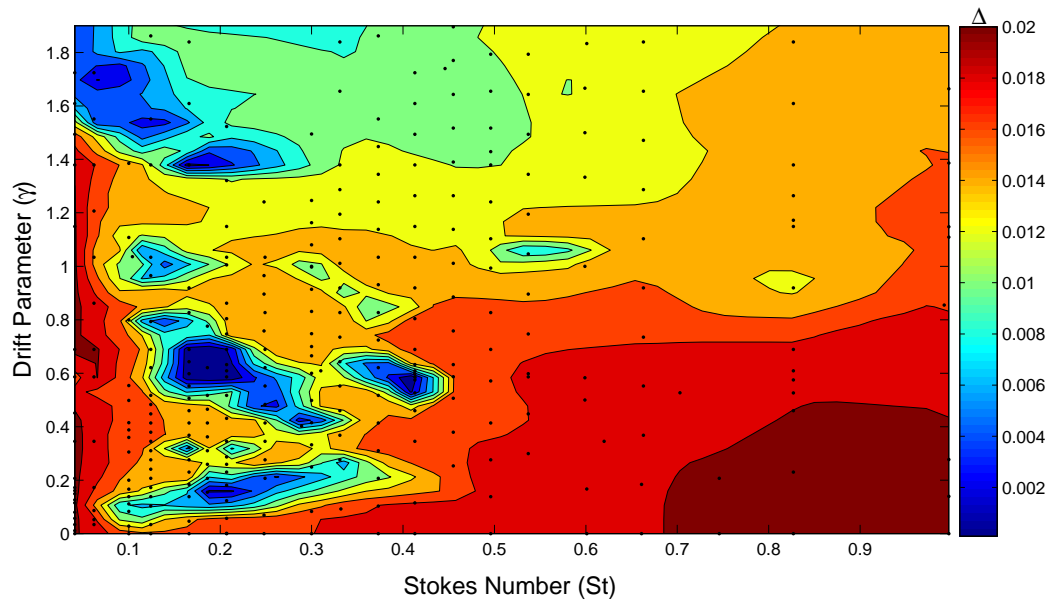


Figure 5.14. Iso-contours of Δ as a function of (St, γ)

5.5 Anisotropy of Lagrangian attractor

In the previous section, we have discovered the Lagrangian attractors in KS representing the strong clustering of inertial particles. The shapes and orientations of these attractors depend on the non-dimensional parameters. For a given pair of St and Fr , the Lagrangian attractors can either settle in a horizontal or vertical direction as shown in Fig. 5.15. It is obvious that the initial uniform distribution first converts into 1D-H attractor and then repositions as 1D-HV and 1D-V attractors with the increasing values of γ .

Quantitatively, BCM and Lacunarity analysis are not able to capture this anisotropic behaviour. So, another advantage of the nearest neighbour analysis is that variations in horizontal Δ_H and vertical Δ_V directions can be identified separately which help to

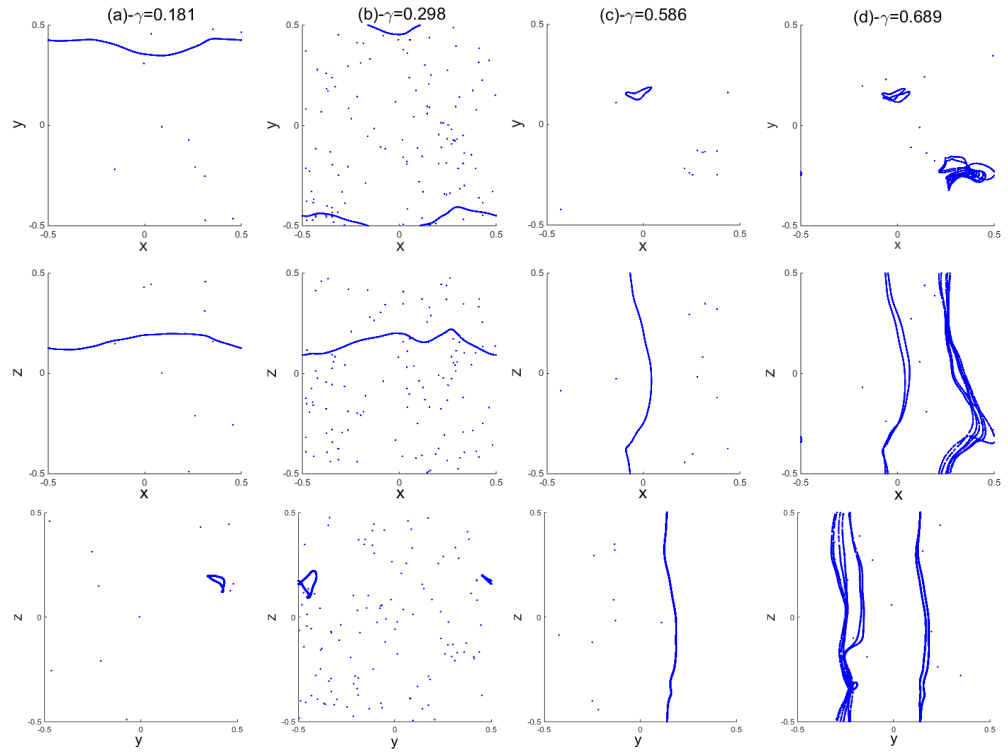


Figure 5.15. 2D-planar views columns (a)-(d) showing different asymptotic 1-D attractor for $St = 0.207$ with different γ .

monitor anisotropic patterns. In practice, Δ_H and Δ_V are defined as follows:

$$\Delta_H = \frac{1}{N_p} \sqrt{\sum_{m=1}^{N_p} (x_m - x_n)^2 + (y_m - y_n)^2} \quad (5.10)$$

$$\Delta_V = \frac{1}{N_p} \sqrt{\sum_{m=1}^{N_p} (z_m - z_n)^2} \quad (5.11)$$

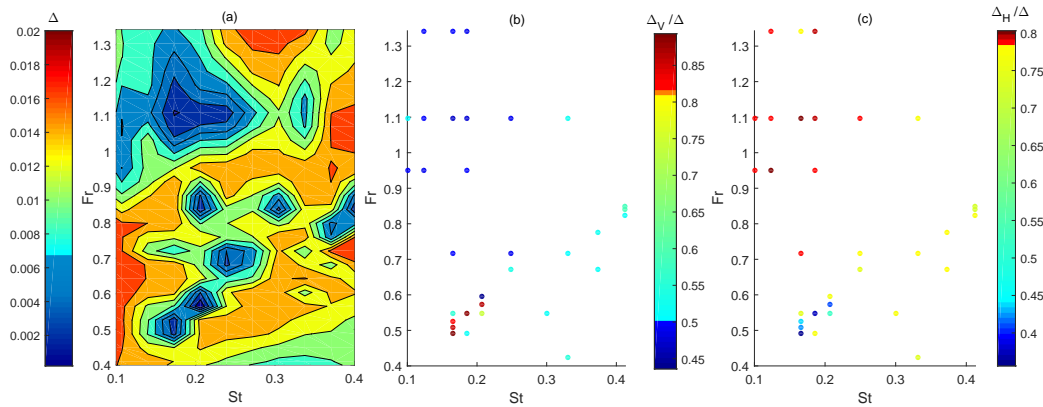


Figure 5.16. (a) Iso-contours of Δ as a function of (St, Fr) , (b) Δ_V/Δ when $\Delta \leq 0.006$, (c) Δ_H/Δ when $\Delta \leq 0.006$.

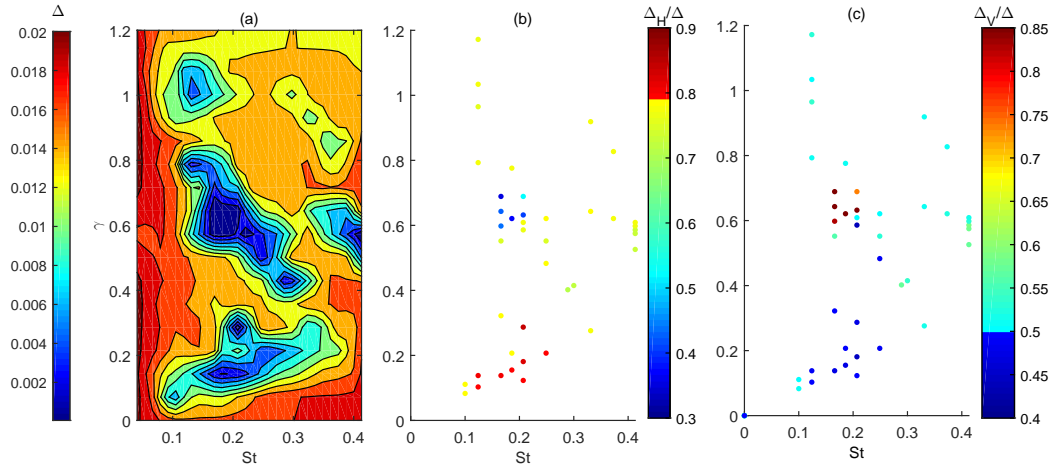


Figure 5.17. (a) Iso-contours of Δ as a function of (St, γ) , (b) Δ_V/Δ when $\Delta \leq 0.006$, (c) Δ_H/Δ when $\Delta \leq 0.006$.

Fig. 5.16(a) shows the iso-contours of Δ as a function of (St, Fr) in the region where one-dimensional Lagrangian attractors are observed, i.e. $0.05 \leq St \leq 0.4$. The two different types of one-dimensional attractor either horizontal (1D-H) or vertical (1D-V) can be further analysed in Figs 5.16(b) and (c). Fig. 5.16(c) shows the ratio Δ_H/Δ where one-dimensional attractors exist, that is when $\Delta \leq 0.008$. $\Delta_H/\Delta \leq 0.5$, that is blue points, indicates 1D-V structures; whereas $\Delta_H/\Delta \geq 0.75$, that is red points, indicates 1D-H structures. Fig. 5.16(b) describes a similar relationship based on Δ_V . So it is clear from the points' colours distribution that horizontal attractors are predominant for large Fr while vertical attractors are prevalent as Fr decreased.

In addition to above analysis, we repeat a similar analysis on the basis of drift parameter γ as shown in Fig. 5.17. There is a clear partition along the ordinate for varying values of St to identify the 1D-H and 1D-V attractors as illustrated by coloured points in Figs. 5.17(b) and (c). For $\gamma > 0.4$, the low values of Δ_H/Δ in Fig. 5.17(b) represent the 1D-V attractors and the amount of γ required to achieve this 1D-V attractor is reduced with the increasing values of St clearly evident from Fig. 5.17(a) (downward blue area for $\gamma > 0.4$). On the basis of the anisotropic analysis, we can define the critical values of non-dimensional parameters differentiating the horizontal and vertical Lagrangian attractors.

5.6 Conclusion

The effect of gravity on the inertial particle clustering is quantified in this chapter. Though a lot of efforts have been made to identify the particle clustering during last three decades, the researchers usually ignored the effect of external forces like gravity

on particle clustering. We have discussed and applied different methods of quantification to inertial particles clustering in KS. In practice, the implementation of each method has some limitations and based on the obtained results we chose the box-counting method and nearest-neighbour analysis to develop a final quantitative analysis.

Finally, the main quantification results are summarised as follows (and as a more synthetic presentation in Fig. 5.18):

- The effect of gravity may reduce or enhance inertial particles clustering (as noticed in Gustavsson *et al.* (2014); Bec *et al.* (2014)) depending on the Stokes number. This effect can lead to strongly anisotropic clusterings (1D or 2D-L) very clearly evidenced by the KS model.
- The 1D structure is better observed with the synthetic flow, as in real flows unsteadiness may prevent the particles from reaching that asymptotic state. These 1D attractors move from the horizontal to the vertical direction as the Fr number decreases.
- For our range of Froude numbers, we found two critical Stokes numbers: for $St > St_{cr1} = 0.3$ there is never occurrence of a horizontal (1D-H) type attractor and no 1D-type attractor is found for $St > St_{cr2} = 0.5$.
- On the basis of anisotropic analysis, we can also deduce the critical values of Froude numbers. From Fig. 5.18, it is observed that there is no 1D-H attractor for $Fr_{cr1} < 0.7$.
- For low values of Froude number $Fr_{cr2} < 0.5$, curtain-like two-dimensional layered structures similar to the curtain-like manifolds already observed in Woittiez & Portela (2008) are recovered as the high gravity prevents the inertial particles from settling uniformly in the turbulent flow.

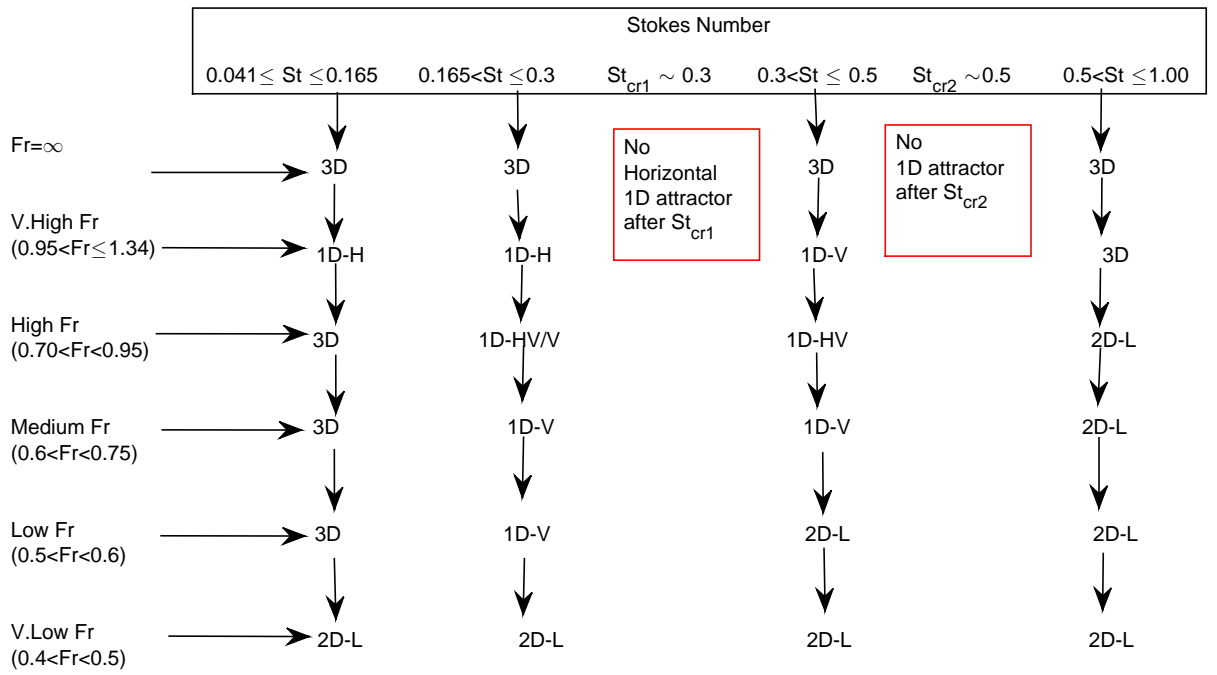


Figure 5.18. Flow chart describing the different attractors in relation to the two critical values of St

Chapter 6

Conclusions and considerations for future studies

6.1 Conclusion

The clustering of inertial particles is studied here in detail using kinematic simulations. We simulated more than a thousand of cases with different particle characteristics and flow conditions. This became only possible because of the synthetic KS model. Our main objective was to emphasize the importance of gravity on inertial particle clustering in turbulent flows and throughout this thesis, we related our results to the gravity effect (Fr). As most of the prior numerical studies dealing with preferential concentration/clustering considered St as the main non-dimensional parameter, particles' inertia was proved to be main cause of preferential concentration/clustering. During the last two years, we notice that the research teams (Gustavsson *et al.*, 2014; Bec *et al.*, 2014; Park & Lee, 2014; Angilella *et al.*, 2014; Jin & He, 2013; Dejoan & Monchaux, 2013) who were only considering the particle's inertia in the past, have taken into account the gravity effect in their studies. As a result, we found quite a brief literature to relate and compare our results.

At the beginning of this work, we set the goals keeping in mind the strength of the KS model. As the Lagrangian tracking and a simpler flow velocity are the attractive features of KS, we aimed to study the particle clustering step by step by modifying the KS Eulerian velocity field. Though each task is investigated and concluded in separate chapters (*Chapters 4-8*), here we summarise our main findings as follows:

- Our results are unique in terms of precision for $0 \leq St \leq 1$ and $0.4 \leq Fr \leq 1.4$. Using the steady KS, we were able to define the ranges of non-dimensional parameters for different types of the Lagrangian attractors. In terms of dimensionality, we found that the one-dimensional attractors exist for a specific range of Stokes number ($St_{cri2} < 0.5$) and Froude number ($Fr > 0.7$). In order to understand the anisotropic behaviour of clustering, the one-dimensional attractors were further categorised into horizontal and vertical attractors. It is also observed that the drift (a combination of the inertia and gravity effect) cause the particles to move in the vertical direction. While the horizontal attractors appear as the result of turbulence structure in the presence of low gravity. Consequently, we observed the variable effect of gravity on the particle clustering which is in agreement with the results of Bec *et al.* (2014); Park & Lee (2014); Dejoan & Monchaux (2013); Jin & He (2013).
- We further investigated the clustering patterns with different spectral conditions. By applying different power laws of energy spectrum, we found the modified ranges of St and Fr which can lead to a one-dimensional attractor. For instance, the St range is changed from [0-0.5] to [0.4-0.85] for $Fr = 0.49$ as the power law is increased from $p = 5/3$ to $p = 2.4$. This shows that the particles with high St can strongly cluster with the modified energy distribution among the scales. Moreover, we also introduced the Kolmogorov Stokes number as a function of p . We found that the range of Stokes number is significantly changed by using Kolmogorov time scale instead of integral time scale. This type of finding can help us to understand the clustering mechanism in the atmospheric and ocean turbulence where energy distribution follows $P \neq 5/3$.
- We also explored the flow structure by applying different vortex region detection methods and then related them with the particle clustering in terms of the centrifugal phenomenology. Firstly, we located the attractors in the strain regions by applying the Q-criterion and vorticity magnitude. Secondly, we calculated the Q-criterion and vorticity on the particles' final positions. The distributions of these quantities in relation to particles initial distribution confirm the appearance of strong attractors in the strain region. Moreover, the 1D-H and 1D-V attractors also differentiated on the basis of Q-criterion. It is noticed that the 1D-H attractors are developed as the result of vorticity differences in the flow structure that hold the attractor in horizontal direction. While the 1D-V attractors arise as a consequence of a combined effect of both turbulence and gravity.

- The effect of temporal variations was introduced to the KS model by considering the different values of unsteadiness parameter λ in the velocity field. We found that the particles' clusters destroy in the unsteady flow. With the help of detailed analysis, we were also able to detect a critical value of the unsteadiness parameter ($\lambda_{cri} = 0.2$) below which one can have the 2D-L attractors. In relation to the gravity, it is observed that the clustering in the unsteady flow is increased with the decreasing values of Fr . This phenomenon reassures that the gravity not only affects the clustering in the steady KS, but also its effect continues with the unsteady conditions.
- Further to this, the unsteadiness flow conditions were also used to see the temporal variations in the Lagrangian attractors. In this way, we could find an effective value of unsteadiness parameter for a given attractor that can destroy it. This mechanism is illustrated by initiating the simulation from different initial positions of the particles. In this regard, we chose the attractors final positions as the starting point of simulation and then unsteadiness parameter was increased step by step. We found that a small amount value of unsteadiness parameter ($\lambda = 0.001$) is enough to destroy the one-dimensional attractor. By comparing two cases with different (St, Fr) and the same unsteadiness parameter, we noticed that a longer time is needed to break a one-dimensional attractor subjected to the lower Fr . It means that the gravity hold the particles together in the unsteady flow as well.
- Finally, we presented a few cases with the modified Reynold numbers by changing the Kolmogorov length scale. With these modified scales, the one-dimensional attractors disappear for $Re_L > 100$, but still some attractors appear whose dimensions may vary from 2D to 3D.

6.2 Considerations for future works

The main goals set for this study have been achieved, but still there is a lack of physics that made the study much simpler than actual multiphase turbulent flows. To make the study physically more appealing, a lot of flow and particle conditions can be added. In this regard, we list some of the future aspects of this research as follows:

- Particle clustering has been studied by using the diverse ranges of St and Fr . To compare our results with recent studies, more work is needed for different ranges of St and Fr .
- We used a mono-dispersed mechanism for seeding the particles and it is also

aimed to see the difference in clustering by considering the bi-dispersed and poly-dispersed seeding.

- The particle-particle and particle-fluid interactions are crucial features, which can affect the clustering in turbulent flows. These features are required to be explored in order to understand some important physical mechanisms such as, collision rate, modification in turbulence, etc.
- The quantification methods applied for the spatial analysis are based on the final positions of particles. It is also recommended to consider other methods having more statistics in contrast to the box counting method and the nearest-neighbour analysis.
- Different energy spectra are applied to the steady KS and it is observed that the particle clustering is considerably affected by the power law variations ranged within $1.5 \leq p \leq 2.5$. We could apply these spectral variations to the unsteady KS as well.
- The range of Reynolds numbers, that can result in the Lagrangian attractors, is one of the important tasks for the upcoming parts of this study. Though we have introduced the effect of variations in Reynolds number using a few cases, more work is required to decide a definite range of Reynolds numbers.
- In the unsteady KS, we also initiated the simulation by choosing different initial positions of the particles. Similar to this, we can further look into the clustering by setting the Lagrangian attractors as a initial position in different numerical simulations such as DNS, LES, etc.
- The homogeneous isotropic kinematic simulation is successfully applied for studying the particle clustering and pursuant to this, we could also aim to set a same kind of study using the stratified and rotating KS.

References

- ALISEDA, A., CARTELLIER, A., HAINAUX, F. & LASHERAS, J. C. 2002 Effect of preferential concentration on the settling velocity of heavy particles in homogeneous isotropic turbulence. *J. Fluid Mech.* **468**, 77–105.
- ANGILELLA, J.-R., VILELA, R. D. & MOTTER, A. E. 2014 Inertial particle trapping in an open vortical flow. *J. Fluid Mech.* **744**, 183–216.
- AYYALASOMAYAJULA, S., GYLFASSON, A., COLLINS, L. R., BODENSCHATZ, E. & WARHAFT, Z. 2006 Lagrangian Measurements of Inertial Particle Accelerations in Grid Generated Wind Tunnel Turbulence. *Phys. Rev. Lett.* **97**, 144507.
- BASSET, A. 1888 *A Treatise on Hydrodynamics*. George Bell and Sons.
- BEC, J. 2005 Multifractal concentrations of inertial particles in smooth random flows. *J. Fluid Mech.* **528**, 255–277.
- BEC, J., BIFERALE, L., CENCINI, M., LANOTTE, A., MUSACCHIO, S. & TOSCHI, F. 2007 Heavy Particle Concentration in Turbulence at Dissipative and Inertial Scales. *Phys. Rev. Lett.* **98**, 084502.
- BEC, J., BIFERALE, L., LANOTTE, A. S., SCAGLIARINI, A. & TOSCHI, F. 2010 Turbulent pair dispersion of inertial particles. *J. Fluid Mech.* **645**, 497–528.
- BEC, J., CENCINI, M. & HILLERBRAND, R. 2007a Clustering of heavy particles in random self-similar flow. *Phys. Rev. E* **75**, 025301.
- BEC, J., CENCINI, M., HILLERBRAND, R. & TURITSYN, K. 2008 Stochastic suspensions of heavy particles. *Physica D: Nonlinear Phenomena* **237** (14–17), 2037–2050.

- BEC, J., HOMANN, H. & RAY, S. S. 2014 Gravity-Driven Enhancement of Heavy Particle Clustering in Turbulent Flow. *Phys. Rev. Lett.* **112**, 184501.
- BOSSE, T., KLEISER, L. & MEIBURG, E. 2006 Small particles in homogeneous turbulence: Settling velocity enhancement by two-way coupling. *Phys. Fluids* **18** (2), 027102.
- BOUSSINESQ, J. 1903 Theorie Analysis de la Chaleur. *Cauthier-Villars, Paris* **2**, 224.
- BROWN, G. L. & ROSHKO, A. 1974 On density effects and large structure in turbulent mixing layers. *J. Fluid Mech.* **64**, 775–816.
- BUEVICH, A. 1966 Motion Resistance of a Particle Suspended in Turbulent Medium. *Fluid dynamics* p. 1119.
- CALZAVARINI, E., KERSCHER, M., LOHSE, D. & TOSCHI, F. 2008 Dimensionality and morphology of particle and bubble clusters in turbulent flow. *J. Fluid Mech.* **607**, 13–24.
- CENCINI, M., BEC, J., BIFERALE, L., BOFFETTA, G., CELANI, A., LANOTTE, A. S., MUSACCHIO, S. & TOSCHI, F. 2006 Dynamics and statistics of heavy particles in turbulent flows. *Journal of Turbulence* **7**, N36.
- CHEN, L., GOTO, S. & VASSILICOS, J. 2006 Turbulent Clustering of Stagnation points and Inertia Particles. *J. Fluid Mech.* **553**, 143–154.
- CHUN, J., KOCH, D. L., RANI, S. L., AHLUWALIA, A. & L.R. COLLINS 2005 Dynamics and statistics of heavy particles in turbulent flows. *J. Fluid Mech.* **536**, 219–251.
- COLEMAN, S. W. & VASSILICOS, J. C. 2009 A unified sweep-stick mechanism to explain particle clustering in two- and three-dimensional homogeneous, isotropic turbulence. *Phys. Fluids* **21** (11).
- COLLINS, L. & KESWANI, A. 2004 Reynolds number scaling of particle clustering in turbulent aerosols. *New J. Phys.* **6**, 1–17.
- CORRSIN, S. & LUMLEY, J. L. 1956 On the equation of motion for a particle in turbulent fluid. *Appl. Sci. Res.* **6A**, 114–116.
- CROWE, C., CHUNG, J. & TROUTT, T. 1988 Particle mixing in free shear flows. *Progress in Energy and Combustion Science* **14** (3), 171 – 194.

- CUZZI, J. N., HOGAN, R. C., PAQUE, J. M. & DOBROVOLSIS, A. R. 2001 Size-selective Concentration of Chondrules and Other Small Particles in Proto-planetary Nebula Turbulence. *The Astrophysical Journal* **546** (1), 496.
- DALE, M. 2000 Lacunarity analysis of spatial pattern: A comparison. *Landscape Ecology* **15** (5), 467–478.
- DEJOAN, A. & MONCHAUX, R. 2013 Preferential concentration and settling of heavy particles in homogeneous turbulence. *Phys. Fluids* **25** (1), 013301.
- EATON, J. & J.R.FESSLER 1994 Preferential concentration of particle by turbulence. *Int. J. Multiphase flow* **20**, 169.
- ELLIOTT, F. W. & MAJDA, A. J. 1996 Pair dispersion over an inertial range spanning many decades. *Phys. Fluids* **8** (4), 1052–1060.
- FALKOVICH, G., FOUXON, A. & STEPANOV, M. 2002 Acceleration of rain initiation by cloud turbulence. *Nature* **419** (6903), 151–154.
- FALKOVICH, G. & PUMIR, A. 2004 Intermittent distribution of heavy particles in a turbulent flow. *Phys. Fluids* **16** (7), L47–L50.
- FERRANTE, A. & ELGHOBASHI, S. 2003 On the physical mechanisms of two-way coupling in particle-laden isotropic turbulence. *Phys. Fluids* **15** (2), 315–329.
- FESSLER, J. R., KULICK, J. D. & EATON, J. K. 1994 Preferential concentration of heavy particles in a turbulent channel flow. *Phys. Fluids* **6** (11), 3742–3749.
- FUNG, J. & VASSILICOS, J. C. 1998 Two-particle dispersion in turbulentlike flows. *Phys. Rev. E* **57** (2), 1677–1690.
- FUNG, J. C. H. 1990 Kinematic Simulation of turbulent flow and particle motion. PhD thesis, University of Cambridge.
- FUNG, J. C. H., HUNT, J. C. R., MALIK, N. A. & PERKINS, R. J. 1992 Kinematic Simulation of homogeneous turbulence by unsteady random Fourier modes. *J. Fluid Mech.* **236**, 281–317.
- GATIGNOL, R. 1983 The Faxen formulae for a rigid particle in an unsteady non-uniform Stokes flow. *J. Mech. Theor. Appl.* **1** (2), 143–160.
- GIBERT, M., XU, H. & BODENSCHATZ, E. 2012 Where do small, weakly inertial particles go in a turbulent flow? *J. Fluid Mech.* **698**, 160–167.

- GOEPFERT, C., MARI, J.-L., CHAREYRON, D. & LANCE, M. 2010 Characterization of a system generating a homogeneous isotropic turbulence field by free synthetic jets. *Exp. Fluids* **48** (5), 809–822.
- GOOD, G. H., IRELAND, P. J., BEWLEY, G. P., BODENSCHATZ, E., COLLINS, L. R. & WARHAFT, Z. 2014 Settling regimes of inertial particles in isotropic turbulence. *J. Fluid Mech.* **759**.
- GOTO, S. & VASSILICOS, J. 2006 Self-Similar Clustering of Inertial Particles and Zero Acceleration Points in Fully Developed Two-Dimensional Turbulence. *Phys. Fluids* **18**, 115103.
- GUSTAVSSON, K., VAJEDI, S. & MEHLIG, B. 2014 Clustering of Particles Falling in a Turbulent Flow. *Phys. Rev. Lett.* **112**, 214501.
- HOGAN, R. C. & CUZZI, J. N. 2001 Stokes and Reynolds number dependence of preferential particle concentration in simulated three-dimensional turbulence. *Phys. Fluids* **13** (10), 2938–2945.
- HOLZNER, M., LIBERZON, A., NIKITIN, N., LTHI, B., KINZELBACH, W. & TSINOBER, A. 2008 A Lagrangian investigation of the small-scale features of turbulent entrainment through particle tracking and direct numerical simulation. *J. Fluid Mech.* **598**, 465–475.
- HWANG, W. & EATON, J. 2004 Creating homogeneous and isotropic turbulence without a mean flow. *Exp. Fluids* **36** (3), 444–454.
- IJZERMANS, R. H. A., MENEGUZ, E. & REEK, M. W. 2010 Segregation of particles in incompressible random flows: singularities, intermittency and random uncorrelated motion. *J. Fluid Mech.* **653**, 99136.
- JIN, G., HE, G. & WANG, L. 2010 Large-eddy simulation of turbulent collision of heavy particles in isotropic turbulence. *Phys. Fluids* **22** (5), 055106.
- JIN, G., W. Y. Z. J. & HE, G. 2013 Turbulent Clustering of Point Particles and Finite-Size Particles in Isotropic Turbulent Flows. *Industrial and engineering chemistry research* **52** (33), 11294–11301.
- KHAN, M. A. I., PUMIR, A. & VASSILICOS, J. C. 2003 Kinematic simulation of multi point turbulent dispersion. *Phys. Rev. E* **68**, 1–13.

- LUCCI, F., FERRANTE, A. & ELGHOBASHI, S. 2010 Modulation of isotropic turbulence by particles of Taylor length-scale size. *J. Fluid Mech.* **650**, 5–55.
- LUCCI, F., FERRANTE, A. & ELGHOBASHI, S. 2011 Is Stokes number an appropriate indicator for turbulence modulation by particles of Taylor-length-scale size? *Phys. Fluids* **23** (2), 025101.
- MALIK, N. A. 2014a A Theory of Turbulent Particle Pair Diffusion, Locality Versus Non-locality. <http://arxiv.org/abs/1405.3625>. .
- MALIK, N. A. 2014b Turbulent Particle Pair Diffusion, Locality Versus Non-locality: Numerical Simulations. <http://arxiv.org/abs/1405.3638>. .
- MALIK, N. A. & VASSILICOS, J. C. 1999 A Lagrangian model for turbulent dispersion with turbulent-like flow structure: comparison with DNS for two-particle statistics. *Phys. Fluids* **11** (6), 1572–1580.
- MAXEY, M. R. 1987 The gravitational settling of aerosol particles in homogeneous turbulence and random flow fields. *J. Fluid Mech.* **174**, 441–465.
- MAXEY, M. R. & RILEY, J. J. 1983 Equation of Motion for a small Rigid in a Nonuniform Flow. *Phys. Fluids* **26** (4), 883–889.
- MENEGUZ, E. & REEKS, M. W. 2011 Statistical properties of particle segregation in homogeneous isotropic turbulence. *J. Fluid Mech.* **686**, 338–351.
- MONCHAUX, R., BOURGOIN, M. & CARTELLIER, A. 2010 Preferential concentration of heavy particles: A Vorono analysis. *Phys. Fluids* **22** (10), 103304.
- NICOLLEAU, F. & ELMAIHY, A. 2004 Study of the development of a 3-D material surface and an iso-concentration field using KS. *J. Fluid Mech.* **517**, 229–249, doi: 10.1017/S0022112004000898.
- NICOLLEAU, F. & ELMAIHY, A. 2006 Study of the effect of the Reynolds number on three- and four-particle diffusion in three-dimensional turbulence using Kinematic Simulation. *Phys Rev. E* **74** (4), 046302, doi:10.1103/PhysRevE.74.046302.
- NICOLLEAU, F., SUNG, K.-S. & VASSILICOS, J. 2013 Vertical motions of heavy inertial particles in stratified turbulence. *Flow, Turbulence and Comb.* **91** (1), 79–103, doi: 10.1007/s10494-013-9456-x.

- NICOLLEAU, F. & VASSILICOS, J. C. 2003 Turbulent Pair Diffusion. *Phys. Rev. Lett.* **90**, 024503.
- NICOLLEAU, F. & YU, G. 2004 Two-particle diffusion and locality assumption. *Phys. Fluids* **16** (4), 2309–2321.
- NICOLLEAU, F. & YU, G. 2007 Turbulence with combined stratification and rotation, limitations of Corrsin’s hypothesis. *Phys. Rev. E* **76** (6), 066302.
- NICOLLEAU, F. C. G. A. & NOWAKOWSKI, A. F. 2011 Presence of a Richardson’s regime in kinematic simulations. *Phys. Rev. E* **83**, 056317.
- OLIVIERI, S., PICANO, F., SARDINA, G., IUDICONE, D. & BRANDT, L. 2014 The effect of the Basset history force on particle clustering in homogeneous and isotropic turbulence. *Phys. Fluids* **26** (4), 041704.
- OSBORNE, D. R., VASSILICOS, J. C., SUNG, K. & HAIGH, J. D. 2006 Fundamentals of pair diffusion in kinematic simulations of turbulence. *Phys. Rev. E* **74**, 036309.
- OSEEN, C. 1927 Hydrodynamik. *Leipzig* p. 132.
- PAN, L., PADOAN, P., SCALO, J., KRITSUK, A. G. & NORMAN, M. L. 2011 Turbulent Clustering of Protoplanetary Dust and Planetesimal Formation. *The Astrophysical Journal* **740** (1), 6.
- PARK, Y. & LEE, C. 2014 Gravity-driven clustering of inertial particles in turbulence. *Phys. Rev. E* **89**, 061004.
- PLOTNICK, R. E., GARDNER, R. H., HARGROVE, W. W., PRESTEGAARD, K. & PERLMUTTER, M. 1996 Lacunarity analysis: A general technique for the analysis of spatial patterns. *Phys. Rev. E* **53**, 5461–5468.
- QURESHI, N. M., ARRIETA, U., BAUDET, C., CARTELLIER, A., GAGNE, Y. & BOURGOIN, M. 2008 Acceleration statistics of inertial particles in turbulent flow. *Eur. Phys. J. B* **66** (4), 531–536.
- RAY, B. & COLLINS, L. R. 2011 Preferential concentration and relative velocity statistics of inertial particles in NavierStokes turbulence with and without filtering. *J. Fluid Mech.* **680**, 488–510.

- RAY, B. & COLLINS, L. R. 2013 Investigation of sub-Kolmogorov inertial particle pair dynamics in turbulence using novel satellite particle simulations. *J. Fluid Mech.* **720**, 192–211.
- RILEY, J. J. 1971 PhD thesis, The John Hopkins University, Baltimore, MD.
- ROSA, B., PARISHANI, H., AYALA, O. & GRABOWSKI, WOJCIECH WAND WANG, L. P. 2013 Kinematic and dynamic collision statistics of cloud droplets from high-resolution simulations. *New J. Phys.* **15**, 045032.
- SALAZAR, J. L. C., DEJONG, J., CAO, L., WOODWARD, S. H., MENG, H. & COLLINS, L. R. 2008 Experimental and numerical investigation of inertial particle clustering in isotropic turbulence. *J. Fluid Mech.* **600**, 245–256.
- SALAZAR, J. P. L. C. & COLLINS, L. R. 2012 Inertial particle relative velocity statistics in homogeneous isotropic turbulence. *J. Fluid Mech.* **696**, 45–66.
- SAPSIS, T. & HALLER, G. 2010 Clustering criterion for inertial particles in two-dimensional time-periodic and three-dimensional steady flows. *Chaos: An Interdisciplinary Journal of Nonlinear Science* **20** (1), 017515.
- SAW, E.-W., SALAZAR, J. P., COLLINS, L. R. & A., S. R. 2012 Spatial clustering of polydisperse inertial particles in turbulence: I. Comparing simulation with theory. *New J. Phys.* **14** (10), 105030.
- SAW, E. W., SHAW, R. A., AYYALASOMAYAJULA, S., CHUANG, P. Y. & GYLFASSON, A. 2008 Inertial Clustering of Particles in High-Reynolds-Number Turbulence. *Phys. Rev. Lett.* **100**, 214501.
- SQUIRES, K. D. & EATON, J. K. 1990 Particle response and turbulence modification in isotropic turbulence. *Phys. Fluids A: Fluid Dynamics (1989-1993)* **2** (7), 1191–1203.
- SQUIRES, K. D. & EATON, J. K. 1991 Measurements of particle dispersion obtained from direct numerical simulations of isotropic turbulence. *J. Fluid Mech.* **226**, 1–35.
- TAGAWA, Y., MERCADO, J., PRAKASH, V., CALZAVARINI, E., SUN, C. & LOHSE, D. 2012 Three-dimensional Lagrangian Vorono analysis for clustering of particles and bubbles in turbulence. *J. Fluid Mech.* **693**, 201–215.

- TANG, L., WEN, F., YANG, Y., CROWE, C. T., CHUNG, J. N. & TROUTT, T. R. 1992 Selforganizing particle dispersion mechanism in a plane wake. *Phys. Fluids A* **4** (10), 2244–2251.
- TCHEN, C. M. 1947 Mean value and correlation problems connected with the motion of small particles suspended in a turbulent fluid. PhD thesis, University of Delft.
- THOMSON, D. J. & DEVENISH, B. J. 2005 Particle pair separation in kinematic simulations. *J. Fluid Mech.* **526**, 277–302.
- WANG, L. P. & MAXEY, M. R. 1993 The Motion of Microbubbles in a forced Isotropic and Homogenous Turbulence. *Applied Scientific Research* **51**, 291–296.
- WANG, Q. & SQUIRES, K. 1996 Large eddy simulation of particle-laden turbulent channel flow. *Phys. Fluids* **8** (5), 1207–1223.
- WOITTIEZ, E. J. P.; JONKER, H. J. & PORTELA, L. M. 2008 On the Combined Effects of Turbulence and Gravity on Droplet Collisions in Clouds: A Numerical Study. *J. Atmos. Sci.* **66** (7), 1926–1943.
- YANG, C. & LEI, U. 1998 The role of the turbulent scales in the settling velocity of heavy particles in homogeneous isotropic turbulence. *J. Fluid Mech.* **371**, 179–205.
- YOSHIMOTO, H. & GOTO, S. 2007 Self-similar clustering of inertial particles in homogeneous turbulence. *J. Fluid Mech.* **577**, 275–286.
- ZIMMERMANN, R., XU, H., GASTEUIL, Y., BOURGOIN, M., VOLK, R., PINTON, J.-F. & BODENSCHATZ, E. 2010 The Lagrangian exploration module: An apparatus for the study of statistically homogeneous and isotropic turbulence. *Rev. Sci. Instrum.* **81** (5), 055112.

Appendix

Appendix A

Quadrat variance method

Quadrat variance analysis is applied to determine the variance of the differences among blocks of different sizes or scales and use the pattern of the variance to determine the scale of the pattern. The methods differ primarily in the number and distribution of blocks being compared (the shape of the logical spatial template). For three dimensional data set, it can be applied as either eight cubed or twenty seven cubed local quadrat system as shown in Figure A.1 and Figure A.2 respectively.

The sum of the values $s_b(x, y, z)$ in the $b \times b \times b$ cube starting at position x, y, z can be defined as;

$$s_b(x, y, z) = \sum_{i=x}^{x+b-1} \sum_{j=y}^{y+b-1} \sum_{k=z}^{z+b-1} dijk \quad (\text{A.1})$$

One block is considered as pivot block with respect to others. The eight-term local quadrat variance (*8TLQV*) for the pivot block is;

$$V_{pivot}(b) = \sum_{x=1}^{n_x+1-2b} \sum_{y=1}^{n_y+1-2b} \sum_{z=1}^{n_z+1-2b} \frac{(7S_p - S_0)^2}{32b^5(n_x + 1 - 2b)(n_y + 1 - 2b)(n_z + 1 - 2b)} \quad (\text{A.2})$$

where n_x, n_y and n_z are the size of the volume along the x-axis, y-axis and z-axis respectively. Because any of 8 blocks can be considered as the pivot (choice of any specific one is arbitrary), the average value of the *8TLQV* variance is calculated as;

$$V_8(b) = \sum_{i=1}^2 \sum_{j=1}^2 \sum_{k=1}^2 \frac{V_{i,j,k}(b)}{8} \quad (\text{A.3})$$

Similarly, we can define the local quadrat variance for twenty seven blocks system and variance can be calculated as;

$$V_{27}(b) = \sum_{x=1}^{n_x+1-3b} \sum_{y=1}^{n_y+1-3b} \sum_{z=1}^{n_z+1-3b} \frac{(26S_p - S_0)^2}{648b^5(n_x + 1 - 2b)(n_y + 1 - 2b)(n_z + 1 - 2b)} \quad (\text{A.4})$$

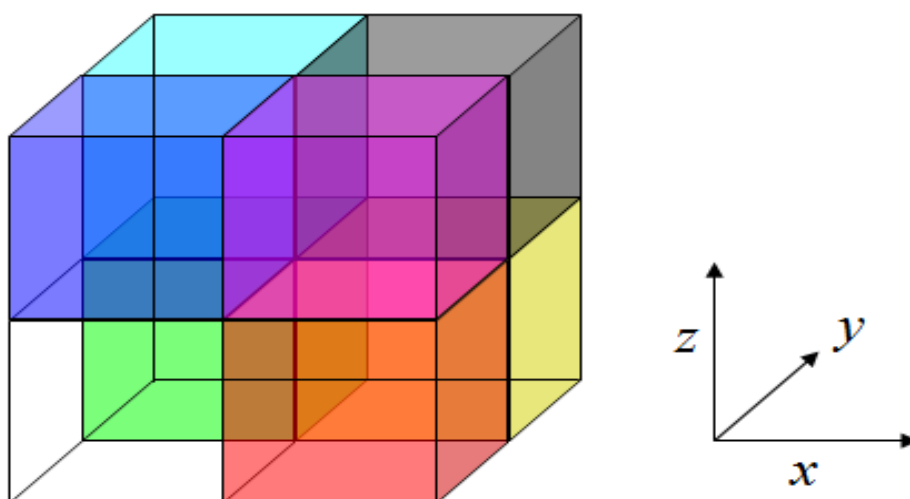


Figure A.1. Representation of eight-term local quadrats

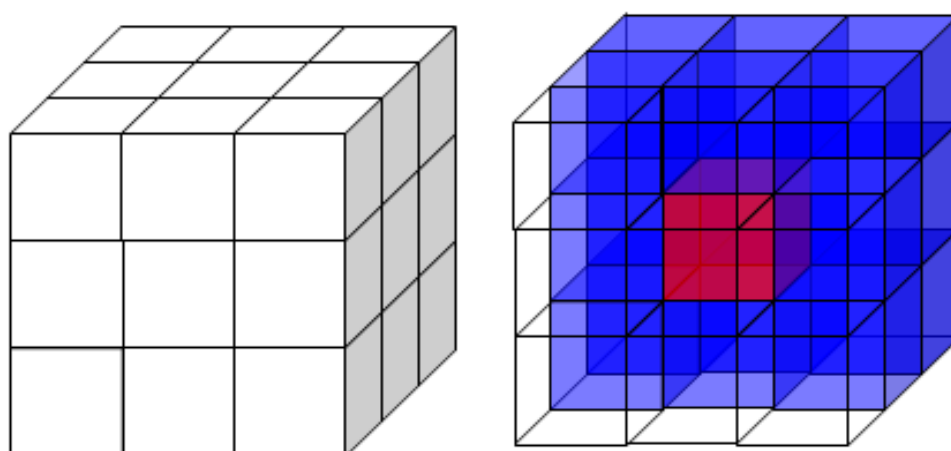


Figure A.2. Representation of twenty seven-term local quadrats

A.0.1 RESULTS USING QUAD VARIANCE ANALYSIS

We apply the 27 – *LTQV* method to identify the clustering (Table 5.1) Fig. A.3(a)-(e). The results shows the clear difference in the curves for different attractors (shown inset). The main problem for this method is very similar to the BCM i.e. only definite shapes of attractator can be captured.

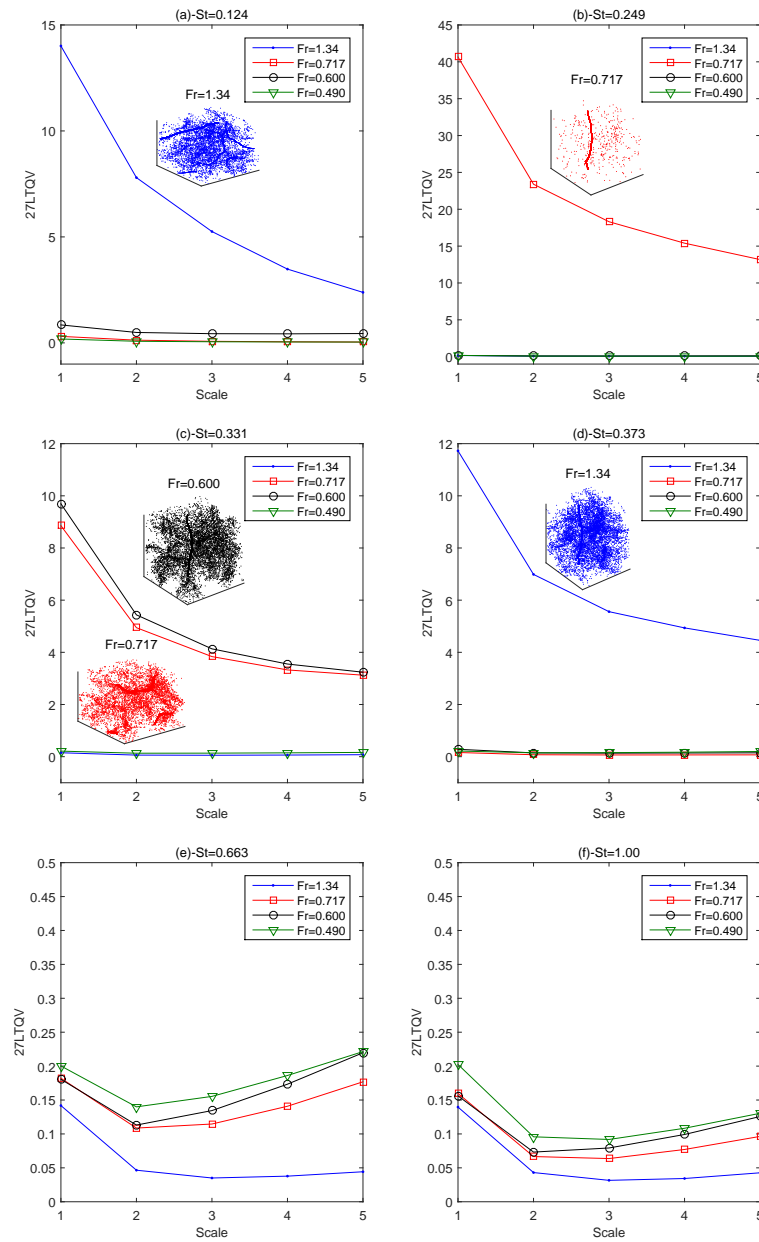


Figure A.3. Results using 27-LTQV method for different values of St with varying Fr at $t=300$

Appendix B

Matlab Script to create Q-criterion and vorticity using velocity field

```

%generating grid and 3d array of velocity
[x y z] = meshgrid(-0.46:0.04:0.5,-0.46:0.04:0.5,-0.46:0.04:0.5);
Fu = TriScatteredInterp(Matrix(:,1),Matrix(:,2),Matrix(:,3), Matrix(:,4)); %u component
Fv = TriScatteredInterp(Matrix(:,1),Matrix(:,2),Matrix(:,3), Matrix(:,5)); %v component
Fw = TriScatteredInterp(Matrix(:,1),Matrix(:,2),Matrix(:,3), Matrix(:,6)); %w component
u = Fu(x,y,z);
w = Fw(x,y,z);
v = Fv(x,y,z);
%gradient of velocities
[dudx,dudy,dudz] = gradient(u,0.04,0.04,0.04);
[dvdx,dvdy,dvdz] = gradient(v,0.04,0.04,0.04);
[dwdx,dwdy,dwdz] = gradient(w,0.04,0.04,0.04);
%creating Q-criteria of flow field
iso_q=180; %+-180 is used
%Definition of Q
q=-0.5*(dudx.^2+dvdy.^2+dwdz.^2)-dudy.*dvdx-dudz.*dwdx-dvdz.*dwdy;
%Plotting a Q isosurface, Q=iso_q
figure()
p=patch(isosurface(x,y,z,q,iso_q));
set(p,'FaceColor','red','EdgeColor','none');
daspect([1,1,1])
axis tight
ax = -1; ay = 1; az = 1;
view([ax,ay,az]);
camroll(240)
camlight
lighting gouraud
cav = curl(x,y,z,u,v,w);
cdata = smooth3( cav,'box',7);
isocolors(x,y,z,cdata,p);
set(p,'FaceColor','interp','EdgeColor','none')
view(150,30); daspect([1 1 1]);axis tight
camlight; lighting phong;

```

Publications

Publications arising from the present work up to the writing:

1. M. Farhan, F. C. G. A. Nicolleau, and A. F. Nowakowski 2015 Effect of gravity on clustering patterns and inertial particle attractors in kinematic simulations *Phys. rev. E*, **91**(4), 043021.
2. M. Farhan, F. C. G. A. Nicolleau and C.J. Keylock 2013 Lagrangian attractors pattern for heavy particle in Kinematic Simulation *Proceedings of the 14th Euromech Turbulence Conference* Lyon, France, 1-4 September 2013.
3. M. Farhan and F. C. G. A. Nicolleau and A. F. Nowakowski 2012 Clustering of laden particles in Kinematic Simulation *ows ERCOFTAC/SIG42 - 8th WSTM - Synthetic turbulence, clustering and fractal geometry*, Paris, France, 28th-29th June 2012.
4. M. Farhan and F. C. G. A. Nicolleau and A. F. Nowakowski 2011 Clustering of laden particles in Kinematic Simulation *ows ERCOFTAC/SIG42 - 7th WSTM - How to assemble and disassemble turbulence and how do things assemble and disassemble in it?*, London, United Kingdom, 22nd-23rd September 2011.
5. M. Farhan and F.C.G.A. Nicolleau and A.F. Nowakowski and J.-R. Angilella 2011 Fractal patterns in turbulent flows for laden particles *Proceedings of the 13th Euromech Turbulence Conference, Journal of Physics: Conference Series* Warsaw, Poland, 11-15 September 2011.